Nonlinear Dyn (2019) 97:797–830
https://doi.org/10.1007/s11071-019-05014-5

ORIGINAL PAPER

Analysis of dynamical behaviors of a 2-DOF friction-induced oscillator with one-sided impact on a conveyor belt

Jinjun Fan · Tianyi Liu · Shoulian Chen

Received: 8 November 2018 / Accepted: 15 May 2019 / Published online: 24 May 2019

Abstract In this paper, the flow switchability theory of discontinuous dynamical systems is used to illustrate the dynamical behavior of a 2-DOF (two degrees of freedom) friction-induced oscillator with one-sided impact on a conveyor belt. All the possible motion states such as stick and non-stick motions, impact motion, and stuck motion for such an oscillator are introduced. The phase space in system can be divided into different domains and boundaries according to the discontinuity caused by the friction force jumping and the impact between the mass and the rigid obstacle. The vector field in each domain is continuous and different from that in its adjacent domain. The flow barrier on the separation boundary is considered in this paper. Once the boundary flow leaves the boundary, the boundary flow barrier on the velocity boundary may exist and the leaving flow barriers on the velocity boundary may also exist. The G-functions on different separation boundaries are defined to illustrate the flow switching on the corresponding boundaries. The analytical conditions of the passable, stick, grazing, impact, and stuck motions are developed through G-functions and analysis of vector fields. Since the motions of the two masses interact with each other, the four-dimensional switching sets are given by the form of direct product and the four-dimensional mappings are given to describe periodic motions with different mapping structures. The analytical prediction of different periodic motions is performed through the mapping dynamics. For a better understanding of the motion switching mechanism in such a 2-DOF oscillator , the time histories of displacement, velocity, G-function and the trajectories in phase space for the passable motion, stick motion, impact motion, grazing motion, stuck motion, and periodic motion in system are given by simulation numerically. This investigation has important significance in the optimization design of machinery with friction and impact etc.

Keywords Discontinuous dynamical system · Flow switchability · Flow barrier · Mapping structure · Periodic motion

J. Fan (✉) · T. Liu (✉) · S. Chen
School of Mathematics and Statistics, Shandong Normal University, Jinan 250014, People's Republic of China
e-mail: fjj18@126.com

T. Liu
e-mail: 1689492604@QQ.com

1 Introduction

In mechanical engineering, discontinuous dynamical systems exist extensively. The reasons causing the discontinuity are various, it is usually related to the impact and friction between two objects or among multiple objects. As examples for such discontinuous dynamical systems, the discontinuities in the dry friction oscillator and the vibrating system are caused by friction and impact, respectively. In fact, some industrial models which are affected by friction and impact exist more complex dynamical behaviors, such as machine tools,

brake systems or turbo machines. The discontinuity caused by impact or friction is advantage for some cases or disadvantage for other cases in engineering applications, so it is necessary to establish such models in practical problems and to study their dynamical behaviors, which can provide us information for applying or controlling them.

Usually, the mathematical models with some kind of discontinuity or non-smoothness are used to investigate the physical phenomena such as impact and dry friction in mechanical systems. Impact and dry friction are abundant in nature, machines and other processes like machine tool chattering and torsional vibration in oil well drill strings etc., which is therefore an important topic in scientific and engineering research. In 1960, Levatan [1] studied the dynamical behavior of a spring-mass system with Coulomb friction and viscous damping. Filippov [2] investigated the differential equations with discontinuous right-hand side by analyzing of a friction oscillator in 1964. He introduced the concept of the differential inclusion and discussed the existence and uniqueness of solutions for discontinuous dynamical systems. After some years, Filippov [3] gave the theory of differential equations with discontinuous right-hand side systematically. More and more models about discontinuous dynamical systems were built since then, and the 1-DOF (single degree of freedom) oscillator was investigated widely. In 1982, Holmes [4] studied the periodic motion and chaotic motion of a ball bouncing vertically on a massive sinusoidally vibrating plate. In 1986, Shaw [5] investigated the stability for periodic motions in the base-driven friction oscillator by using the method of Poincare mapping. A class of harmonically excited 1-DOF oscillators with piecewise linear characteristics were investigated and the stability analysis for periodic motions was presented by Natsiavas [6] in 1998. In 2000, Andreaus and Casini [7] analyzed the motion of 1-DOF system with dry friction on a base with a constant velocity, and obtained the periodic orbit in system by numerical approaches. In 2002, Andreaus and Casini [8] investigated the dynamical behavior of an oscillator with impact and friction, and presented the closed-form solutions. In 2005 and 2006, Casini et al. [9,10] numerically studied the dynamics of a stop-belt friction oscillator and made the analytical and experimental investigations on the dynamic behavior of a non-smooth rotational oscillator, which exhibits multiple discontinuity boundaries in phase space. Other examples for 1-DOF oscillator see [11–16]. Compared with 1-DOF oscillator, the motion of the multi-degree of freedom oscillator is more complicated. Awrejcewicz and Delfs [17,18] studied a self-excited roll-slide oscillator with 2-DOF (two degrees of freedom) and gave the stability of periodic orbits in 1990. In 1992, Foale and Bishop [19] discussed the motion of a forced linear oscillator with instantaneous impact at one or two stops. In 1997, Hinriches et al. [20,21] investigated an impact oscillator and a self-sustained friction oscillator, which are two types of non-smooth oscillators. The stick and non-stick motions can be observed. The bifurcation behavior of such system was predicted by numerical simulations. Since 2006, Pascal [22–24] began to study the dynamics and stability of 2-DOF oscillators with an elastic stop. The dynamics of coupled oscillators excited by dry friction and the dynamical behaviors in stick-slip oscillators were investigated. After some years, Pascal [25] discussed a new model of dry friction oscillator colliding with a rigid obstacle by using Coulomb friction law. Balachandran et al. [26–29] investigated the dynamical behaviors for a beam-mass structure with the influence of resonance and low excitation levels, a thin-walled structure subjected to impact excitations and an elastic structure affected by harmonic or periodic excitations etc. In 2018 and 2019, Lenci et al. [30,31] studied the nonlinear oscillations of an Euler–Bernoulli beam hinged at one end and having a roller support sliding on an inclined line at the other end and the dynamic behavior of a ball bouncing on a flexible beam. Other discontinuous systems with impulsive or Boolean control are investigated in [32–43].

In 2001, two discontinuous bifurcations in mechanical stick-slip systems affected by dry friction were presented by Galvanetto [44]. In 2004, Leine and Nijmeijer [45] systematically studied the dynamical behaviors of Filippov systems and used mechanical systems with dry friction which constitute an important subclass of Filippov systems as examples to illustrate the theory and methods of dealing with the mechanical Filippov systems, and established a bridge between engineering-oriented and mathematics-oriented research in this field. In 2008, Bernardo et al. [46] introduced a qualitative theory for non-smooth systems which is similar to the qualitative theory of smooth systems, and gave the general techniques for analyzing the bifurcations that are unique to non-smooth dynamical systems [so-called discontinuity-induced bifurcations (DIBs for short)], and also gave a consistent classification of all known

DIBs for piecewise-smooth continuous-time dynamical systems (flows), including such diverse phenomena as sliding, chattering, grazing and corner collision etc. In 2016, Lancioni et al. [47] modeled the motion of a windshield wiper blade by a mass–spring–damper system on a moving frictional surface and investigated the dynamical behavior of such system. Attention is focused on the causes of squeal, reversal and chattering noises, and remedies for reducing or avoiding them were proposed. Theory and applications of piecewise-smooth dynamical systems can see Refs. [45,46] in detail.

For most practical problems or applications in the field of mechanical engineering, the motion regions of objects are usually dynamic and the dynamic friction force and maximum static friction force is not equal. Thus the switching motions on dynamic boundaries and the stability of the periodic motions and so on need to be further studied enough. Moreover, there are relatively few results about the multi-degree of freedom systems in the coexistence of friction and impact. In 2005, Luo [48,49] developed the theory of flow switchability on discontinuous boundaries between two adjacent domains to investigate discontinuous dynamical systems. By using such theory, Luo and Gegg [50] presented the force criteria for stick and non-stick motions in a periodically forced friction-induced oscillator in 2006, and gave the numerical simulation of some motions in system. The G-function for discontinuous dynamical systems was further introduced in Luo [51] and the non-passable flows of sink and source to the separation boundary were discussed. In 2007, Luo and Thapa [52] investigated the nonlinear dynamics of a brake system driven by a periodic excitation. The switching conditions of the sliding motions were developed. For a 2-DOF friction-induced oscillator on a constant speed belt, Luo and Mao [53] discussed all the possible stick and non-stick motions in such a model and gave the corresponding analytical conditions of switching motions on discontinuous boundaries in system. The systematic elaboration of the switching theory of flow in discontinuous dynamical systems and some of its applications can be referred to Luo [54,55]. Using such theory, more and more results of discontinuous dynamical systems in mechanical engineering are obtained. In 2012, Luo and Huang [56] studied discontinuous dynamics of a nonlinear, self-excited, friction-induced, periodically forced oscillator. In 2015, Fu et al. [57–59] discussed the dry friction oscillator with impulsive effect or impact, and presented the analytical prediction for several periodic motions. From 2016 to 2019, Fan et al. [60–70] studied the discontinuous dynamical behaviors of several oscillation systems derived from mechanical engineering and the synchronization of two different dynamical systems.

In this paper, the flow switching theory for discontinuous dynamical systems will be applied to perform a theoretical and numerical investigation concerning the non-smooth dynamics of a 2-DOF oscillator in the coexistence of friction and impacts and the inequality of dynamic friction force and maximum static friction force. The flow switching theory of discontinuous dynamic system regards the motion of objects and the friction or collision between objects as occurring in the dynamic domain and on its dynamic boundary, which becomes one of the important tools to study such mechanical problem. Using G-function as the main research tool, the motion switching mechanism in such a 2-DOF oscillator system will be studied from a new perspective, which would facilitate a better explanation of the discontinuous dynamic behavior in mechanical systems. The 2-DOF system studied in this paper is complex and several configurations can occur. This paper will be focused on providing a complete analytical description of all the possible motions with the relevant switching conditions in system on multiple discontinuity boundaries and carrying out the numerical simulations of stick motion, impact motion, grazing motion, periodic motions and so on through the time history responses of displacement, velocity, G-function and the trajectories in phase space for such system. The rest of the paper is organized as follows. In Sect. 2, the physical model of the 2-DOF friction-induced oscillator with one-sided impact on a conveyor belt is introduced. In Sect. 3, the phase space for each mass is partitioned into different domains and boundaries due to the discontinuity caused by friction and impact. The G-functions are defined to illustrate the flow switching mechanism on different separation boundaries and the switching conditions for different motions are given by the form of theorem in Sect. 4. In Sect. 5, the four-dimensional switching sets and mappings are introduced to illustrate the periodic motions in the 2-DOF friction-induced oscillator. For a better understanding of the complex dynamical behaviors of this oscillator system, the numerical simulations are given in Sect. 6. Finally, Sect. 7 concludes the whole paper.

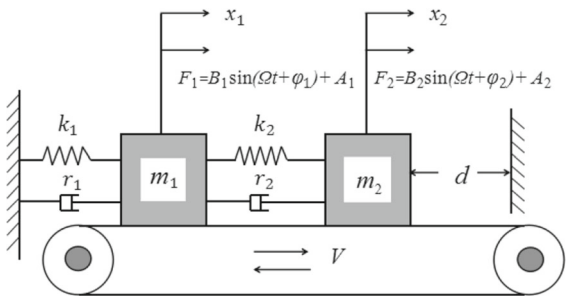

Fig. 1 Physical model

2 Physical model

A new 2-DOF, friction-induced oscillator with one-sided impact on a conveyor belt will be investigated in this paper. The corresponding physical model is shown in Fig. 1. The system consists of two masses $m_\alpha(\alpha = 1, 2)$ which are in contact with a belt moving at a constant velocity of V and are subjected to two periodic excitation forces. The two masses are connected by a spring of stiffness k_2 and a damper of coefficient r_2. The mass m_1 is attached to the fixed wall by the linear spring of stiffness k_1 and the damper of coefficient r_1. The distance between the mass m_2 and the right fixed rigid obstacle is d. The mass m_2 can impact with the fixed rigid obstacle and the restitution coefficient of impact is R ($R \in (0, 1)$). The two periodic excitations acting on the two masses are

$$F_\alpha = B_\alpha \sin(\Omega t + \varphi_\alpha) + A_\alpha \quad (\alpha = 1, 2), \tag{1}$$

where B_α, Ω, φ_α and A_α are amplitude, frequency, phase angle and the constant force, respectively. Through prestressing the masses m_1 and m_2, the constant force magnitudes of A_1 and A_2 could be adjusted to adapt to different working environments. The displacements of the two masses $m_\alpha(\alpha = 1, 2)$ are represented by $x_\alpha(\alpha = 1, 2)$, where the origins of the coordinates are set at their own equilibrium positions, i.e., when the conveyor belt is at rest and the object is not subjected to external force and the spring to which the object is connected has no extension and the damper to which the object is connected has no damping force, the position of each object is defined as its equilibrium position. The friction force $F_{\mathrm{f}}^{(\alpha)}(\dot{x}_\alpha)(\alpha \in \{1, 2\})$ between the mass $m_\alpha(\alpha \in \{1, 2\})$ and the belt shown in Fig. 2 can be described as

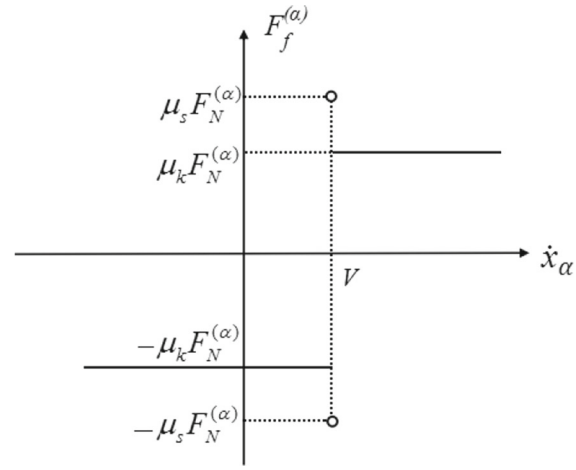

Fig. 2 Friction forces ($\alpha = 1, 2$)

$$F_{\mathrm{f}}^{(\alpha)}(\dot{x}_\alpha) \begin{cases} = \mu_{\mathrm{k}} F_{\mathrm{N}}^{(\alpha)}, & \dot{x}_\alpha > V, \\ \in [-\mu_{\mathrm{s}} F_{\mathrm{N}}^{(\alpha)}, \mu_{\mathrm{s}} F_{\mathrm{N}}^{(\alpha)}], & \dot{x}_\alpha = V, \\ = -\mu_{\mathrm{k}} F_{\mathrm{N}}^{(\alpha)}, & \dot{x}_\alpha < V, \end{cases} \tag{2}$$

where $\dot{x}_\alpha = \mathrm{d}x_\alpha/\mathrm{d}t$, μ_{k} and μ_{s} are the kinetic and static friction coefficients on the contact surface and $F_{\mathrm{N}}^{(\alpha)}$ is the normal force to contact surface, $F_{\mathrm{N}}^{(\alpha)} = m_\alpha g$ and g is the acceleration of gravity. The range of the static friction force is $[-\mu_{\mathrm{s}} F_{\mathrm{N}}^{(\alpha)}, \mu_{\mathrm{s}} F_{\mathrm{N}}^{(\alpha)}]$, where $\mu_{\mathrm{s}} F_{\mathrm{N}}^{(\alpha)}$ represents the maximum static friction force. The kinetic friction force is $\mu_{\mathrm{k}} F_{\mathrm{N}}^{(\alpha)}$ or $-\mu_{\mathrm{k}} F_{\mathrm{N}}^{(\alpha)}$ once the relative motion occurs between the mass m_α and the belt.

The non-friction forces exerting on the two masses $m_\alpha(\alpha = 1, 2)$ in the x_α-direction are defined as

$$\begin{aligned} F_{\mathrm{s}}^{(1)} &= B_1 \sin(\Omega t + \varphi_1) + A_1 - k_1 x_1 - r_1 \dot{x}_1 \\ &\quad - k_2(x_1 - x_2) - r_2(\dot{x}_1 - \dot{x}_2), \\ F_{\mathrm{s}}^{(2)} &= B_2 \sin(\Omega t + \varphi_2) + A_2 - k_2(x_2 - x_1) \\ &\quad - r_2(\dot{x}_2 - \dot{x}_1). \end{aligned} \tag{3}$$

The motion of the system can be generally fallen into two categories: the mass m_2 cannot contact with the fixed rigid obstacle (i.e., $x_2 < d$), and the mass m_2 contacts with the fixed rigid obstacle (i.e., $x_2 = d$). For the first category (i.e., $x_2 < d$), both the masses have two kinds of motion states: non-stick motion and stick motion. If the mass $m_\alpha(\alpha \in \{1, 2\})$ moves along the belt, i.e., the velocity of the mass m_α is different to

that of the belt, such motion is called non-stick motion or free-flight motion. For this case, the mass has the relative motion to the belt, and the non-friction force can overcome the maximum static friction force. For the non-stick motion of the masses $m_\alpha(\alpha = 1, 2)$, the resultant forces acting on the two masses are

$$\begin{aligned} F^{(1)} &= B_1\sin(\Omega t + \varphi_1) + A_1 - k_1x_1 - r_1\dot{x}_1 \\ &\quad - k_2(x_1 - x_2) - r_2(\dot{x}_1 - \dot{x}_2) \\ &\quad - \mu_k F_N^{(1)}\mathrm{sgn}(\dot{x}_1 - V), \\ F^{(2)} &= B_2\sin(\Omega t + \varphi_2) + A_2 - k_2(x_2 - x_1) \\ &\quad - r_2(\dot{x}_2 - \dot{x}_1) - \mu_k F_N^{(2)}\mathrm{sgn}(\dot{x}_2 - V). \end{aligned} \tag{4}$$

If the velocity of the mass $m_\alpha(\alpha \in \{1, 2\})$ is equal to that of the belt, the corresponding motion is called stick motion. For this case, the non-friction force cannot overcome the maximum static friction force acting on the corresponding mass (i.e., $|F_s^{(\alpha)}| \le \mu_s F_N^{(\alpha)}, \alpha \in \{1, 2\}$), and the mass moves together with the belt at this time. For the stick motion, the equation of motion for the mass $m_\alpha(\alpha \in \{1, 2\})$ is

$$\ddot{x}_\alpha = 0 \quad \text{for } \dot{x}_\alpha = V \text{ and } \alpha \in \{1, 2\}. \tag{5}$$

From the above discussion, the motion when the mass m_2 does not touch with the right-hand obstacle can be divided into four cases.

Case I non-stick motion $(\dot{x}_\alpha \ne V, \alpha = 1, 2)$.

The equations of non-stick motion for the two masses $m_\alpha(\alpha = 1, 2)$ are

$$\begin{aligned} &m_1\ddot{x}_1 + k_1x_1 + r_1\dot{x}_1 + k_2(x_1 - x_2) + r_2(\dot{x}_1 - \dot{x}_2) \\ &\quad = B_1\sin(\Omega t + \varphi_1) + A_1 - \mu_k m_1 g\mathrm{sgn}(\dot{x}_1 - V), \\ &m_2\ddot{x}_2 + k_2(x_2 - x_1) + r_2(\dot{x}_2 - \dot{x}_1) \\ &\quad = B_2\sin(\Omega t + \varphi_2) + A_2 - \mu_k m_2 g\mathrm{sgn}(\dot{x}_2 - V). \end{aligned} \tag{6}$$

Case II single stick motion $(\dot{x}_1 = V, \dot{x}_2 \ne V)$.

The mass m_1 has the stick motion and the mass m_2 has the non-stick motion. The equations for the two masses $m_\alpha(\alpha = 1, 2)$ are

$$\begin{aligned} &\ddot{x}_1 = 0 \text{ for } \dot{x}_1 = V \text{ with } |F_s^{(1)}| \le \mu_s F_N^{(1)}, \\ &m_2\ddot{x}_2 + k_2(x_2 - x_1) + r_2(\dot{x}_2 - \dot{x}_1) \\ &\quad = B_2\sin(\Omega t + \varphi_2) + A_2 - \mu_k m_2 g\mathrm{sgn}(\dot{x}_2 - V). \end{aligned} \tag{7}$$

Case III single stick motion $(\dot{x}_1 \ne V, \dot{x}_2 = V)$.

The mass m_1 has the non-stick motion and the mass m_2 has the stick motion. The equations for the two masses $m_\alpha(\alpha = 1, 2)$ are

$$\begin{aligned} &m_1\ddot{x}_1 + k_1x_1 + r_1\dot{x}_1 + k_2(x_1 - x_2) + r_2(\dot{x}_1 - \dot{x}_2) \\ &\quad = B_1\sin(\Omega t + \varphi_1) + A_1 - \mu_k m_1 g\mathrm{sgn}(\dot{x}_1 - V), \\ &\ddot{x}_2 = 0 \quad \text{for } \dot{x}_2 = V \text{ with } |F_s^{(2)}| \le \mu_s F_N^{(2)}. \end{aligned} \tag{8}$$

Case IV double stick motion $(\dot{x}_\alpha = V, \alpha = 1, 2)$.

The equations of stick motion for the two masses are

$$\begin{aligned} &\ddot{x}_1 = 0 \quad \text{for } \dot{x}_1 = V \text{ with } |F_s^{(1)}| \le \mu_s F_N^{(1)}, \\ &\ddot{x}_2 = 0 \quad \text{for } \dot{x}_2 = V \text{ with } |F_s^{(2)}| \le \mu_s F_N^{(2)}. \end{aligned} \tag{9}$$

When the mass m_2 contacts with the fixed rigid obstacle, the mass m_1 still has the stick or non-stick motion as the above discussion. For the stick motion of the mass m_1, the corresponding equation is

$$\ddot{x}_1 = 0 \quad \text{for } \dot{x}_1 = V \text{ with } |F_s^{(1)}| \le \mu_s F_N^{(1)}. \tag{10}$$

For the non-stick motion of the mass m_1, the corresponding equation is

$$\begin{aligned} &m_1\ddot{x}_1 + k_1x_1 + r_1\dot{x}_1 + k_2(x_1 - x_2) + r_2(\dot{x}_1 - \dot{x}_2) \\ &\quad = B_1\sin(\Omega t + \varphi_1) + A_1 \\ &\quad -\mu_k m_1 g\mathrm{sgn}(\dot{x}_1 - V). \end{aligned} \tag{11}$$

The motion of the mass m_2 has two cases. The first case is that the mass m_2 contacts with the obstacle with the nonzero velocity and then separates with the obstacle immediately, such case is called impact motion. The second case is that the mass m_2 contacts with the obstacle with zero velocity and continues to contact with the obstacle for a period of time, such case is called stuck motion. For the impact motion, the impact relation between the mass m_2 and the obstacle is

$$x_2^+ = x_2^-, \quad x_2 = d; \quad \dot{x}_2^+ = -R\dot{x}_2^- \ (R \in (0, 1)), \tag{12}$$

where $()^+$ and $()^-$ represent after and before an impact between the mass m_2 and the fixed rigid obstacle. For the stuck motion, the corresponding equation is

$$x_2 = d, \quad \dot{x}_2 = 0; \quad \text{and } F^{(2)} \ge 0 \text{ at } x_2 = d. \tag{13}$$

3 Domains and boundaries

Because the impact between the mass m_2 and the rigid obstacle can make the velocity of the mass m_2 change immediately, and the friction force is dependent on the direction of the relative velocity between the mass m_α

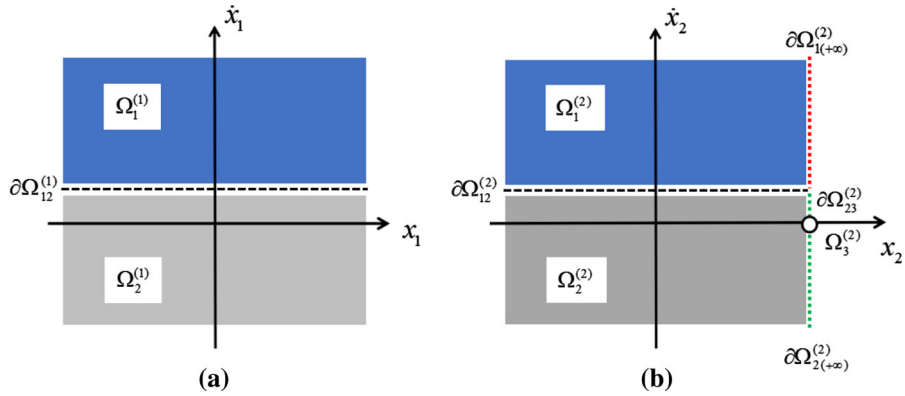

Fig. 3 Domains and boundaries with the mass m_2 touching the obstacle: **a** mass m_1 and **b** mass m_2. (Color figure online)

($\alpha \in \{1, 2\}$) and the traveling belt, the motions of the 2-DOF impact oscillator become discontinuous and more complex. In order to analyze the discontinuous dynamical behaviors of the masses $m_\alpha(\alpha = 1, 2)$, the phase spaces of the two masses can be divided into different domains and different boundaries based on impact and friction.

The corresponding non-stick domains $\Omega_i^{(\alpha)}$ $(i = 1, 2; \alpha = 1, 2)$ for the masses $m_\alpha(\alpha = 1, 2)$ and the stuck domain $\Omega_3^{(2)}$ for the mass m_2 are defined as

$$\begin{aligned}
\Omega_1^{(1)} &= \{(x_1, \dot{x}_1) \mid x_1 \in (-\infty, \infty), \dot{x}_1 - V > 0\},\\
\Omega_2^{(1)} &= \{(x_1, \dot{x}_1) \mid x_1 \in (-\infty, \infty), \dot{x}_1 - V < 0\},\\
\Omega_1^{(2)} &= \{(x_2, \dot{x}_2) \mid x_2 \in (-\infty, d), \dot{x}_2 - V > 0\},\\
\Omega_2^{(2)} &= \{(x_2, \dot{x}_2) \mid x_2 \in (-\infty, d), \dot{x}_2 - V < 0\},\\
\Omega_3^{(2)} &= \{(x_2, \dot{x}_2) \mid x_2 = d, \dot{x}_2 = 0\},
\end{aligned} \tag{14}$$

and the boundaries are defined as

$$\begin{aligned}
\partial\Omega_{12}^{(1)} &\equiv \partial\Omega_{21}^{(1)}\\
&= \{(x_1, \dot{x}_1) \mid \varphi_{12}^{(1)} \equiv \dot{x}_1 - V = 0,\\
&\qquad x_1 \in (-\infty, \infty)\},\\
\partial\Omega_{12}^{(2)} &\equiv \partial\Omega_{21}^{(2)}\\
&= \{(x_2, \dot{x}_2) \mid \varphi_{12}^{(2)} \equiv \dot{x}_2 - V = 0,\\
&\qquad x_2 \in (-\infty, d)\},\\
\partial\Omega_{1(+\infty)}^{(2)} &= \{(x_2, \dot{x}_2) \mid \varphi_{1(+\infty)}^{(2)} \equiv x_2 - d = 0,\\
&\qquad \dot{x}_2 - V > 0\},\\
\partial\Omega_{2(+\infty)}^{(2)} &= \{(x_2, \dot{x}_2) \mid \varphi_{2(+\infty)}^{(2)} \equiv x_2 - d = 0,\\
&\qquad \dot{x}_2 - V < 0 \text{ and } \dot{x}_2 \neq 0\},\\
\partial\Omega_{23}^{(2)} &\equiv \partial\Omega_{32}^{(2)}\\
&= \{(x_2, \dot{x}_2) \mid \varphi_{23}^{(2)} \equiv \dot{x}_2 = 0,\\
&\qquad x_2 - d = 0\},
\end{aligned} \tag{15}$$

where the velocity boundaries $\partial\Omega_{12}^{(\alpha)}(\alpha = 1, 2)$ are the passable or stick boundaries, i.e., the flow in system can pass through or slide on them. The impact boundaries $\partial\Omega_{i(+\infty)}^{(2)}(i = 1, 2)$ are the permanent boundaries, which means that the flow in system cannot pass through them. The boundary $\partial\Omega_{23}^{(2)}$ denotes the stuck boundary formed by the domain $\Omega_2^{(2)}$ and the stuck domain $\Omega_3^{(2)}$.

The partitions of the domains and boundaries for the masses m_1 and m_2 are shown in Fig. 3a and b, respectively. The domains $\Omega_1^{(\alpha)}$ and $\Omega_2^{(\alpha)}(\alpha = 1, 2)$ are covered by blue areas and gray areas. The velocity boundaries $\partial\Omega_{12}^{(\alpha)}(\alpha = 1, 2)$ are represented by the black dashed curves. The impact boundaries $\partial\Omega_{1(+\infty)}^{(2)}$ and $\partial\Omega_{2(+\infty)}^{(2)}$ are depicted by red dotted line and green dotted line, respectively. The hollow circle in Fig. 3b denotes the stuck domain Ω_3 and the stuck boundary $\partial\Omega_{23}^{(2)}$.

Based on the above discussion, the state vectors and the vectors of field vector for the motions of the masses m_1 and m_2 are introduced as

$$\begin{aligned}
&\mathbf{x}_1^{(\lambda_1)} = (x_1^{(\lambda_1)}, \dot{x}_1^{(\lambda_1)})^{\mathrm{T}},\\
&\mathbf{x}_2^{(\lambda_2)} = (x_2^{(\lambda_2)}, \dot{x}_2^{(\lambda_2)})^{\mathrm{T}},
\end{aligned} \tag{16}$$

$$\begin{aligned}
&\mathbf{F}_1^{(\lambda_1)}(\mathbf{x}_1^{(\lambda_1)}, \mathbf{x}_2^{(\lambda_2)}, t)\\
&\quad = (\dot{x}_1^{(\lambda_1)}, F_1^{(\lambda_1)}(\mathbf{x}_1^{(\lambda_1)}, \mathbf{x}_2^{(\lambda_2)}, t))^{\mathrm{T}},\\
&\mathbf{F}_2^{(\lambda_2)}(\mathbf{x}_2^{(\lambda_2)}, \mathbf{x}_1^{(\lambda_1)}, t)\\
&\quad = (\dot{x}_2^{(\lambda_2)}, F_2^{(\lambda_2)}(\mathbf{x}_2^{(\lambda_2)}, \mathbf{x}_1^{(\lambda_1)}, t))^{\mathrm{T}},
\end{aligned} \tag{17}$$

where $\lambda_1 = 0, 1, 2$, $\lambda_2 = 0, 1, 2, 3$; $\lambda_\alpha = 0$ ($\alpha \in \{1, 2\}$) represents the stick motion of the mass m_α ($\alpha \in \{1, 2\}$) on the boundary $\partial\Omega_{12}^{(\alpha)}$; $\lambda_\alpha = 1, 2$ ($\alpha = 1, 2$) stand for the free-flight motion for the masses m_α ($\alpha = 1, 2$) in domains $\Omega_1^{(\alpha)}$ and $\Omega_2^{(\alpha)}$, respectively; $\lambda_2 = 3$

denotes that the mass m_2 has a stuck motion, i.e., the mass m_2 contacts the obstacle on the right with zero velocity and stays in touch for a while.

The equations of motion for the two masses $m_\alpha(\alpha = 1, 2)$ can be rewritten in the vector form of

$$\dot{\mathbf{x}}_1^{(\lambda_1)} = \mathbf{F}_1^{(\lambda_1)}(\mathbf{x}_1^{(\lambda_1)}, \mathbf{x}_2^{(\lambda_2)}, t), \tag{18}$$

$$\dot{\mathbf{x}}_2^{(\lambda_2)} = \mathbf{F}_2^{(\lambda_2)}(\mathbf{x}_2^{(\lambda_2)}, \mathbf{x}_1^{(\lambda_1)}, t), \tag{19}$$

where $\lambda_1 = 0, 1, 2$ and $\lambda_2 = 0, 1, 2, 3$.

For convenience, the following notations will be used below:

$$\begin{aligned}
&a_\alpha = \frac{A_\alpha}{m_\alpha}, \quad b_\alpha = \frac{B_\alpha}{m_\alpha}, \quad c_\alpha = \frac{r_\alpha}{m_\alpha},\\
&d_\alpha = \frac{k_\alpha}{m_\alpha} \quad (\alpha = 1, 2), \quad p = \frac{k_2}{m_1},\\
&q = \frac{r_2}{m_1}, \quad F_{\mathrm{f_k}}^{(1)} = \mu_\mathrm{k} g, \quad F_{\mathrm{f_k}}^{(2)} = -\mu_\mathrm{k} g,\\
&\mathbf{F}_1^{(\lambda_1)} \equiv \mathbf{F}_1^{(\lambda_1)}(\mathbf{x}_1^{(\lambda_1)}, t) \equiv \mathbf{F}_1^{(\lambda_1)}(\mathbf{x}_1^{(\lambda_1)}, \mathbf{x}_2^{(\lambda_2)}, t),\\
&\mathbf{F}_2^{(\lambda_2)} \equiv \mathbf{F}_2^{(\lambda_2)}(\mathbf{x}_2^{(\lambda_2)}, t) \equiv \mathbf{F}_2^{(\lambda_2)}(\mathbf{x}_2^{(\lambda_2)}, \mathbf{x}_1^{(\lambda_1)}, t),\\
&F_1^{(\lambda_1)} \equiv F_1^{(\lambda_1)}(\mathbf{x}_1^{(\lambda_1)}, t) \equiv F_1^{(\lambda_1)}(\mathbf{x}_1^{(\lambda_1)}, \mathbf{x}_2^{(\lambda_2)}, t),\\
&F_2^{(\lambda_2)} \equiv F_2^{(\lambda_2)}(\mathbf{x}_2^{(\lambda_2)}, t) \equiv F_2^{(\lambda_2)}(\mathbf{x}_2^{(\lambda_2)}, \mathbf{x}_1^{(\lambda_1)}, t),
\end{aligned} \tag{20}$$

where $\lambda_1 = 0, 1, 2$ and $\lambda_2 = 0, 1, 2, 3$.

For the non-stick motions ($\lambda_1 = 1, 2$, $\lambda_2 = 1, 2$) of the two masses m_1 and m_2 in the domains $\Omega_1^{(\alpha)}$ and $\Omega_2^{(\alpha)}$ ($\alpha = 1, 2$), the forces of per unit mass acting on the masses m_1 and m_2 are

$$\begin{aligned}
F_1^{(\lambda_1)} = {} & b_1\sin(\Omega t + \varphi_1) + a_1 - d_1 x_1^{(\lambda_1)} - c_1\dot{x}_1^{(\lambda_1)}\\
& - p(x_1^{(\lambda_1)} - x_2^{(\lambda_2)}) - q(\dot{x}_1^{(\lambda_1)} - \dot{x}_2^{(\lambda_2)})\\
& - \mu_\mathrm{k} g\,\mathrm{sgn}(\dot{x}_1^{(\lambda_1)} - V),\\
F_2^{(\lambda_2)} = {} & b_2\sin(\Omega t + \varphi_2) + a_2 - d_2(x_2^{(\lambda_2)} - x_1^{(\lambda_1)})\\
& c_2(\dot{x}_2^{(\lambda_2)} - \dot{x}_1^{(\lambda_1)}) - \mu_\mathrm{k} g\,\mathrm{sgn}(\dot{x}_2^{(\lambda_2)} - V).
\end{aligned} \tag{21}$$

For the single stick motion ($\lambda_1 = 0$, $\lambda_2 = 1, 2$) of the masses m_1 and m_2, the forces of per unit mass acting on the masses m_1 and m_2 are

$$\begin{aligned}
F_1^{(0)} = {} & \ddot{x}_1^{(0)} = \dot{V} = 0,\\
F_2^{(\lambda_2)} = {} & b_2\sin(\Omega t + \varphi_2) + a_2 - d_2(x_2^{(\lambda_2)} - x_1^{(\lambda_1)})\\
& - c_2(\dot{x}_2^{(\lambda_2)} - \dot{x}_1^{(\lambda_1)}) - \mu_\mathrm{k} g\,\mathrm{sgn}(\dot{x}_2^{(\lambda_2)} - V).
\end{aligned} \tag{22}$$

For the single stick motion ($\lambda_1 = 1, 2$, $\lambda_2 = 0$) of the masses m_1 and m_2, the forces of per unit mass acting on the masses m_1 and m_2 are

$$\begin{aligned}
F_1^{(\lambda_1)} = {} & b_1\sin(\Omega t + \varphi_1) + a_1 - d_1 x_1^{(\lambda_1)} - c_1\dot{x}_1^{(\lambda_1)}\\
& - p(x_1^{(\lambda_1)} - x_2^{(\lambda_2)}) - q(\dot{x}_1^{(\lambda_1)} - \dot{x}_2^{(\lambda_2)})\\
& - \mu_\mathrm{k} g\,\mathrm{sgn}(\dot{x}_1^{(\lambda_1)} - V),\\
F_2^{(0)} = {} & \ddot{x}_2^{(0)} = \dot{V} = 0.
\end{aligned} \tag{23}$$

For the double stick motion ($\lambda_\alpha = 0, \alpha = 1, 2$) of the two masses m_α ($\alpha = 1, 2$) on the corresponding boundaries $\partial\Omega_{12}^{(\alpha)}$ ($\alpha = 1, 2$), the forces of per unit mass acting on the masses m_1 and m_2 are

$$\begin{aligned}
&F_1^{(0)} = \ddot{x}_1^{(0)} = \dot{V} = 0,\\
&F_2^{(0)} = \ddot{x}_2^{(0)} = \dot{V} = 0.
\end{aligned} \tag{24}$$

For the non-stick motion ($\lambda_1 = 1, 2$) for the mass m_1 and the stuck motion ($\lambda_2 = 3$) for the mass m_2 on the stuck domain $\Omega_3^{(2)}$ or the stuck boundary $\partial\Omega_{23}^{(2)}$ of the mass m_2, the forces of per unit mass acting on the masses m_1 and m_2 are

$$\begin{aligned}
F_1^{(\lambda_1)} = {} & b_1\sin(\Omega t + \varphi_1) + a_1 - d_1 x_1^{(\lambda_1)}\\
& - c_1\dot{x}_1^{(\lambda_1)} - p(x_1^{(\lambda_1)} - d) - q\dot{x}_1^{(\lambda_1)}\\
& - \mu_\mathrm{k} g\,\mathrm{sgn}(\dot{x}_1^{(\lambda_1)} - V),\\
F_2^{(3)} = {} & b_2\sin(\Omega t + \varphi_2) + a_2 - d_2(d - x_1^{(\lambda_1)})\\
& + c_2\dot{x}_1^{(\lambda_1)} + \mu_\mathrm{k} g.
\end{aligned} \tag{25}$$

For the stick motion ($\lambda_1 = 0$) of the mass m_1 and the stuck motion ($\lambda_2 = 3$) of the mass m_2 on the stuck domain $\Omega_3^{(2)}$ or stuck boundary $\partial\Omega_{23}^{(2)}$, the forces of per unit mass acting on the masses m_1 and m_2 are

$$\begin{aligned}
F_1^{(0)} = {} & \ddot{x}_1^{(0)} = \dot{V} = 0,\\
F_2^{(3)} = {} & b_2\sin(\Omega t + \varphi_2) + a_2 - d_2(d - x_1^{(0)})\\
& + c_2 V + \mu_\mathrm{k} g.
\end{aligned} \tag{26}$$

Since the kinetic and static friction coefficients on the contact surface between the mass $m_\alpha(\alpha \in 1, 2)$ and the belt is unequal, i.e., the maximum static friction force is not equal to the dynamic friction force for the mass m_α, the flow barrier exists on the velocity boundary $\partial\Omega_{12}^{(\alpha)}(\alpha \in \{1, 2\})$ and the flow barrier vector fields for $\mathbf{x}_m^{(\alpha)} = (x_{\alpha m}, \dot{x}_{\alpha m}) \in \partial\Omega_{12}^{(\alpha)}(\alpha \in \{1, 2\})$ at time t_m are

$$\begin{aligned}
&\mathbf{F}_1^{(0\succ 0_\lambda)}(\mathbf{x}_m^{(1)}, t_m, \tau^{(\lambda)})\\
&\quad \equiv \mathbf{F}_1^{(0\succ 0_\lambda)}(\mathbf{x}_m^{(1)}, \mathbf{x}_2^{(\lambda_2)}, t_m, \tau^{(\lambda)})\\
&\quad = (\dot{x}_{1m}, F_1^{(0\succ 0_\lambda)}(\mathbf{x}_m^{(1)}, \mathbf{x}_2^{(\lambda_2)}, t_m, \tau^{(\lambda)}))^\mathrm{T},\\
&\mathbf{F}_2^{(0\succ 0_\lambda)}(\mathbf{x}_m^{(2)}, t_m, \tau^{(\lambda)})\\
&\quad \equiv \mathbf{F}_2^{(0\succ 0_\lambda)}(\mathbf{x}_m^{(2)}, \mathbf{x}_1^{(\lambda_1)}, t_m, \tau^{(\lambda)})
\end{aligned}$$

$$= (\dot{x}_{2m}, F_2^{(0\succ 0_\lambda)}(\mathbf{x}_m^{(2)}, \mathbf{x}_1^{(\lambda_1)}, t_m, \tau^{(\lambda)}))^{\mathrm{T}}, \quad (27)$$

where

$$\begin{aligned} &F_1^{(0\succ 0_\lambda)}(\mathbf{x}_m^{(1)}, t_m, \tau^{(\lambda)}) \\ &\equiv F_1^{(0\succ 0_\lambda)}(\mathbf{x}_m^{(1)}, \mathbf{x}_2^{(\lambda_2)}, t_m, \tau^{(\lambda)}) \\ &= b_1 \sin(\Omega t_m + \varphi_1) + a_1 - d_1 x_{1m} \\ &\quad -c_1 \dot{x}_{1m} - p(x_{1m} - x_2^{(\lambda_2)}) \\ &\quad -q(\dot{x}_{1m} - \dot{x}_2^{(\lambda_2)}) - F_{\mathrm{f_s}}^{(\lambda)}(\tau^{(\lambda)}), \\ &F_2^{(0\succ 0_\lambda)}(\mathbf{x}_m^{(2)}, t_m, \tau^{(\lambda)}) \\ &\equiv F_2^{(0\succ 0_\lambda)}(\mathbf{x}_m^{(2)}, \mathbf{x}_1^{(\lambda_1)}, t_m, \tau^{(\lambda)}) \\ &= b_2 \sin(\Omega t_m + \varphi_2) + a_2 \\ &\quad -d_2(x_{2m} - x_1^{(\lambda_1)}) \\ &\quad -c_2(\dot{x}_{2m} - \dot{x}_1^{(\lambda_1)}) - F_{\mathrm{f_s}}^{(\lambda)}(\tau^{(\lambda)}), \end{aligned} \quad (28)$$

and $\lambda = 1, 2,\ \tau^{(\lambda)} \in [\tau_1^{(\lambda)}, \tau_2^{(\lambda)}],\ \lambda_1 \in \{0, 1, 2\},\ \lambda_2 \in \{0, 1, 2, 3\}$.

From Eq. (3), the static friction forces $F_{\mathrm{f_s}}^{(\lambda)}(\tau^{(\lambda)})$ $(\lambda = 1, 2)$ of per unit mass exerting on the masses m_α $(\alpha = 1, 2)$ on the boundaries $\partial\Omega_{12}^{(\alpha)}$ $(\alpha = 1, 2)$ are

$$\begin{aligned} &F_{\mathrm{f_s}}^{(1)}(\tau^{(1)}) \in (-\infty, \mu_{\mathrm{s}} g] \quad \text{and} \\ &F_{\mathrm{f_s}}^{(2)}(\tau^{(2)}) \in [-\mu_{\mathrm{s}} g, +\infty). \end{aligned} \quad (29)$$

The boundary flow barrier on the λ-side ($\lambda \in \{1, 2\}$) of the boundary $\partial\Omega_{12}^{(\alpha)}$ for $\mathbf{x}_m^{(\alpha)} = (x_{\alpha m}, \dot{x}_{\alpha m}) \in \partial\Omega_{12}^{(\alpha)}$ $(\alpha \in \{1, 2\})$ at time t_m is

$$\begin{aligned} &\mathbf{F}_\alpha^{(0\succ 0_\lambda)}(\mathbf{x}_m^{(\alpha)}, t_m, \tau_1^{(\lambda)}) \\ &= (\dot{x}_{\alpha m}, F_\alpha^{(0\succ 0_\lambda)}(\mathbf{x}_m^{(\alpha)}, t_m, \tau_1^{(\lambda)}))^{\mathrm{T}}, \end{aligned} \quad (30)$$

where

$$\begin{aligned} &F_1^{(0\succ 0_\lambda)}(\mathbf{x}_m^{(1)}, t_m, \tau_1^{(\lambda)}) \\ &\equiv b_1 \sin(\Omega t_m + \varphi_1) + a_1 \\ &\quad -d_1 x_{1m} - c_1 \dot{x}_{1m} \\ &\quad -p(x_{1m} - x_2^{(\lambda_2)}) \\ &\quad -q(\dot{x}_{1m} - \dot{x}_2^{(\lambda_2)}) - F_{\mathrm{f_s}}^{(\lambda)}(\tau_1^{(\lambda)}), \\ &F_2^{(0\succ 0_\lambda)}(\mathbf{x}_m^{(2)}, t_m, \tau_1^{(\lambda)}) \\ &\equiv b_2 \sin(\Omega t_m + \varphi_2) + a_2 \\ &\quad -d_2(x_{2m} - x_1^{(\lambda_1)}) \\ &\quad -c_2(\dot{x}_{2m} - \dot{x}_1^{(\lambda_1)}) - F_{\mathrm{f_s}}^{(\lambda)}(\tau_1^{(\lambda)}); \end{aligned} \quad (31)$$

$$\begin{aligned} &\mathbf{F}_\alpha^{(0\succ 0_1)}(\mathbf{x}_m^{(\alpha)}, t_m, \tau_2^{(1)}) = (\dot{x}_{\alpha m}, +\infty)^{\mathrm{T}}, \\ &\mathbf{F}_\alpha^{(0\succ 0_2)}(\mathbf{x}_m^{(\alpha)}, t_m, \tau_2^{(2)}) = (\dot{x}_{\alpha m}, -\infty)^{\mathrm{T}}, \end{aligned} \quad (32)$$

and $\lambda_1 \in \{0, 1, 2\},\ \lambda_2 \in \{0, 1, 2, 3\}$.

4 Switching conditions

For the 2-DOF friction-induced oscillator with one-sided impact on a conveyor belt described in Sect. 2, the analytical conditions of flow switchability will be discussed in this section. The definition of G-functions and the conditions of several kinds of flow switchability on separate boundaries were given in Luo [48,49], and the theory of flow switching in discontinuous dynamical systems were presented in a detailed manner in Luo [54,55]. Based on the fundamental theory of discontinuous dynamical systems, the corresponding definitions and theorems will be given in the following.

From Eq. (15), the velocity boundaries $\partial\Omega_{12}^{(\alpha)}$ $(\alpha = 1, 2)$, the impact boundaries $\partial\Omega_{i(+\infty)}^{(2)}$ $(i = 1, 2)$ and the stuck boundary $\partial\Omega_{23}^{(2)}$ are independent of time and the normal vectors of the velocity boundaries, the impact boundaries and the stuck boundary are obtained by

$$\begin{aligned} \mathbf{n}_{\partial\Omega_{12}^{(\alpha)}} &\equiv {}^t\mathbf{n}_{\partial\Omega_{12}^{(\alpha)}} \\ &= \nabla\varphi_{12}^{(\alpha)} = \left(\frac{\partial\varphi_{12}^{(\alpha)}}{\partial x_\alpha}, \frac{\partial\varphi_{12}^{(\alpha)}}{\partial\dot{x}_\alpha}\right)^{\mathrm{T}} = (0, 1)^{\mathrm{T}}, \end{aligned} \quad (33)$$

$$\begin{aligned} \mathbf{n}_{\partial\Omega_{i(+\infty)}^{(2)}} &\equiv {}^t\mathbf{n}_{\partial\Omega_{i(+\infty)}^{(2)}} \\ &= \nabla\varphi_{i(+\infty)}^{(2)} = \left(\frac{\partial\varphi_{i(+\infty)}^{(2)}}{\partial x_2}, \frac{\partial\varphi_{i(+\infty)}^{(2)}}{\partial\dot{x}_2}\right)^{\mathrm{T}} \\ &= (1, 0)^{\mathrm{T}}, \end{aligned} \quad (34)$$

$$\begin{aligned} \mathbf{n}_{\partial\Omega_{23}^{(2)}} &\equiv {}^t\mathbf{n}_{\partial\Omega_{23}^{(2)}} \\ &= \nabla\varphi_{23}^{(2)} = \left(\frac{\partial\varphi_{23}^{(2)}}{\partial x_2}, \frac{\partial\varphi_{23}^{(2)}}{\partial\dot{x}_2}\right)^{\mathrm{T}} \\ &= (0, 1)^{\mathrm{T}}, \end{aligned} \quad (35)$$

where $\nabla = (\partial/\partial x, \partial/\partial\dot{x})^{\mathrm{T}}$.

For the 2-DOF oscillator described in Sect. 2, the corresponding zeroth-order G–functions and first-order G-functions are defined as follows.

Definition 1 (i) For the 2-DOF one-sided impact model described in Sect. 2, the zeroth-order G-function $G_{\partial\Omega_{12}^{(\alpha)}}^{(0,\lambda)}$ of the flow $\mathbf{x}_\alpha^{(\lambda)}(t)$ in domain $\Omega_\lambda^{(\alpha)}$ $(\alpha, \lambda \in \{1, 2\})$ to the flow $\mathbf{x}_\alpha^{(0)}(t)$ on the velocity boundary $\partial\Omega_{12}^{(\alpha)}$ $(\alpha \in \{1, 2\})$ is defined as

$$G_{\partial\Omega_{12}^{(\alpha)}}^{(0,\lambda)}(\mathbf{x}_m^{(\alpha)}, t_{m\pm}) = \mathbf{n}_{\partial\Omega_{12}^{(\alpha)}}^{\mathrm{T}} \cdot \mathbf{F}_\alpha^{(\lambda)}(\mathbf{x}_m^{(\alpha)}, t_{m\pm}), \quad (36)$$

where $\mathbf{x}_{\alpha}^{(\lambda)}(t_{m\pm}) = \mathbf{x}_{\alpha}^{(0)}(t_m) = \mathbf{x}_m^{(\alpha)} \in \partial\Omega_{12}^{(\alpha)}$, the time $t_{m\pm} = t_m \pm 0$ reflects the flow in the domain instead of the separation boundary.

(ii) For the 2-DOF one-sided impact model described in Sect. 2, the zeroth-order G-function $G^{(0,\lambda)}_{\partial\Omega^{(2)}_{i(+\infty)}}$ $(\lambda, i \in \{1,2\})$ of the flow $\mathbf{x}_2^{(\lambda)}(t)$ in domain $\Omega_{\lambda}^{(2)}(\lambda \in \{1,2\})$ to the flow $\mathbf{x}_2^{(4)}(t)$ on the impact boundary $\partial\Omega^{(2)}_{i(+\infty)}$ $(i \in \{1,2\})$ is defined as

$$G^{(0,\lambda)}_{\partial\Omega^{(2)}_{i(+\infty)}}(\mathbf{x}_m^{(2)}, t_{m\pm}) = \mathbf{n}^{\mathrm{T}}_{\partial\Omega^{(2)}_{i(+\infty)}} \cdot \mathbf{F}_2^{(\lambda)}(\mathbf{x}_m^{(2)}, t_{m\pm}), \tag{37}$$

where $\mathbf{x}_2^{(\lambda)}(t_{m\pm}) = \mathbf{x}_2^{(4)}(t_m) = \mathbf{x}_m^{(2)} \equiv (x_{2m}, \dot{x}_{2m}) \in \partial\Omega^{(2)}_{i(+\infty)}$.

(iii) For the 2-DOF one-sided impact model described in Sect. 2, the zeroth-order G-function $G^{(0,\lambda)}_{\partial\Omega^{(2)}_{23}}$ of the flow $\mathbf{x}_2^{(\lambda)}(t)$ in domain $\Omega_{\lambda}^{(2)}$ $(\lambda \in \{2,3\})$ to the flow $\mathbf{x}_2^{(3)}(t)$ on the stuck boundary $\partial\Omega_{23}^{(2)}$ is defined as

$$G^{(0,\lambda)}_{\partial\Omega^{(2)}_{23}}(\mathbf{x}_m^{(2)}, t_{m\pm}) = \mathbf{n}^{\mathrm{T}}_{\partial\Omega^{(2)}_{23}} \cdot \mathbf{F}_2^{(\lambda)}(\mathbf{x}_m^{(2)}, t_{m\pm}), \tag{38}$$

where $\mathbf{x}_2^{(\lambda)}(t_{m\pm}) = \mathbf{x}_2^{(3)}(t_m) = \mathbf{x}_m^{(2)} \in \partial\Omega_{23}^{(2)}$.

Definition 2 (i) For the 2-DOF one-sided impact model described in Sect. 2, the first-order G-function $G^{(1,\lambda)}_{\partial\Omega^{(\alpha)}_{12}}$ of the flow $\mathbf{x}_{\alpha}^{(\lambda)}(t)$ in domain $\Omega_{\lambda}^{(\alpha)}$ $(\alpha, \lambda \in \{1,2\})$ to the flow $\mathbf{x}_{\alpha}^{(0)}(t)$ on the velocity boundary $\partial\Omega_{12}^{(\alpha)}$ $(\alpha \in \{1,2\})$ is defined as

$$G^{(1,\lambda)}_{\partial\Omega^{(\alpha)}_{12}}(\mathbf{x}_m^{(\alpha)}, t_{m\pm}) = \mathbf{n}^{\mathrm{T}}_{\partial\Omega^{(\alpha)}_{12}} \cdot D\mathbf{F}_{\alpha}^{(\lambda)}(\mathbf{x}_m^{(\alpha)}, t_{m\pm}), \tag{39}$$

where $\mathbf{x}_{\alpha}^{(\lambda)}(t_{m\pm}) = \mathbf{x}_{\alpha}^{(0)}(t_m) = \mathbf{x}_m^{(\alpha)} \in \partial\Omega_{12}^{(\alpha)}$.

(ii) For the 2-DOF one-sided impact model described in Sect. 2, the first-order G-function $G^{(1,\lambda)}_{\partial\Omega^{(2)}_{i(+\infty)}}$ $(\lambda, i \in \{1,2\})$ of the flow $\mathbf{x}_2^{(\lambda)}(t)$ in domain $\Omega_{\lambda}^{(2)}$ $(\lambda \in \{1,2\})$ to the flow $\mathbf{x}_2^{(4)}(t)$ on the impact boundary $\partial\Omega^{(2)}_{i(+\infty)}$ $(i \in \{1,2\})$ is defined as

$$G^{(1,\lambda)}_{\partial\Omega^{(2)}_{i(+\infty)}}(\mathbf{x}_m^{(2)}, t_{m\pm}) = \mathbf{n}^{\mathrm{T}}_{\partial\Omega^{(2)}_{i(+\infty)}} \cdot D\mathbf{F}_2^{(\lambda)}(\mathbf{x}_m^{(2)}, t_{m\pm}), \tag{40}$$

where $\mathbf{x}_2^{(\lambda)}(t_{m\pm}) = \mathbf{x}_2^{(4)}(t_m) = \mathbf{x}_m^{(2)} \equiv (x_{2m}, \dot{x}_{2m}) \in \partial\Omega^{(2)}_{i(+\infty)}$.

(iii) For the 2-DOF one-sided impact model described in Sect. 2, the first-order G-function $G^{(1,\lambda)}_{\partial\Omega^{(2)}_{23}}$ of the flow $\mathbf{x}_2^{(\lambda)}(t)$ in domain $\Omega_{\lambda}^{(2)}$ $(\lambda \in \{2,3\})$ to the flow $\mathbf{x}_2^{(3)}(t)$ on the stuck boundary $\partial\Omega_{23}^{(2)}$ is defined as

$$G^{(1,\lambda)}_{\partial\Omega^{(2)}_{23}}(\mathbf{x}_m^{(2)}, t_{m\pm}) = \mathbf{n}^{\mathrm{T}}_{\partial\Omega^{(2)}_{23}} \cdot D\mathbf{F}_2^{(\lambda)}(\mathbf{x}_m^{(2)}, t_{m\pm}), \tag{41}$$

where $\mathbf{x}_2^{(\lambda)}(t_{m\pm}) = \mathbf{x}_2^{(3)}(t_m) = \mathbf{x}_m^{(2)} \in \partial\Omega_{23}^{(2)}$.

The G-functions can be used to judge the situation of the flow switchability when the flow of motion reaches to the separate boundary. If the flow barrier exists on the separate boundary, the flow property on the boundary with flow barrier should be investigated. For the 2-DOF one-sided impact model considered in this paper, the dynamic friction force is not equal to the maximum static friction force, so there exist the flow barriers on the velocity boundaries. The G-functions for the flow barrier should be introduced. The corresponding definition is given as follows.

Definition 3 For the 2-DOF one-sided impact model described in Sect. 2, there is a point $\mathbf{x}_{\alpha}^{(0)}(t_m) \equiv \mathbf{x}_m^{(0)} = \mathbf{x}_m \in \partial\Omega_{12}^{(\alpha)}$ $(\alpha \in \{1,2\})$ at time t_m between two adjacent domains $\Omega_1^{(\alpha)}$ and $\Omega_2^{(\alpha)}$. There are two vector fields of $\mathbf{F}_{\alpha}^{(\rho\succ\gamma)}(\mathbf{x}_{\alpha}^{(\lambda)}, t, \tau^{(\lambda)})$ for $\tau^{(\lambda)} \in [\tau_1^{(\lambda)}, \tau_2^{(\lambda)}]$ $(\rho, \gamma \in \{0,1,2\}, \lambda \in \{1,2\}$ and $\rho \neq \gamma$ if $\rho \neq 0)$ and $\mathbf{F}_{\alpha}^{(0)}(\mathbf{x}_{\alpha}^{(0)}, t)$ on the boundary $\partial\Omega_{12}^{(\alpha)}$. For the point $\mathbf{x}_{\alpha}^{(\lambda)}(t_m) \equiv \mathbf{x}_m^{(\alpha)} = \mathbf{x}_m$, the G-function of the vector field $\mathbf{F}_{\alpha}^{(\rho\succ\gamma)}(\mathbf{x}_{\alpha}^{(\lambda)}, t, \tau^{(\lambda)})$ is defined as

$$G^{(0,\rho\succ\gamma)}_{\partial\Omega^{(\alpha)}_{12}}(\mathbf{x}_m^{(\alpha)}, t_{m\pm}, \tau^{(\lambda)}) = \mathbf{n}^{\mathrm{T}}_{\partial\Omega^{(\alpha)}_{12}} \cdot [\mathbf{F}_{\alpha}^{(\rho\succ\gamma)}(\mathbf{x}_{\alpha}^{(\lambda)}, t, \tau^{(\lambda)}) - \mathbf{F}_{\alpha}^{(0)}(\mathbf{x}_{\alpha}^{(0)}, t)]\Big|_{(\mathbf{x}_m^{(\alpha)}, \mathbf{x}_m^{(0)}, t_{m\pm})}; \tag{42}$$

and the higher-order G-function of the vector field $\mathbf{F}_{\alpha}^{(\rho\succ\gamma)}(\mathbf{x}_{\alpha}^{(\lambda)}, t, \tau^{(\lambda)})$ is defined for $k_\lambda = 0, 1, 2, \ldots$ as

$$
\begin{aligned}
&G^{(k_\lambda,\rho\succ\gamma)}_{\partial\Omega^{(\alpha)}_{12}}(\mathbf{x}^{(\alpha)}_m, t_{m\pm}, \tau^{(\lambda)})\\
&\quad = \Sigma^{k_\lambda+1}_{r=1} C^r_{k_\lambda+1} D^{k_\lambda+1-r}_0 \mathbf{n}^{\mathrm{T}}_{\partial\Omega^{(\alpha)}_{12}}\\
&\quad\quad \cdot [D^{r-1}_\lambda \mathbf{F}^{(\rho\succ\gamma)}_\alpha(\mathbf{x}^{(\lambda)}_\alpha, t, \tau^{(\lambda)})\\
&\quad\quad - D^{r-1}_0 \mathbf{F}^{(0)}_\alpha(\mathbf{x}^{(0)}_\alpha, t)]\Big|_{(\mathbf{x}^{(\alpha)}_m, \mathbf{x}^{(0)}_m, t_{m\pm})},
\end{aligned}
\tag{43}
$$

where $D_0(\cdot) \equiv \dfrac{\partial(\cdot)}{\partial \mathbf{x}^{(0)}_\alpha}\dot{\mathbf{x}}^{(0)}_\alpha + \dfrac{\partial(\cdot)}{\partial t}$, $D_\lambda(\cdot) \equiv \dfrac{\partial(\cdot)}{\partial \mathbf{x}^{(\lambda)}_\alpha}\dot{\mathbf{x}}^{(\lambda)}_\alpha + \dfrac{\partial(\cdot)}{\partial t}$.

Since the velocity boundaries $\partial\Omega^{(\alpha)}_{12}(\alpha = 1, 2)$ are straight lines in phase space, the normal vectors are constant vectors. So $D\mathbf{n}_{\partial\Omega^{(\alpha)}_{12}} = 0\,(\alpha = 1, 2)$ can be obtained. Note that $\mathbf{n}^{\mathrm{T}}_{\partial\Omega^{(\alpha)}_{12}} \cdot \mathbf{F}^{(0)}_\alpha(\mathbf{x}^{(0)}_\alpha(t_{m\pm}), t_{m\pm}, \lambda) = 0$, thus the zeroth-order and first-order G-functions of the flow barrier on $\mathbf{x}^{(\alpha)}_m \in \partial\Omega^{(\alpha)}_{12}(\alpha = 1, 2)$ at time t_m can be expressed by

$$
\begin{aligned}
&G^{(0,0\succ 0_\lambda)}_{\partial\Omega^{(\alpha)}_{12}}(\mathbf{x}^{(\alpha)}_m, t_{m\pm}, \tau^{(\lambda)})\\
&\quad = \mathbf{n}^{\mathrm{T}}_{\partial\Omega^{(\alpha)}_{12}} \cdot \mathbf{F}^{(0\succ 0_\lambda)}_\alpha(\mathbf{x}^{(\alpha)}_m, t_{m\pm}, \tau^{(\lambda)}),\\
&G^{(1,0\succ 0_\lambda)}_{\partial\Omega^{(\alpha)}_{12}}(\mathbf{x}^{(\alpha)}_m, t_{m\pm}, \tau^{(\lambda)})\\
&\quad = \mathbf{n}^{\mathrm{T}}_{\partial\Omega^{(\alpha)}_{12}} \cdot D\mathbf{F}^{(0\succ 0_\lambda)}_\alpha(\mathbf{x}^{(\alpha)}_m, t_{m\pm}, \tau^{(\lambda)}).
\end{aligned}
\tag{44}
$$

For simplicity, the following notations are adopted:

$$
\begin{aligned}
&F^{(j)}_\alpha(t_{m\pm}) \equiv F^{(j)}_\alpha(\mathbf{x}^{(\alpha)}_m, t_{m\pm}),\\
&DF^{(j)}_\alpha(t_{m\pm}) \equiv DF^{(j)}_\alpha(\mathbf{x}^{(\alpha)}_m, t_{m\pm}),\\
&G^{(0,\lambda)}_{\partial\Omega^{(\alpha)}_{12}}(t_{m\pm}) \equiv G^{(0,\lambda)}_{\partial\Omega^{(\alpha)}_{12}}(\mathbf{x}^{(\alpha)}_m, t_{m\pm}),\\
&G^{(1,\lambda)}_{\partial\Omega^{(\alpha)}_{12}}(t_{m\pm}) \equiv G^{(1,\lambda)}_{\partial\Omega^{(\alpha)}_{12}}(\mathbf{x}^{(\alpha)}_m, t_{m\pm}),\\
&G^{(0,\lambda)}_{\partial\Omega^{(2)}_{i(+\infty)}}(t_{m\pm}) \equiv G^{(0,\lambda)}_{\partial\Omega^{(2)}_{i(+\infty)}}(\mathbf{x}^{(2)}_m, t_{m\pm}),\\
&G^{(0,0\succ 0_\lambda)}_{\partial\Omega^{(\alpha)}_{12}}(t_{m\pm}) \equiv G^{(0,0\succ 0_\lambda)}_{\partial\Omega^{(\alpha)}_{12}}(\mathbf{x}^{(\alpha)}_m, t_{m\pm}, \tau^{(\lambda)}),\\
&G^{(1,0\succ 0_\lambda)}_{\partial\Omega^{(\alpha)}_{12}}(t_{m\pm}) \equiv G^{(1,0\succ 0_\lambda)}_{\partial\Omega^{(\alpha)}_{12}}(\mathbf{x}^{(\alpha)}_m, t_{m\pm}, \tau^{(\lambda)}),
\end{aligned}
\tag{45}
$$

where $\alpha, \lambda, i \in \{1, 2\}$ and $j \in \{1, 2, 3\}$.

According to the different situations when the flows reach to the separate boundaries, the analytical conditions of the passable flows, the appearance and vanishing of the stick motion and the stuck motion will be given in the form of theorems.

Theorem 1 *For the physical model with one-sided impact described in Sect. 2, the following conditions can guarantee that the flow in domain $\Omega^{(\alpha)}_i$ passes through the boundary $\partial\Omega^{(\alpha)}_{ij}$ at $(\mathbf{x}^{(\alpha)}_m, t_m)$ and enters into the domain $\Omega^{(\alpha)}_j(\alpha \in \{1, 2\}; i, j \in \{1, 2\}, i \neq j)$ for the mass $m_\alpha(\alpha \in \{1, 2\})$:*

$$
\left.
\begin{aligned}
&F^{(1)}_\alpha(\mathbf{x}^{(\alpha)}_m, t_{m-}) < 0,\\
&F^{(2)}_\alpha(\mathbf{x}^{(\alpha)}_m, t_{m+}) < 0
\end{aligned}
\right\} \text{ for } \Omega^{(\alpha)}_1 \to \Omega^{(\alpha)}_2, \tag{46}
$$

$$
\left.
\begin{aligned}
&F^{(2)}_\alpha(\mathbf{x}^{(\alpha)}_m, t_{m-}) > 0,\\
&F^{(1)}_\alpha(\mathbf{x}^{(\alpha)}_m, t_{m+}) > 0
\end{aligned}
\right\} \text{ for } \Omega^{(\alpha)}_2 \to \Omega^{(\alpha)}_1, \tag{47}
$$

where $\mathbf{x}^{(\alpha)}_m \in \partial\Omega^{(\alpha)}_{ij}$.

Proof By the theory of flow switchability, the zeroth-order G-functions are needed to judge the passable flow from one domain to another domain. For passable motion, the switching conditions are

$$
\begin{aligned}
&G^{(0,1)}_{\partial\Omega^{(\alpha)}_{12}}(\mathbf{x}^{(\alpha)}_m, t_{m-}) < 0,\ G^{(0,2)}_{\partial\Omega^{(\alpha)}_{12}}(\mathbf{x}^{(\alpha)}_m, t_{m+}) < 0\\
&\quad \text{for } \Omega^{(\alpha)}_1 \to \Omega^{(\alpha)}_2,\\
&G^{(0,2)}_{\partial\Omega^{(\alpha)}_{21}}(\mathbf{x}^{(\alpha)}_m, t_{m-}) > 0,\ G^{(0,1)}_{\partial\Omega^{(\alpha)}_{21}}(\mathbf{x}^{(\alpha)}_m, t_{m+}) > 0\\
&\quad \text{for } \Omega^{(\alpha)}_2 \to \Omega^{(\alpha)}_1.
\end{aligned}
\tag{48}
$$

For a more intuitive presentation, the process is described in Fig. 4. The G-function for the velocity boundary $\partial\Omega^{(\alpha)}_{12}(\alpha \in \{1, 2\})$ is given in Definition 1 (i). Combining with Eqs. (17) and (33), the corresponding G-functions can be obtained:

$$
\begin{aligned}
&G^{(0,1)}_{\partial\Omega^{(\alpha)}_{12}}(\mathbf{x}_m, t_{m\pm}) = \mathbf{n}^{\mathrm{T}}_{\partial\Omega^{(\alpha)}_{12}} \cdot \mathbf{F}^{(1)}_\alpha(\mathbf{x}^{(\alpha)}_m, t_{m\pm})\\
&\quad = F^{(1)}_\alpha(\mathbf{x}_m, t_{m\pm}),\\
&G^{(0,2)}_{\partial\Omega^{(\alpha)}_{12}}(\mathbf{x}_m, t_{m\pm}) = \mathbf{n}^{\mathrm{T}}_{\partial\Omega^{(\alpha)}_{12}} \cdot \mathbf{F}^{(2)}_\alpha(\mathbf{x}^{(\alpha)}_m, t_{m\pm})\\
&\quad = F^{(2)}_\alpha(\mathbf{x}_m, t_{m\pm}).
\end{aligned}
\tag{49}
$$

From Eqs. (48) and (49), Eqs. (46) and (47) can be obtained. The proof is completed. □

Remark 1 The direction of the friction force acting on the corresponding mass changes with the speed of the mass m_α $(\alpha \in \{1, 2\})$. The velocity of the mass $m_\alpha(\alpha \in \{1, 2\})$ is not equal to that of the belt before time t_m. At time t_m, the relative velocity between the

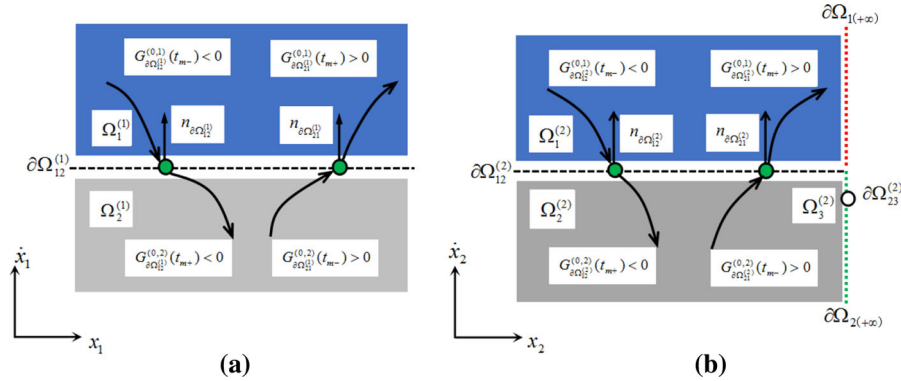

Fig. 4 The passable motions on the velocity boundaries (assuming $V > 0$): **a** mass m_1 and **b** mass m_2

mass and the belt is zero, that is to say that the flow reaches to the velocity boundary. And after time t_m, the direction of the relative motion between the mass $m_\alpha(\alpha \in \{1,2\})$ and the belt is changed, so the direction of the friction force is opposite to the direction before time t_m, this means that the flow passes through the velocity boundary from one domain to another one.

Theorem 2 *For the physical model with one-sided impact described in Sect. 2, the stick motion exists on* $\mathbf{x}_m^{(\alpha)} \in \partial\Omega_{ij}^{(\alpha)}(\alpha \in \{1,2\}; i, j \in \{1,2\}, i \neq j)$ *at time* t_m *for the mass* $m_\alpha(\alpha \in \{1,2\})$ *if and only if*

$$\begin{aligned} &F_\alpha^{(0\succ 0_1)}(\mathbf{x}_m^{(\alpha)}, t_{m-}, \tau_1^{(1)}) < 0, \\ &F_\alpha^{(0\succ 0_2)}(\mathbf{x}_m^{(\alpha)}, t_{m-}, \tau_1^{(2)}) > 0. \end{aligned} \tag{50}$$

Proof The mass $m_\alpha(\alpha \in \{1,2\})$ moves together with the belt for some time, this motion is called the stick motion. The zeroth-order G-functions are needed to judge the stick motion on the velocity boundary. The analytical conditions of the stick motion existing on the velocity boundary $\partial\Omega_{12}^{(\alpha)}$ with flow barriers are

$$\begin{aligned} &G_{\partial\Omega_{12}^{(\alpha)}}^{(0,0\succ 0_1)}(\mathbf{x}_m^{(\alpha)}, t_{m-}, \tau_1^{(1)}) < 0, \\ &G_{\partial\Omega_{12}^{(\alpha)}}^{(0,0\succ 0_2)}(\mathbf{x}_m^{(\alpha)}, t_{m-}, \tau_1^{(2)}) > 0. \end{aligned} \tag{51}$$

By Definition 3 and Eqs. (30), (33), the corresponding G-functions can be computed as

$$\begin{aligned} &G_{\partial\Omega_{12}^{(\alpha)}}^{(0,0\succ 0_1)}(\mathbf{x}_m^{(\alpha)}, t_{m-}, \tau_1^{(1)}) \\ &\quad = \mathbf{n}_{\partial\Omega_{12}^{(\alpha)}}^{\mathrm{T}} \cdot \mathbf{F}_\alpha^{(0\succ 0_1)}(\mathbf{x}_m^{(\alpha)}, t_{m-}, \tau^{(1)}) \\ &\quad = F_\alpha^{(0\succ 0_1)}(\mathbf{x}_m^{(\alpha)}, t_{m-}, \tau_1^{(1)}), \\ &G_{\partial\Omega_{12}^{(\alpha)}}^{(0,0\succ 0_2)}(\mathbf{x}_m^{(\alpha)}, t_{m-}, \tau_1^{(2)}) \\ &\quad = \mathbf{n}_{\partial\Omega_{12}^{(\alpha)}}^{\mathrm{T}} \cdot \mathbf{F}_\alpha^{(0\succ 0_2)}(\mathbf{x}_m^{(\alpha)}, t_{m-}, \tau^{(2)}) \\ &\quad = F_\alpha^{(0\succ 0_2)}(\mathbf{x}_m^{(\alpha)}, t_{m-}, \tau_1^{(2)}). \end{aligned} \tag{52}$$

From Eqs. (51) and (52), the conclusion of this theorem holds. □

Remark 2 If the non-friction force acting on the mass $m_\alpha(\alpha \in \{1,2\})$ cannot overcome the maximum static friction force between the mass and the belt(i.e., $|F_s^{(\alpha)}| \leq \mu_s F_N^{(\alpha)}, \alpha \in \{1,2\}$), the mass will move together with the belt. When the mass $m_\alpha(\alpha \in \{1,2\})$ has the stick motion, the relative velocity between the mass and the belt is zero. If the conditions in Theorem 2 are satisfied, the mass will move together with the belt for some time.

Theorem 3 *For the physical model with one-sided impact described in Sect. 2, the appearance of stick motion on* $\mathbf{x}_m^{(\alpha)} \in \partial\Omega_{ij}^{(\alpha)}(\alpha \in \{1,2\}; i, j \in \{1,2\}, i \neq j)$ *at time* t_m *for the mass* $m_\alpha(\alpha \in \{1,2\})$ *requires*

$$F_\alpha^{(1)}(\mathbf{x}_m^{(\alpha)}, t_{m-}) < 0, \quad F_\alpha^{(2)}(\mathbf{x}_m^{(\alpha)}, t_{m-}) > 0. \tag{53}$$

Proof When the motion of the mass $m_\alpha(\alpha \in \{1,2\})$ switches from non-stick motion to stick motion, the stick motion occurs at this time. By the theory of flow switchability, the onset of stick motion is that the flows in domain $\Omega_i^{(\alpha)}$ and domain $\Omega_j^{(\alpha)}$ come to the velocity boundary $\partial\Omega_{ij}^{(\alpha)}(\alpha \in \{1,2\}; i, j \in \{1,2\}, i \neq j)$ at the

same time t_m. The zeroth-order G-functions are needed to judge the appearing of stick motion on the velocity boundary. The analytical conditions of the appearing of stick motion from $\Omega_1^{(\alpha)}$ or $\Omega_2^{(\alpha)}$ to the boundary $\partial\Omega_{12}^{(\alpha)}$ are

$$G^{(0,1)}_{\partial\Omega_{12}^{(\alpha)}}(\mathbf{x}_m^{(\alpha)}, t_{m-}) < 0, \quad G^{(0,2)}_{\partial\Omega_{12}^{(\alpha)}}(\mathbf{x}_m^{(\alpha)}, t_{m-}) > 0. \quad (54)$$

From Eqs. (49) and (54), the conclusion of this theorem holds. □

Remark 3 The onset of stick motion is that the motion of the mass $m_\alpha(\alpha \in \{1, 2\})$ is changed from non-stick motion to stick motion. At this moment, the force in domain $\Omega_1^{(\alpha)}$ is negative, and the force in domain $\Omega_2^{(\alpha)}$ is positive at the same time when the flow is from domain $\Omega_1^{(\alpha)}$ or $\Omega_2^{(\alpha)}$ to the velocity boundary. The conditions in Theorem 3 is just the sufficient conditions of the appearance of the stick motion, and it can guarantee that the stick motion occurs. The sufficient and necessary conditions of the appearance of the stick motion can be referred in Luo [51,54] or [55].

Theorem 4 *For the physical model with one-sided impact described in Sect. 2, once the stick motion is formed on the velocity boundary* $\partial\Omega_{ij}^{(\alpha)}$ $(\alpha \in \{1, 2\}$; $i, j \in \{1, 2\}, i \neq j)$ *with flow barrier, the vanishing of the stick motion on the* δ*-side* $(\delta \in \{1, 2\})$ *at time* t_m *and point* $\mathbf{x}_m^{(\alpha)} \in \partial\Omega_{ij}^{(\alpha)}$ *for the mass* m_α $(\alpha \in \{1, 2\})$ *requires*

$$\left.\begin{aligned} &F_\alpha^{(0\succ 0_1)}(\mathbf{x}_m^{(\alpha)}, t_{m-}, \tau_1^{(1)}) < 0 \\ &F_\alpha^{(0\succ 0_2)}(\mathbf{x}_m^{(\alpha)}, t_{m\mp}, \tau_1^{(2)}) = 0, \\ &DF_\alpha^{(0\succ 0_2)}(\mathbf{x}_m^{(\alpha)}, t_{m\mp}, \tau_1^{(2)}) < 0 \end{aligned}\right\} \text{from } \partial\Omega_{12}^{(\alpha)} \to \Omega_2^{(\alpha)}; \quad (55)$$

and

$$\left.\begin{aligned} &F_\alpha^{(0\succ 0_2)}(\mathbf{x}_m^{(\alpha)}, t_{m-}, \tau_1^{(2)}) > 0 \\ &F_\alpha^{(0\succ 0_1)}(\mathbf{x}_m^{(\alpha)}, t_{m\mp}, \tau_1^{(1)}) = 0, \\ &DF_\alpha^{(0\succ 0_1)}(\mathbf{x}_m^{(\alpha)}, t_{m\mp}, \tau_1^{(1)}) > 0 \end{aligned}\right\} \text{from } \partial\Omega_{12}^{(\alpha)} \to \Omega_1^{(\alpha)}. \quad (56)$$

Proof The mass $m_\alpha(\alpha \in \{1, 2\})$ moves together with the belt for some time, but at time t_m the non-friction force on the horizontal direction can overcome the maximum static friction force of the mass, which results in the relative motion between the mass and the belt after this time. By the theory of flow switchability, the vanishing of stick motion is that the flow sliding on the velocity boundary $\partial\Omega_{ij}^{(\alpha)}(\alpha \in \{1, 2\}; i, j \in \{1, 2\}, i \neq j)$ will enter into domain $\Omega_i^{(\alpha)}$ or domain $\Omega_j^{(\alpha)}$. The zeroth-order and first-order G-functions are needed to judge the vanishing of stick motion on the velocity boundary $\partial\Omega_{ij}^{(\alpha)}(\alpha \in \{1, 2\}; i, j \in \{1, 2\}, i \neq j)$. The switching conditions of the vanishing of stick motion on the 2–side of the boundary $\partial\Omega_{21}^{(\alpha)}(\alpha \in \{1, 2\})$ with flow barrier are

$$\left.\begin{aligned} &G^{(0,0\succ 0_1)}_{\partial\Omega_{12}^{(\alpha)}}(\mathbf{x}_m^{(\alpha)}, t_{m-}, \tau_1^{(1)}) < 0 \\ &G^{(0,0\succ 0_2)}_{\partial\Omega_{12}^{(\alpha)}}(\mathbf{x}_m^{(\alpha)}, t_{m\mp}, \tau_1^{(2)}) = 0, \\ &G^{(1,0\succ 0_2)}_{\partial\Omega_{12}^{(\alpha)}}(\mathbf{x}_m^{(\alpha)}, t_{m\mp}, \tau_1^{(2)}) < 0. \end{aligned}\right\} \quad (57)$$

By Eqs. (30), (33) and (44), the corresponding flow barrier G-functions can be computed as

$$\begin{aligned} &G^{(0,0\succ 0_\lambda)}_{\partial\Omega_{21}^{(\alpha)}}(\mathbf{x}_m^{(\alpha)}, t_{m\mp}, \tau_1^{(\lambda)}) \\ &= \mathbf{n}^{\mathrm{T}}_{\partial\Omega_{21}^{(\alpha)}} \cdot \mathbf{F}_\alpha^{(0\succ 0_\lambda)}(\mathbf{x}_m^{(\alpha)}, t_{m\mp}, \tau_1^{(\lambda)}) \\ &= F_\alpha^{(0\succ 0_\lambda)}(\mathbf{x}_m^{(\alpha)}, t_{m\mp}, \tau_1^{(\lambda)}), \end{aligned} \quad (58)$$

$$\begin{aligned} &G^{(1,0\succ 0_\lambda)}_{\partial\Omega_{21}^{(\alpha)}}(\mathbf{x}_m^{(\alpha)}, t_{m\mp}, \tau_1^{(\lambda)}) \\ &= \mathbf{n}^{\mathrm{T}}_{\partial\Omega_{21}^{(\alpha)}} \cdot D\mathbf{F}_\alpha^{(0\succ 0_\lambda)}(\mathbf{x}_m^{(\alpha)}, t_{m\mp}, \tau_1^{(\lambda)}) \\ &= DF_\alpha^{(0\succ 0_\lambda)}(\mathbf{x}_m^{(\alpha)}, t_{m\mp}, \tau_1^{(\lambda)}), \end{aligned} \quad (59)$$

where $\lambda \in \{1, 2\}$.

From Eqs. (57), (58) and (59), Eq. (55) holds. Similarly, the switching conditions of the vanishing of stick motion on the 1–side of the boundary $\partial\Omega_{12}^{(\alpha)}(\alpha \in \{1, 2\})$ with flow barrier can be obtained, i.e., Eq. (56) holds. The proof is completed. □

Remark 4 The flow barrier exists on the velocity boundary because of the static friction force. When the non-friction force is greater than the maximum static friction force, the flow on the boundary will overcome the flow barrier and enter to the corresponding domain, i.e., the stick motion will vanish. Before time

t_m, the non-friction force cannot overcome the maximum static friction force for the mass $m_\alpha(\alpha \in \{1,2\})$, the mass moves together with the belt at the same velocity. After time t_m, the non-friction force can overcome the maximum static friction force, the relative velocity between the mass and the belt is not equal to zero. That is to say, the mass begins to slip on the belt, and the stick motion will disappear at time t_m. If the conditions in Theorem 4 can be satisfied, the mass will have the relative motion to the belt.

The four kinds of process of the stick motion for the mass m_1 are depicted in Fig. 5, and the stick motion for the mass m_2 is similar to that of the mass m_1.

Theorem 5 (i) *For the physical model with one-sided impact described in Sect. 2, the grazing motion on* $\mathbf{x}_m^{(\alpha)} \in \partial\Omega_{12}^{(\alpha)}(\alpha \in \{1,2\})$ *for the mass* $m_\alpha(\alpha \in \{1,2\})$ *in domain* $\Omega_1^{(\alpha)}(\alpha \in \{1,2\})$ *at time* t_m *appears if and only if*

$$F_\alpha^{(1)}(\mathbf{x}_m^{(\alpha)}, t_{m\pm}) = 0,\ DF_\alpha^{(1)}(\mathbf{x}_m^{(\alpha)}, t_{m\pm}) > 0. \tag{60}$$

(ii) *For the physical model with one-sided impact described in Sect. 2, the grazing motion on* $\mathbf{x}_m^{(\alpha)} \in \partial\Omega_{21}^{(\alpha)}$ $(\alpha \in \{1,2\})$ *for the mass* $m_\alpha(\alpha \in \{1,2\})$ *in domain* $\Omega_2^{(\alpha)}(\alpha \in \{1,2\})$ *at time* t_m *appears if and only if*

$$F_\alpha^{(2)}(\mathbf{x}_m^{(\alpha)}, t_{m\pm}) = 0,\ DF_\alpha^{(2)}(\mathbf{x}_m^{(\alpha)}, t_{m\pm}) < 0. \tag{61}$$

Proof Before and after time t_m, the velocity of the mass $m_\alpha(\alpha \in \{1,2\})$ is greater (or less) than the velocity of the belt, and at time t_m, the velocities of the mass m_α $(\alpha \in \{1,2\})$ and the belt are equal. This means that the direction of the relative velocity between mass $m_\alpha(\alpha \in \{1,2\})$ and the belt does not change before and after time t_m. By the theory of flow switchability, the domain flow comes to the velocity boundary, and is tangential to it at time t_m. After time t_m, the flow returns to the original domain. The zeroth-order and first-order G-functions are needed to judge the grazing motion on the velocity boundary. The switching conditions of the grazing motion on the boundary $\partial\Omega_{12}^{(\alpha)}$ in domain $\Omega_j^{(\alpha)}$ $(\alpha, j \in \{1,2\})$ are

$$\left.\begin{aligned} &G_{\partial\Omega_{12}^{(\alpha)}}^{(0,j)}(\mathbf{x}_m^{(\alpha)}, t_{m\pm}) = 0,\\ &(-1)^{j+1} G_{\partial\Omega_{12}^{(\alpha)}}^{(1,j)}(\mathbf{x}_m^{(\alpha)}, t_{m\pm}) > 0. \end{aligned}\right\} \tag{62}$$

It is depicted in Fig. 6. By Eqs. (17), (33), (36) and (39), the corresponding G-functions can be computed as

$$\begin{aligned} G_{\partial\Omega_{12}^{(\alpha)}}^{(0,j)}(\mathbf{x}_m^{(\alpha)}, t_{m\pm}) &= \mathbf{n}_{\partial\Omega_{12}^{(\alpha)}}^{\mathrm{T}} \cdot \mathbf{F}_\alpha^{(j)}(\mathbf{x}_m^{(\alpha)}, t_{m\pm})\\ &= F_\alpha^{(j)}(\mathbf{x}_m^{(\alpha)}, t_{m\pm}),\\ G_{\partial\Omega_{12}^{(\alpha)}}^{(1,j)}(\mathbf{x}_m^{(\alpha)}, t_{m\pm}) &= \mathbf{n}_{\partial\Omega_{12}^{(\alpha)}}^{\mathrm{T}} \cdot D\mathbf{F}_\alpha^{(j)}(\mathbf{x}_m^{(\alpha)}, t_{m\pm})\\ &= DF_\alpha^{(j)}(\mathbf{x}_m^{(\alpha)}, t_{m\pm}). \end{aligned} \tag{63}$$

From Eqs. (62) and (63), (i) and (ii) hold. □

Remark 5 The mass $m_\alpha(\alpha \in \{1,2\})$ moves on the belt at a variable velocity. The varying of the velocity will cause the appearance of grazing motion. From the view of flow switching in discontinuous dynamical systems, the grazing motion is that the domain flow reaches to the boundary and is tangential to the boundary. After that, the flow returns to this domain again. The zeroth-order G-function is zero, it means that the flow is tangential to the velocity boundary. The first-order G-function is used to judge the trend of the flow at the next moment.

Theorem 6 *For the physical model with one-sided impact described in Sect. 2, the impact motion on* $\mathbf{x}_m^{(2)} \in \partial\Omega_{i(+\infty)}^{(2)}(i = 1,2)$ *occurs for the mass* m_2 *at time* t_m *if the following conditions are satisfied:*

$$\left.\begin{aligned} &\dot{x}_2^{(1)}(t_{m-}) > 0,\\ &\dot{x}_2^{(2)}(t_{m+}) < 0 \end{aligned}\right\} \text{ on } \partial\Omega_{1(+\infty)}^{(2)}; \tag{64}$$

$$\left.\begin{aligned} &\dot{x}_2^{(2)}(t_{m-}) > 0,\\ &\dot{x}_2^{(2)}(t_{m+}) < 0 \end{aligned}\right\} \text{ on } \partial\Omega_{2(+\infty)}^{(2)}. \tag{65}$$

Proof The mass m_2 impacts with the right-hand rigid obstacle when the mass touches the obstacle with the nonzero velocity and separates with the obstacle immediately, which means that the flow in the domain reaches to the impact boundary $\partial\Omega_{i(+\infty)}^{(2)}(i \in \{1,2\})$ at time t_m by the theory of flow switchability. Because the

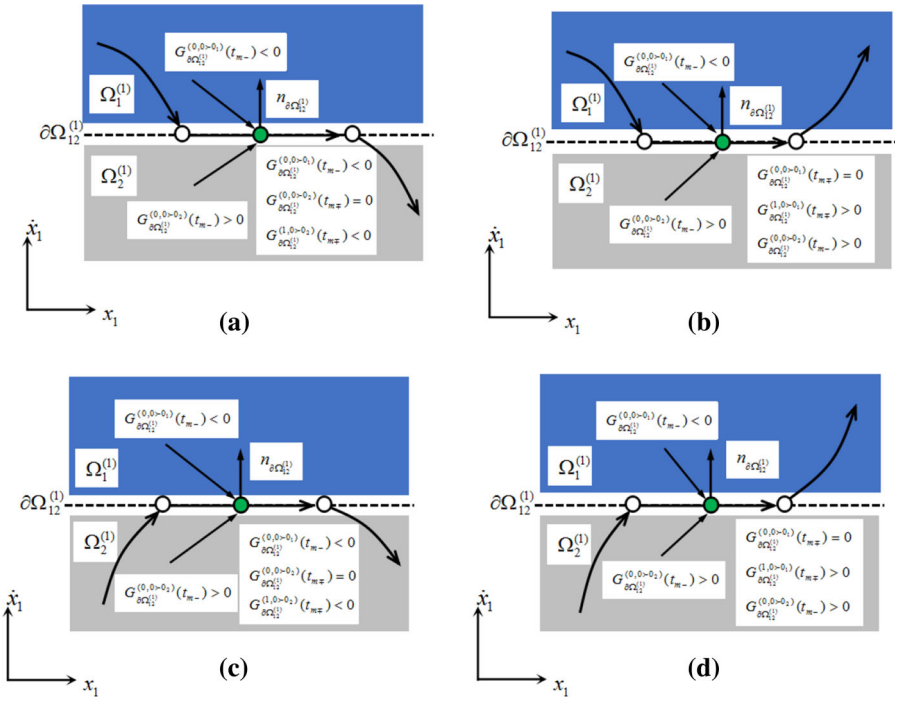

Fig. 5 The four kinds of stick motion on the velocity boundary for the mass m_1, and the mass m_2 is similar

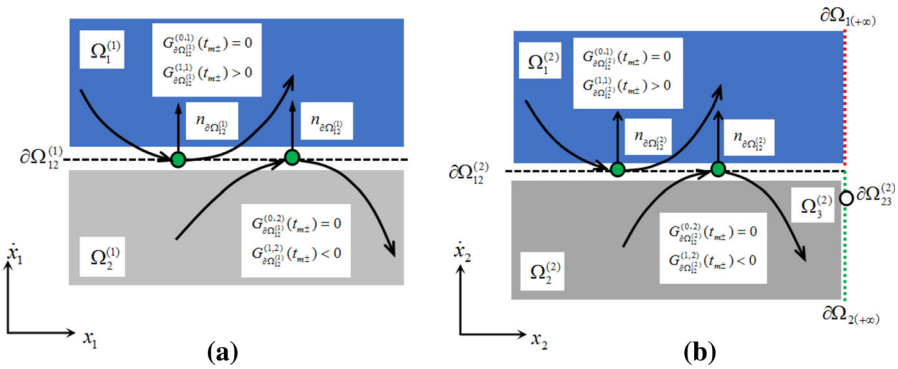

Fig. 6 The grazing motions on the velocity boundaries for the two masses $m_\alpha(\alpha = 1, 2)$: **a** mass m_1 and **b** mass m_2

impact boundary is the non-passable boundary, the flow will return to the free movement domain. The switching conditions of the impact motion are

$$\left.\begin{aligned} &G^{(0,1)}_{\partial\Omega^{(2)}_{1(+\infty)}}(\mathbf{x}^{(2)}_m, t_{m-}) > 0,\\ &G^{(0,2)}_{\partial\Omega^{(2)}_{2(+\infty)}}(\mathbf{x}^{(2)}_m, t_{m+}) < 0 \end{aligned}\right\} \text{on } \partial\Omega^{(2)}_{1(+\infty)}; \tag{66}$$

$$\left.\begin{aligned} &G^{(0,2)}_{\partial\Omega^{(2)}_{2(+\infty)}}(\mathbf{x}^{(2)}_m, t_{m-}) > 0,\\ &G^{(0,2)}_{\partial\Omega^{(2)}_{2(+\infty)}}(\mathbf{x}^{(2)}_m, t_{m+}) < 0 \end{aligned}\right\} \text{on } \partial\Omega^{(2)}_{2(+\infty)}. \tag{67}$$

The process of the impact motion is described in Fig. 6. By Eqs. (17), (34) and (37), the corresponding G-functions can be obtained as follows:

$$\begin{aligned} G^{(0,1)}_{\partial\Omega^{(2)}_{1(+\infty)}}(\mathbf{x}^{(2)}_m, t_{m-}) &= \mathbf{n}^{\mathrm{T}}_{\partial\Omega^{(2)}_{1(+\infty)}} \cdot \mathbf{F}^{(1)}_2(\mathbf{x}^{(2)}_m, t_{m-})\\ &= \dot{x}^{(1)}_2(t_{m-}),\\ G^{(0,2)}_{\partial\Omega^{(2)}_{2(+\infty)}}(\mathbf{x}^{(2)}_m, t_{m\pm}) &= \mathbf{n}^{\mathrm{T}}_{\partial\Omega^{(2)}_{2(+\infty)}} \cdot \mathbf{F}^{(2)}_2(\mathbf{x}^{(2)}_m, t_{m\pm})\\ &= \dot{x}^{(2)}_2(t_{m\pm}). \end{aligned} \tag{68}$$

The proof is completed by Eqs. (66), (67) and (68). □

Remark 6 When the mass m_2 impacts the rigid obstacle at time t_m, the mass m_2 approaches to it with a

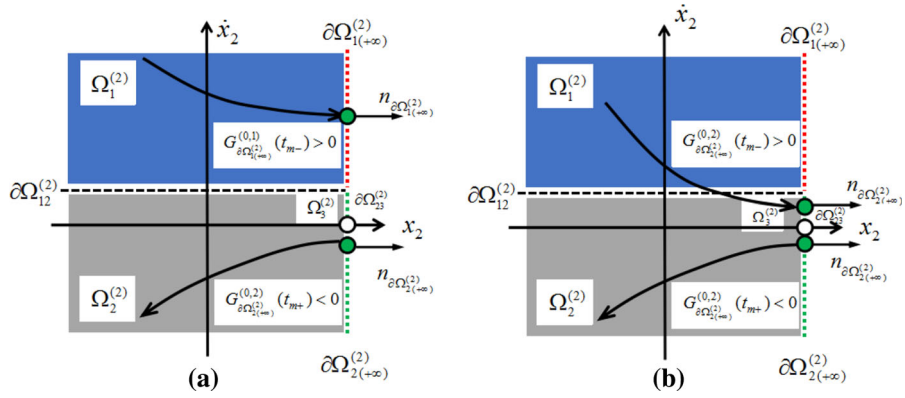

Fig. 7 The impact motion between the mass m_2 and the right-hand rigid obstacle: **a** on $\partial\Omega^{(2)}_{1(+\infty)}$; **b** on $\partial\Omega^{(2)}_{2(+\infty)}$

positive velocity before time t_m and leaves it with a negative velocity after time t_m, as shown in Fig. 7. The conditions in Theorem 6 can guarantee that the mass m_2 will impact with the rigid obstacle and vice versa.

Theorem 7 *For the physical model with one-sided impact described in Sect. 2, the stuck motion on* $\mathbf{x}^{(2)}_m \in \partial\Omega^{(2)}_{23}$ *(stuck boundary) at time* t_m *for the mass* m_2 *appears if and only if*

$$F^{(2)}_2(\mathbf{x}^{(2)}_m, t_{m-}) > 0, \quad F^{(3)}_2(\mathbf{x}^{(2)}_m, t_{m+}) > 0. \tag{69}$$

Proof The mass m_2 touches with the right-hand rigid obstacle with the zero velocity for some time, such motion is called stuck motion. By the theory of the flow switchability, the stuck motion is that the flow in free movement domain comes to the stuck boundary and tries to pass through the stuck boundary and to enter into the stuck domain. The zeroth-order G-functions are needed to judge the onset of stuck motion on the stuck boundary. The switching conditions are

$$G^{(0,2)}_{\partial\Omega^{(2)}_{23}}(\mathbf{x}^{(2)}_m, t_{m-}) > 0, \quad G^{(0,3)}_{\partial\Omega^{(2)}_{23}}(\mathbf{x}^{(2)}_m, t_{m+}) > 0. \tag{70}$$

By Eqs. (17), (35) and (38), the corresponding G-functions can be computed as

$$\begin{aligned} G^{(0,2)}_{\partial\Omega^{(2)}_{23}}(\mathbf{x}^{(2)}_m, t_{m-}) &= \mathbf{n}^{\mathrm{T}}_{\partial\Omega^{(2)}_{23}} \cdot \mathbf{F}^{(2)}_2(\mathbf{x}^{(2)}_m, t_{m-}) \\ &= F^{(2)}_2(\mathbf{x}^{(2)}_m, t_{m-}), \\ G^{(0,3)}_{\partial\Omega^{(2)}_{23}}(\mathbf{x}^{(2)}_m, t_{m+}) &= \mathbf{n}^{\mathrm{T}}_{\partial\Omega^{(2)}_{23}} \cdot \mathbf{F}^{(3)}_2(\mathbf{x}^{(2)}_m, t_{m+}) \\ &= F^{(3)}_2(\mathbf{x}^{(2)}_m, t_{m+}). \end{aligned} \tag{71}$$

From Eqs. (70) and (71), the conclusion of this theorem holds, as shown in Fig. 8. □

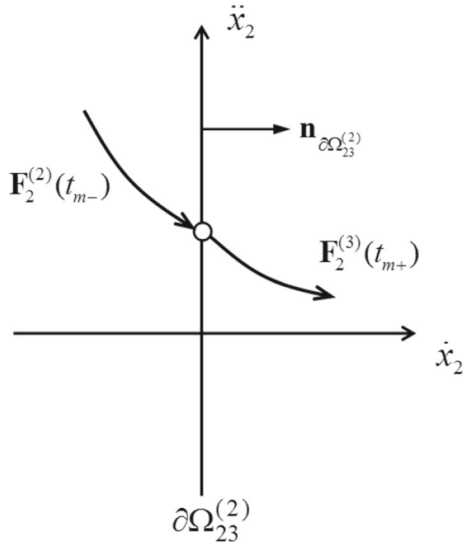

Fig. 8 The onset of stuck motion between the mass m_2 and the right-hand rigid obstacle

Remark 7 When the mass m_2 reaches to the right-hand rigid obstacle with zero velocity and continues to push it, this obstacle will give an opposite and equal reaction force to the mass at the same time due to the right-hand rigid obstacle being fixed. This will make the mass keep the stuck motion for some time. So the mass m_2 has a stuck motion if the conditions in Theorem 7 are satisfied.

Theorem 8 *For the physical model with one-sided impact described in Sect. 2, once the stuck motion is formed on the stuck boundary* $\partial\Omega^{(2)}_{23}$*, the stuck motion will vanish on* $\mathbf{x}^{(2)}_m \in \partial\Omega^{(2)}_{23}$ *at time* t_m *for the mass* m_2 *if and only if*

$$F^{(3)}_2(\mathbf{x}^{(2)}_m, t_{m-}) = 0, \; DF^{(3)}_2(\mathbf{x}^{(2)}_m, t_{m-}) < 0,$$

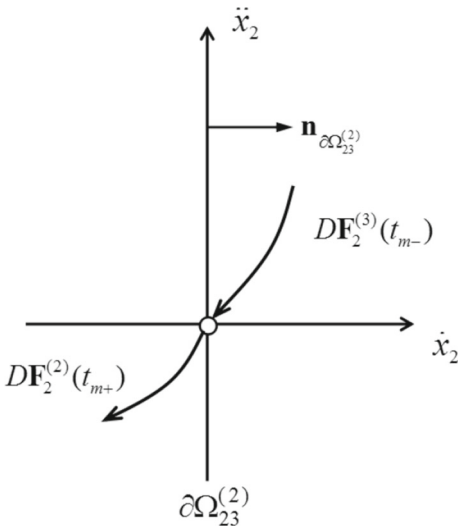

Fig. 9 The vanishing of stuck motion between the mass m_2 and the right-hand rigid obstacle

$$F_2^{(2)}(\mathbf{x}_m^{(2)}, t_{m+}) = 0,\ DF_2^{(2)}(\mathbf{x}_m^{(2)}, t_{m+}) < 0 \quad \text{for} \quad \partial\Omega_{23}^{(2)} \to \Omega_2^{(2)}. \tag{72}$$

Proof When the mass m_2 has a stuck motion on the stuck boundary $\partial\Omega_{23}^{(2)}$, the velocity of the mass is zero. If it has a tendency to leave the right-hand rigid obstacle, the acceleration of the mass m_2 will change. By the theory of flow switchability, the vanishing of the stuck motion is that the flow on the stuck boundary $\partial\Omega_{23}^{(2)}$ will come into the free movement domain $\Omega_2^{(2)}$. The zeroth-order and first-order G-functions are needed to judge the vanishing of stuck motion on the stuck boundary. The switching conditions of disappearance of stuck motion are

$$\begin{aligned} &G^{(0,3)}_{\partial\Omega_{23}^{(2)}}(\mathbf{x}_m^{(2)}, t_{m-}) = 0,\ G^{(1,3)}_{\partial\Omega_{23}^{(2)}}(\mathbf{x}_m^{(2)}, t_{m-}) < 0,\\ &G^{(0,2)}_{\partial\Omega_{23}^{(2)}}(\mathbf{x}_m^{(2)}, t_{m+}) = 0,\ G^{(1,2)}_{\partial\Omega_{23}^{(2)}}(\mathbf{x}_m^{(2)}, t_{m+}) < 0\\ &\quad \text{for} \quad \partial\Omega_{23}^{(2)} \to \Omega_2^{(2)}. \end{aligned} \tag{73}$$

The vanishing of stuck motion is shown in Fig. 9. By (17), (35), (38) and (41), the corresponding G-functions can be computed as

$$\begin{aligned} G^{(0,3)}_{\partial\Omega_{23}^{(2)}}(\mathbf{x}_m^{(2)}, t_{m-}) &= \mathbf{n}^{\mathrm{T}}_{\partial\Omega_{23}^{(2)}} \cdot \mathbf{F}_2^{(3)}(\mathbf{x}_m^{(2)}, t_{m-})\\ &= F_2^{(3)}(\mathbf{x}_m^{(2)}, t_{m-}),\\ G^{(1,3)}_{\partial\Omega_{23}^{(2)}}(\mathbf{x}_m^{(2)}, t_{m-}) &= \mathbf{n}^{\mathrm{T}}_{\partial\Omega_{23}^{(2)}} \cdot D\mathbf{F}_2^{(3)}(\mathbf{x}_m^{(2)}, t_{m-})\\ &= DF_2^{(3)}(\mathbf{x}_m^{(2)}, t_{m-}), \end{aligned} \tag{74}$$

$$\begin{aligned} G^{(0,2)}_{\partial\Omega_{23}^{(2)}}(\mathbf{x}_m^{(2)}, t_{m+}) &= \mathbf{n}^{\mathrm{T}}_{\partial\Omega_{23}^{(2)}} \cdot \mathbf{F}_2^{(2)}(\mathbf{x}_m^{(2)}, t_{m+})\\ &= F_2^{(2)}(\mathbf{x}_m^{(2)}, t_{m+}),\\ G^{(1,2)}_{\partial\Omega_{23}^{(2)}}(\mathbf{x}_m^{(2)}, t_{m+}) &= \mathbf{n}^{\mathrm{T}}_{\partial\Omega_{23}^{(2)}} \cdot D\mathbf{F}_2^{(2)}(\mathbf{x}_m^{(2)}, t_{m+})\\ &= DF_2^{(2)}(\mathbf{x}_m^{(2)}, t_{m+}). \end{aligned} \tag{75}$$

From Eqs. (73), (74) and (75), the conclusion of this theorem holds. □

Remark 8 Before time t_m, the mass m_2 is stuck on the right-hand obstacle, which means that a pair of equilibrium forces acting on the mass keep the system at equilibrium for this time. At time t_m, the stuck motion will vanish when the mass m_2 will leave the rigid obstacle. The zeroth-order G-function represents the acceleration of the mass and the zeroth-order G-function means the jerk. So the zeroth-order G-function and first-order G-function are needed to judge the vanishing of stuck motion. If the conditions in Theorem 8 are satisfied, the stuck motion for the mass m_2 will vanish on the stuck boundary $\partial\Omega_{23}^{(2)}$.

5 Mapping structures and periodic motions

In order to better discuss periodic motions and other motions of the 2-DOF friction-induced oscillator with one-sided impact on a conveyer belt described in Sect. 2, the corresponding mapping structures will be introduced through the discontinuous boundaries, as shown in Appendix A. By connecting some of these mappings, it is possible to define periodic solutions of the system.

Based on the mappings defined in Appendix A, a periodic motion of the two masses $m_\alpha (\alpha = 1, 2)$ with impact and stick is considered by the following simple mapping structure

$$P = (P_{3c} \circ P_{8a})^{M_3} \circ (P_{3c} \circ P_{2a})^{M_2} \circ (P_{1c} \circ P_{1a} \circ P_{1b})^{M_1}, \tag{76}$$

where M_1, M_2 and M_3 are positive integers or zero, and $P^0 = I$; or a more general periodic motion is considered with the following general mapping structure

$$\begin{aligned} P = {} & (P_{3c} \circ P_{8a})^{M_{3s}} \circ (P_{3c} \circ P_{2a})^{M_{2s}}\\ & \circ (P_{1c} \circ P_{1a} \circ P_{1b})^{M_{1s}} \circ \cdots \circ (P_{3c} \circ P_{8a})^{M_{31}}\\ & \circ (P_{3c} \circ P_{2a})^{M_{21}} \circ (P_{1c} \circ P_{1a} \circ P_{1b})^{M_{11}}, \end{aligned} \tag{77}$$

where $M_{1\xi}$, $M_{2\xi}$ and $M_{3\xi}(\xi = 1, 2, \ldots, s)$ are positive integers or zero.

Consider another periodic motion of the masses m_1 and m_2 with stuck and stick expressed by the following mapping structure

$$P = (P_{7c} \circ P_{6a} \circ P_{5c} \circ P_{4a})^{M_3} \circ (P_{7c} \circ P_{4a})^{M_2} \circ (P_{1c} \circ P_{1a} \circ P_{1b})^{M_1}, \tag{78}$$

where M_1, M_2 and M_3 are positive integers or zero, and $P^0 = I$; or consider a more general periodic motion with the following general mapping structure

$$\begin{aligned} P = {} & (P_{7c} \circ P_{6a} \circ P_{5c} \circ P_{4a})^{M_{3s}} \circ (P_{7c} \circ P_{4a})^{M_{2s}} \\ & \circ (P_{1c} \circ P_{1a} \circ P_{1b})^{M_{1s}} \circ \cdots \\ & \circ (P_{7c} \circ P_{6a} \circ P_{5c} \circ P_{4a})^{M_{31}} \\ & \circ (P_{7c} \circ P_{4a})^{M_{21}} \circ (P_{1c} \circ P_{1a} \circ P_{1b})^{M_{11}}, \end{aligned} \tag{79}$$

where $M_{1\xi}$, $M_{2\xi}$ and $M_{3\xi}$ $(\xi = 1, 2, \ldots, s)$ are positive integers or zero.

In a similar fashion, a complex periodic motion of the masses m_1 and m_2 with stuck, impact and stick described by the following general mapping structure can be also considered:

$$\begin{aligned} P = {} & (P_{7c} \circ P_{6a} \circ P_{5c} \circ P_{4a})^{M_5} \circ (P_{7c} \circ P_{4a})^{M_4} \\ & \circ (P_{3c} \circ P_{8a})^{M_3} \circ (P_{3c} \circ P_{2a})^{M_2} \\ & \circ (P_{1c} \circ P_{1a} \circ P_{1b})^{M_1}, \end{aligned} \tag{80}$$

where M_1, M_2, M_3, M_4 and M_5 are positive integers or zero, and $P^0 = I$; or consider more general periodic motion with the following general mapping structure

$$\begin{aligned} P = {} & (P_{7c} \circ P_{6a} \circ P_{5c} \circ P_{4a})^{M_{5s}} \circ (P_{7c} \circ P_{4a})^{M_{4s}} \\ & \circ (P_{3c} \circ P_{8a})^{M_{3s}} \circ (P_{3c} \circ P_{2a})^{M_{2s}} \\ & \circ (P_{1c} \circ P_{1a} \circ P_{1b})^{M_{1s}} \circ \cdots \\ & \circ (P_{7c} \circ P_{6a} \circ P_{5c} \circ P_{4a})^{M_{51}} \circ (P_{7c} \circ P_{4a})^{M_{41}} \\ & \circ (P_{3c} \circ P_{8a})^{M_{31}} \circ (P_{3c} \circ P_{2a})^{M_{21}} \\ & \circ (P_{1c} \circ P_{1a} \circ P_{1b})^{M_{11}}, \end{aligned} \tag{81}$$

where $M_{1\xi}$, $M_{2\xi}$, $M_{3\xi}$, $M_{4\xi}$ and $M_{5\xi}(\xi = 1, 2, \ldots, s)$ are positive integers or zero.

In addition, other periodic motions for the masses m_1 and m_2 can be also considered as in Eq. (81).

Theorem 9 *For periodic motion with the above mapping structure described in Eq. (81), the switching sets for a specific regular motion can be determined through solving a set of nonlinear equations.*

Proof A set of nonlinear equations are

$$\begin{aligned} & \mathbf{f}^{(1b)}(\mathbf{m}_k, \mathbf{m}_{k+1}) = 0, \\ & \mathbf{f}^{(1a)}(\mathbf{m}_{k+1}, \mathbf{m}_{k+2}) = 0, \\ & \mathbf{f}^{(1c)}(\mathbf{m}_{k+2}, \mathbf{m}_{k+3}) = 0, \ldots, \\ & \mathbf{f}^{(1b)}(\mathbf{m}_{k+3M_{11}-3}, \\ & \quad \mathbf{m}_{k+3M_{11}-2}) = 0, \\ & \mathbf{f}^{(1a)}(\mathbf{m}_{k+3M_{11}-2}, \mathbf{m}_{k+3M_{11}-1}) = 0, \\ & \mathbf{f}^{(1c)}(\mathbf{m}_{k+3M_{11}-1}, \mathbf{m}_{k+3M_{11}}) = 0; \end{aligned} \tag{82(1-1)}$$

$$\begin{aligned} & \mathbf{f}^{(2a)}(\mathbf{m}_{k+3M_{11}}, \mathbf{m}_{k+3M_{11}+1}) = 0, \\ & \mathbf{f}^{(3c)}(\mathbf{m}_{k+3M_{11}+1}, \mathbf{m}_{k+3M_{11}+2}) = 0, \ldots, \\ & \mathbf{f}^{(2a)}(\mathbf{m}_{k+3M_{11}+2M_{21}-2}, \\ & \quad \mathbf{m}_{k+3M_{11}+2M_{21}-1}) = 0, \\ & \mathbf{f}^{(3c)}(\mathbf{m}_{k+3M_{11}+2M_{21}-1}, \\ & \quad \mathbf{m}_{k+3M_{11}+2M_{21}}) = 0; \end{aligned} \tag{82(1-2)}$$

$$\begin{aligned} & \mathbf{f}^{(8a)}(\mathbf{m}_{k+3M_{11}+2M_{21}}, \\ & \quad \mathbf{m}_{k+3M_{11}+2M_{21}+1}) = 0, \\ & \mathbf{f}^{(3c)}(\mathbf{m}_{k+3M_{11}+2M_{21}+1}, \\ & \quad \mathbf{m}_{k+3M_{11}+2M_{21}+2}) = 0, \ldots, \\ & \mathbf{f}^{(8a)}(\mathbf{m}_{k+3M_{11}+2M_{21}+2M_{31}-2}, \\ & \quad \mathbf{m}_{k+3M_{11}+2M_{21}+2M_{31}-1}) = 0, \\ & \mathbf{f}^{(3c)}(\mathbf{m}_{k+3M_{11}+2M_{21}+2M_{31}-1}, \\ & \quad \mathbf{m}_{k+3M_{11}+2M_{21}+2M_{31}}) = 0; \end{aligned} \tag{82(1-3)}$$

$$\begin{aligned} & \mathbf{f}^{(4a)}(\mathbf{m}_{k+3M_{11}+2M_{21}+2M_{31}}, \\ & \quad \mathbf{m}_{k+3M_{11}+2M_{21}+2M_{31}+1}) = 0, \\ & \mathbf{f}^{(7c)}(\mathbf{m}_{k+3M_{11}+2M_{21}+2M_{31}+1}, \\ & \quad \mathbf{m}_{k+3M_{11}+2M_{21}+2M_{31}+2}) = 0, \ldots, \\ & \mathbf{f}^{(4a)}(\mathbf{m}_{k+3M_{11}+2M_{21}+2M_{31}+2M_{41}-2}, \\ & \quad \mathbf{m}_{k+3M_{11}+2M_{21}+2M_{31}+2M_{41}-1}) = 0, \\ & \mathbf{f}^{(7c)}(\mathbf{m}_{k+3M_{11}+2M_{21}+2M_{31}+2M_{41}-1}, \\ & \quad \mathbf{m}_{k+3M_{11}+2M_{21}+2M_{31}+2M_{41}}) = 0; \end{aligned} \tag{82(1-4)}$$

$$\mathbf{f}^{(4a)}(\mathbf{m}_{k+3M_{11}+2M_{21}+2M_{31}+2M_{41}},\ \mathbf{m}_{k+3M_{11}+2M_{21}+2M_{31}+2M_{41}+1})=0,$$
$$\mathbf{f}^{(5c)}(\mathbf{m}_{k+3M_{11}+2M_{21}+2M_{31}+2M_{41}+1},\ \mathbf{m}_{k+3M_{11}+2M_{21}+2M_{31}+2M_{41}+2})=0,$$
$$\mathbf{f}^{(6a)}(\mathbf{m}_{k+3M_{11}+2M_{21}+2M_{31}+2M_{41}+2},\ \mathbf{m}_{k+3M_{11}+2M_{21}+2M_{31}+2M_{41}+3})=0,$$
$$\mathbf{f}^{(7c)}(\mathbf{m}_{k+3M_{11}+2M_{21}+2M_{31}+2M_{41}+3},\ \mathbf{m}_{k+3M_{11}+2M_{21}+2M_{31}+2M_{41}+4})=0,\ldots,$$
$$\mathbf{f}^{(4a)}(\mathbf{m}_{k+3M_{11}+2M_{21}+2M_{31}+2M_{41}+4M_{51}-4},\ \mathbf{m}_{k+3M_{11}+2M_{21}+2M_{31}+2M_{41}+4M_{51}-3})=0,$$
$$\mathbf{f}^{(5c)}(\mathbf{m}_{k+3M_{11}+2M_{21}+2M_{31}+2M_{41}+4M_{51}-3},\ \mathbf{m}_{k+3M_{11}+2M_{21}+2M_{31}+2M_{41}+4M_{51}-2})=0,$$
$$\mathbf{f}^{(6a)}(\mathbf{m}_{k+3M_{11}+2M_{21}+2M_{31}+2M_{41}+4M_{51}-2},\ \mathbf{m}_{k+3M_{11}+2M_{21}+2M_{31}+2M_{41}+4M_{51}-1})=0,$$
$$\mathbf{f}^{(7c)}(\mathbf{m}_{k+3M_{11}+2M_{21}+2M_{31}+2M_{41}+4M_{51}-1},\ \mathbf{m}_{k+3M_{11}+2M_{21}+2M_{31}+2M_{41}+4M_{51}})=0;\quad (82(1\text{-}5))$$

$$\vdots$$

$$\mathbf{f}^{(1b)}(\mathbf{m}_{k+3\sum_{i=1}^{s-1}M_{1i}+2\sum_{i=1}^{s-1}M_{2i}+2\sum_{i=1}^{s-1}M_{3i}+2\sum_{i=1}^{s-1}M_{4i}+4\sum_{i=1}^{s-1}M_{5i}},\ \mathbf{m}_{k+3\sum_{i=1}^{s-1}M_{1i}+2\sum_{i=1}^{s-1}M_{2i}+2\sum_{i=1}^{s-1}M_{3i}+2\sum_{i=1}^{s-1}M_{4i}+4\sum_{i=1}^{s-1}M_{5i}+1})=0,$$
$$\mathbf{f}^{(1a)}(\mathbf{m}_{k+3\sum_{i=1}^{s-1}M_{1i}+2\sum_{i=1}^{s-1}M_{2i}+2\sum_{i=1}^{s-1}M_{3i}+2\sum_{i=1}^{s-1}M_{4i}+4\sum_{i=1}^{s-1}M_{5i}+1},\ \mathbf{m}_{k+3\sum_{i=1}^{s-1}M_{1i}+2\sum_{i=1}^{s-1}M_{2i}+2\sum_{i=1}^{s-1}M_{3i}+2\sum_{i=1}^{s-1}M_{4i}+4\sum_{i=1}^{s-1}M_{5i}+2})=0,$$
$$\mathbf{f}^{(1c)}(\mathbf{m}_{k+3\sum_{i=1}^{s-1}M_{1i}+2\sum_{i=1}^{s-1}M_{2i}+2\sum_{i=1}^{s-1}M_{3i}+2\sum_{i=1}^{s-1}M_{4i}+4\sum_{i=1}^{s-1}M_{5i}+2},\ \mathbf{m}_{k+3\sum_{i=1}^{s-1}M_{1i}+2\sum_{i=1}^{s-1}M_{2i}+2\sum_{i=1}^{s-1}M_{3i}+2\sum_{i=1}^{s-1}M_{4i}+4\sum_{i=1}^{s-1}M_{5i}+3})=0,\ldots,$$

$$\mathbf{f}^{(1b)}(\mathbf{m}_{k+3\sum_{i=1}^{s}M_{1i}+2\sum_{i=1}^{s-1}M_{2i}+2\sum_{i=1}^{s-1}M_{3i}+2\sum_{i=1}^{s-1}M_{4i}+4\sum_{i=1}^{s-1}M_{5i}-3},\ \mathbf{m}_{k+3\sum_{i=1}^{s}M_{1i}+2\sum_{i=1}^{s-1}M_{2i}+2\sum_{i=1}^{s-1}M_{3i}+2\sum_{i=1}^{s-1}M_{4i}+4\sum_{i=1}^{s-1}M_{5i}-2})=0,$$
$$\mathbf{f}^{(1a)}(\mathbf{m}_{k+3\sum_{i=1}^{s-1}M_{1i}+2\sum_{i=1}^{s-1}M_{2i}+2\sum_{i=1}^{s-1}M_{3i}+2\sum_{i=1}^{s-1}M_{4i}+4\sum_{i=1}^{s-1}M_{5i}-2},\ \mathbf{m}_{k+3\sum_{i=1}^{s}M_{1i}+2\sum_{i=1}^{s-1}M_{2i}+2\sum_{i=1}^{s-1}M_{3i}+2\sum_{i=1}^{s-1}M_{4i}+4\sum_{i=1}^{s-1}M_{5i}-1})=0,$$
$$\mathbf{f}^{(1c)}(\mathbf{m}_{k+3\sum_{i=1}^{s-1}M_{1i}+2\sum_{i=1}^{s-1}M_{2i}+2\sum_{i=1}^{s-1}M_{3i}+2\sum_{i=1}^{s-1}M_{4i}+4\sum_{i=1}^{s-1}M_{5i}-1},\ \mathbf{m}_{k+3\sum_{i=1}^{s}M_{1i}+2\sum_{i=1}^{s-1}M_{2i}+2\sum_{i=1}^{s-1}M_{3i}+2\sum_{i=1}^{s-1}M_{4i}+4\sum_{i=1}^{s-1}M_{5i}})=0;\quad (82(s\text{-}1))$$

$$\mathbf{f}^{(2a)}(\mathbf{m}_{k+3\sum_{i=1}^{s}M_{1i}+2\sum_{i=1}^{s-1}M_{2i}+2\sum_{i=1}^{s-1}M_{3i}+2\sum_{i=1}^{s-1}M_{4i}+4\sum_{i=1}^{s-1}M_{5i}},\ \mathbf{m}_{k+3\sum_{i=1}^{s}M_{1i}+2\sum_{i=1}^{s-1}M_{2i}+2\sum_{i=1}^{s-1}M_{3i}+2\sum_{i=1}^{s-1}M_{4i}+4\sum_{i=1}^{s-1}M_{5i}+1})=0,$$
$$\mathbf{f}^{(3c)}(\mathbf{m}_{k+3\sum_{i=1}^{s}M_{1i}+2\sum_{i=1}^{s-1}M_{2i}+2\sum_{i=1}^{s-1}M_{3i}+2\sum_{i=1}^{s-1}M_{4i}+4\sum_{i=1}^{s-1}M_{5i}+1},$$

$$
\begin{aligned}
&\mathbf{m}_{k+3\sum_{i=1}^{s} M_{1i}+2\sum_{i=1}^{s-1} M_{2i}} \\
&+2\sum_{i=1}^{s-1} M_{3i}+2\sum_{i=1}^{s-1} M_{4i} \\
&+4\sum_{i=1}^{s-1} M_{5i}+2) = 0, \ldots, \\
\mathbf{f}^{(2a)}(&\mathbf{m}_{k+3\sum_{i=1}^{s} M_{1i}+2\sum_{i=1}^{s} M_{2i}} \\
&+2\sum_{i=1}^{s-1} M_{3i}+2\sum_{i=1}^{s-1} M_{4i} \\
&+4\sum_{i=1}^{s-1} M_{5i}-2, \\
&\mathbf{m}_{k+3\sum_{i=1}^{s} M_{1i}+2\sum_{i=1}^{s} M_{2i}} \\
&+2\sum_{i=1}^{s-1} M_{3i}+2\sum_{i=1}^{s-1} M_{4i} \\
&+4\sum_{i=1}^{s-1} M_{5i}-1) = 0, \\
\mathbf{f}^{(3c)}(&\mathbf{m}_{k+3\sum_{i=1}^{s} M_{1i}+2\sum_{i=1}^{s} M_{2i}} \\
&+2\sum_{i=1}^{s-1} M_{3i}+2\sum_{i=1}^{s-1} M_{4i} \\
&+4\sum_{i=1}^{s-1} M_{5i}-1, \\
&\mathbf{m}_{k+3\sum_{i=1}^{s} M_{1i}+2\sum_{i=1}^{s} M_{2i}} \\
&+2\sum_{i=1}^{s-1} M_{3i}+2\sum_{i=1}^{s-1} M_{4i} \\
&+4\sum_{i=1}^{s-1} M_{5i}) = 0;
\end{aligned}
\tag{82(s-2)}
$$

$$
\begin{aligned}
\mathbf{f}^{(8a)}(&\mathbf{m}_{k+3\sum_{i=1}^{s} M_{1i}+2\sum_{i=1}^{s} M_{2i}} \\
&+2\sum_{i=1}^{s-1} M_{3i}+2\sum_{i=1}^{s-1} M_{4i} \\
&+4\sum_{i=1}^{s-1} M_{5i}, \\
&\mathbf{m}_{k+3\sum_{i=1}^{s} M_{1i}+2\sum_{i=1}^{s} M_{2i}} \\
&+2\sum_{i=1}^{s-1} M_{3i}+2\sum_{i=1}^{s-1} M_{4i} \\
&+4\sum_{i=1}^{s-1} M_{5i}+1) = 0, \\
\mathbf{f}^{(3c)}(&\mathbf{m}_{k+3\sum_{i=1}^{s} M_{1i}+2\sum_{i=1}^{s} M_{2i}} \\
&+2\sum_{i=1}^{s-1} M_{3i}+2\sum_{i=1}^{s-1} M_{4i} \\
&+4\sum_{i=1}^{s-1} M_{5i}+1, \\
&\mathbf{m}_{k+3\sum_{i=1}^{s} M_{1i}+2\sum_{i=1}^{s} M_{2i}} \\
&+2\sum_{i=1}^{s-1} M_{3i}+2\sum_{i=1}^{s-1} M_{4i} \\
&+4\sum_{i=1}^{s-1} M_{5i}+2) = 0, \ldots, \\
\mathbf{f}^{(8a)}(&\mathbf{m}_{k+3\sum_{i=1}^{s} M_{1i}+2\sum_{i=1}^{s} M_{2i}} \\
&+2\sum_{i=1}^{s} M_{3i}+2\sum_{i=1}^{s-1} M_{4i} \\
&+4\sum_{i=1}^{s-1} M_{5i}-2, \\
&\mathbf{m}_{k+3\sum_{i=1}^{s} M_{1i}+2\sum_{i=1}^{s} M_{2i}} \\
&+2\sum_{i=1}^{s} M_{3i}+2\sum_{i=1}^{s-1} M_{4i} \\
&+4\sum_{i=1}^{s-1} M_{5i}-1) = 0, \\
\mathbf{f}^{(3c)}(&\mathbf{m}_{k+3\sum_{i=1}^{s} M_{1i}+2\sum_{i=1}^{s} M_{2i}} \\
&+2\sum_{i=1}^{s} M_{3i}+2\sum_{i=1}^{s-1} M_{4i} \\
&+4\sum_{i=1}^{s-1} M_{5i}-1, \\
&\mathbf{m}_{k+3\sum_{i=1}^{s} M_{1i}+2\sum_{i=1}^{s} M_{2i}} \\
&+2\sum_{i=1}^{s} M_{3i}+2\sum_{i=1}^{s-1} M_{4i} \\
&+4\sum_{i=1}^{s-1} M_{5i}) = 0;
\end{aligned}
\tag{82(s-3)}
$$

$$
\begin{aligned}
\mathbf{f}^{(4a)}(&\mathbf{m}_{k+3\sum_{i=1}^{s} M_{1i}+2\sum_{i=1}^{s} M_{2i}} \\
&+2\sum_{i=1}^{s} M_{3i}+2\sum_{i=1}^{s-1} M_{4i} \\
&+4\sum_{i=1}^{s-1} M_{5i}, \\
&\mathbf{m}_{k+3\sum_{i=1}^{s} M_{1i}+2\sum_{i=1}^{s} M_{2i}} \\
&+2\sum_{i=1}^{s} M_{3i}+2\sum_{i=1}^{s-1} M_{4i} \\
&+4\sum_{i=1}^{s-1} M_{5i}+1) = 0, \\
\mathbf{f}^{(7c)}(&\mathbf{m}_{k+3\sum_{i=1}^{s} M_{1i}+2\sum_{i=1}^{s} M_{2i}} \\
&+2\sum_{i=1}^{s} M_{3i}+2\sum_{i=1}^{s-1} M_{4i} \\
&+4\sum_{i=1}^{s-1} M_{5i}+1, \\
&\mathbf{m}_{k+3\sum_{i=1}^{s} M_{1i}+2\sum_{i=1}^{s} M_{2i}} \\
&+2\sum_{i=1}^{s} M_{3i}+2\sum_{i=1}^{s-1} M_{4i} \\
&+4\sum_{i=1}^{s-1} M_{5i}+2) = 0, \ldots, \\
\mathbf{f}^{(4a)}(&\mathbf{m}_{k+3\sum_{i=1}^{s} M_{1i}+2\sum_{i=1}^{s} M_{2i}} \\
&+2\sum_{i=1}^{s} M_{3i}+2\sum_{i=1}^{s} M_{4i} \\
&+4\sum_{i=1}^{s-1} M_{5i}-2, \\
&\mathbf{m}_{k+3\sum_{i=1}^{s} M_{1i}+2\sum_{i=1}^{s} M_{2i}} \\
&+2\sum_{i=1}^{s} M_{3i}+2\sum_{i=1}^{s} M_{4i} \\
&+4\sum_{i=1}^{s-1} M_{5i}-1) = 0, \\
\mathbf{f}^{(7c)}(&\mathbf{m}_{k+3\sum_{i=1}^{s} M_{1i}+2\sum_{i=1}^{s} M_{2i}} \\
&+2\sum_{i=1}^{s} M_{3i}+2\sum_{i=1}^{s} M_{4i} \\
&+4\sum_{i=1}^{s-1} M_{5i}-1, \\
&\mathbf{m}_{k+3\sum_{i=1}^{s} M_{1i}+2\sum_{i=1}^{s} M_{2i}} \\
&+2\sum_{i=1}^{s} M_{3i}+2\sum_{i=1}^{s} M_{4i} \\
&+4\sum_{i=1}^{s-1} M_{5i}) = 0;
\end{aligned}
\tag{82(s-4)}
$$

$$
\begin{aligned}
&\mathbf{f}^{(4a)}(\mathbf{m}_{k+3\sum_{i=1}^{s} M_{1i}+2\sum_{i=1}^{s} M_{2i}+2\sum_{i=1}^{s} M_{3i}} \\
&\quad +2\sum_{i=1}^{s} M_{4i}+4\sum_{i=1}^{s-1} M_{5i}, \\
&\quad \mathbf{m}_{k+3\sum_{i=1}^{s} M_{1i}+2\sum_{i=1}^{s} M_{2i}+2\sum_{i=1}^{s} M_{3i}} \\
&\quad +2\sum_{i=1}^{s-1} M_{4i}+4\sum_{i=1}^{s-1} M_{5i}+1) = 0, \\
&\mathbf{f}^{(5c)}(\mathbf{m}_{k+3\sum_{i=1}^{s} M_{1i}+2\sum_{i=1}^{s} M_{2i}+2\sum_{i=1}^{s} M_{3i}} \\
&\quad +2\sum_{i=1}^{s} M_{4i}+4\sum_{i=1}^{s-1} M_{5i}+1, \\
&\quad \mathbf{m}_{k+3\sum_{i=1}^{s} M_{1i}+2\sum_{i=1}^{s} M_{2i}+2\sum_{i=1}^{s} M_{3i}} \\
&\quad +2\sum_{i=1}^{s-1} M_{4i}+4\sum_{i=1}^{s-1} M_{5i}+2) = 0, \\
&\mathbf{f}^{(6a)}(\mathbf{m}_{k+3\sum_{i=1}^{s} M_{1i}+2\sum_{i=1}^{s} M_{2i}+2\sum_{i=1}^{s} M_{3i}} \\
&\quad +2\sum_{i=1}^{s} M_{4i}+4\sum_{i=1}^{s-1} M_{5i}+1, \\
&\quad \mathbf{m}_{k+3\sum_{i=1}^{s} M_{1i}+2\sum_{i=1}^{s} M_{2i}+2\sum_{i=1}^{s} M_{3i}} \\
&\quad +2\sum_{i=1}^{s-1} M_{4i}+4\sum_{i=1}^{s-1} M_{5i}+2) = 0, \\
&\mathbf{f}^{(7c)}(\mathbf{m}_{k+3\sum_{i=1}^{s} M_{1i}+2\sum_{i=1}^{s} M_{2i}+2\sum_{i=1}^{s} M_{3i}} \\
&\quad +2\sum_{i=1}^{s} M_{4i}+4\sum_{i=1}^{s-1} M_{5i}+3, \\
&\quad \mathbf{m}_{k+3\sum_{i=1}^{s} M_{1i}+2\sum_{i=1}^{s} M_{2i}+2\sum_{i=1}^{s} M_{3i}} \\
&\quad +2\sum_{i=1}^{s-1} M_{4i}+4\sum_{i=1}^{s-1} M_{5i}+4) = 0, \ldots, \\
&\mathbf{f}^{(4a)}(\mathbf{m}_{k+3\sum_{i=1}^{s} M_{1i}+2\sum_{i=1}^{s} M_{2i}+2\sum_{i=1}^{s} M_{3i}} \\
&\quad +2\sum_{i=1}^{s} M_{4i}+4\sum_{i=1}^{s} M_{5i}-4, \\
&\quad \mathbf{m}_{k+3\sum_{i=1}^{s} M_{1i}+2\sum_{i=1}^{s} M_{2i}+2\sum_{i=1}^{s} M_{3i}} \\
&\quad +2\sum_{i=1}^{s-1} M_{4i}+4\sum_{i=1}^{s} M_{5i}-3) = 0, \\
&\mathbf{f}^{(5c)}(\mathbf{m}_{k+3\sum_{i=1}^{s} M_{1i}+2\sum_{i=1}^{s} M_{2i}+2\sum_{i=1}^{s} M_{3i}} \\
&\quad +2\sum_{i=1}^{s} M_{4i}+4\sum_{i=1}^{s} M_{5i}-3, \\
&\quad \mathbf{m}_{k+3\sum_{i=1}^{s} M_{1i}+2\sum_{i=1}^{s} M_{2i}+2\sum_{i=1}^{s} M_{3i}} \\
&\quad +2\sum_{i=1}^{s-1} M_{4i}+4\sum_{i=1}^{s} M_{5i}-2) = 0, \\
&\mathbf{f}^{(6a)}(\mathbf{m}_{k+3\sum_{i=1}^{s} M_{1i}+2\sum_{i=1}^{s} M_{2i}+2\sum_{i=1}^{s} M_{3i}} \\
&\quad +2\sum_{i=1}^{s} M_{4i}+4\sum_{i=1}^{s} M_{5i}-2, \\
&\quad \mathbf{m}_{k+3\sum_{i=1}^{s} M_{1i}+2\sum_{i=1}^{s} M_{2i}+2\sum_{i=1}^{s} M_{3i}} \\
&\quad +2\sum_{i=1}^{s-1} M_{4i}+4\sum_{i=1}^{s} M_{5i}-1) = 0, \\
&\mathbf{f}^{(7c)}(\mathbf{m}_{k+3\sum_{i=1}^{s} M_{1i}+2\sum_{i=1}^{s} M_{2i}+2\sum_{i=1}^{s} M_{3i}} \\
&\quad +2\sum_{i=1}^{s} M_{4i}+4\sum_{i=1}^{s} M_{5i}-1, \\
&\quad \mathbf{m}_{k+3\sum_{i=1}^{s} M_{1i}+2\sum_{i=1}^{s} M_{2i}+2\sum_{i=1}^{s} M_{3i}} \\
&\quad +2\sum_{i=1}^{s-1} M_{4i}+4\sum_{i=1}^{s} M_{5i}) = 0. \qquad (82\text{(s-5)})
\end{aligned}
$$

The periodic motion pertaining to such a mapping requires

$$
\begin{aligned}
&\mathbf{m}_{k+3\sum_{i=1}^{s} M_{1i}+2\sum_{i=1}^{s} M_{2i}+2\sum_{i=1}^{s} M_{3i}} \\
&\quad +2\sum_{i=1}^{s} M_{4i}+4\sum_{i=1}^{s} M_{5i} = \mathbf{m}_k, \qquad (83)
\end{aligned}
$$

i.e.,

$$
\begin{aligned}
&x^{(\alpha)}_{k+3\sum_{i=1}^{s} M_{1i}+2\sum_{i=1}^{s} M_{2i}+2\sum_{i=1}^{s} M_{3i}} \\
&\quad +2\sum_{i=1}^{s} M_{4i}+4\sum_{i=1}^{s} M_{5i} = x^{(\alpha)}_k, \\
&\dot{x}^{(\alpha)}_{k+3\sum_{i=1}^{s} M_{1i}+2\sum_{i=1}^{s} M_{2i}+2\sum_{i=1}^{s} M_{3i}} \\
&\quad +2\sum_{i=1}^{s} M_{4i}+4\sum_{i=1}^{s} M_{5i} = \dot{x}^{(\alpha)}_k, \\
&\Omega t_{k+3\sum_{i=1}^{s} M_{1i}+2\sum_{i=1}^{s} M_{2i}+2\sum_{i=1}^{s} M_{3i}} \\
&\quad +2\sum_{i=1}^{s} M_{4i}+4\sum_{i=1}^{s} M_{5i} = \Omega t_k + 2N\pi, \qquad (84)
\end{aligned}
$$

where N is a positive integer.

Solving Eqs. (82) and (83) or (84) can generate the switching sets for periodic motions. The proof is completed. □

6 Numerical simulations

The conditions of switching between one configuration to another one in the 2-DOF friction-induced oscillator with one-sided impact on a conveyer belt have been discussed in Sect. 4, and the corresponding mapping structures for periodic motions have been investigated in Sect. 5. To illustrate the analytical conditions for switchability more vividly, several kinds of motions such as stick motion, impact motion, grazing motion and periodic motions for the system will be demonstrated through the numerical simulations in this section. The trajectories in phase space, time history responses of displacement, velocity and force of per unit mass will be presented in Figs. 10, 11, 12, 13, 14, and 15a, b, c and d, respectively. In these pictures, the velocity boundary $\partial\Omega_{12}^{(\alpha)}(\alpha \in \{1, 2\})$ and the displacement boundary $\partial\Omega_{i(+\infty)}^{(2)}(i \in \{1, 2\})$ are respectively depicted by black and blue thick dotted lines. The green filled dots and the hollow dots represent the starting points and the switching points of the corresponding motions, respectively. The responses of motion for the mass m_1 and mass m_2 are pictured by red curves and black curves, respectively. In Figs. 13 and 14d–f, the red and blue lines represent the forces in domains $\Omega_1^{(1)}$ and $\Omega_2^{(1)}$ for the mass m_1, and the forces in domains $\Omega_1^{(2)}$ and $\Omega_2^{(2)}$ for the mass m_2 are denoted by black and purple lines.

Consider a set of system parameters as $m_1 = 4$ kg, $m_2 = 1$ kg, $k_1 = 4$ N/m, $k_2 = 1$ N/m, $r_1 = 0.05$ N/m^2, $r_2 = 0.5$ N/m^2, $B_1 = -15$ N, $B_2 = 15$ N, $\varphi_1 = 0$ rad, $\varphi_2 = 0$ rad, $A_1 = 0$ N, $A_2 = 0$ N, $\Omega = 2.25$ rad/s, $\mu_k = 0.55$, $\mu_s = 0.654$; $g = 9.8$ m/s^2, $V = 2$ m/s, $d = 5$ m to establish a stick motion of the mass m_1. The trajectories in phase plane, time histories of displacement, velocity, force of per unit mass and the first-order force of per unit mass are shown in Fig. 10a–e with the initial conditions $t_0 = 2.8363$ s, $x_{10} = -4.7155$ m, $\dot{x}_{10} = 5.1647$ m/s, $x_{20} = -8.1777$ m, $\dot{x}_{20} = 2$ m/s. In the group of pictures, the appearance and vanishing points of stick motion are signed by yellow and blue filled circles, respectively, the regions shaded by gray color represent the stick areas. In Fig. 10d, the forces for the mass m_1 in domains $\Omega_1^{(1)}$ and $\Omega_2^{(1)}$ are described by red and blue lines, respectively. And for the mass m_2, the forces $F_2^{(1)}$ and $F_2^{(2)}$ are depicted by black and purple lines, respectively. For the first derivative of the force(first-order force for short) of the mass m_1 in Fig. 10e, the red line represents the first-order force in domain $\Omega_1^{(1)}$ and the blue line describes the first-order force in domain $\Omega_2^{(1)}$. It can be seen that the initial point for the mass m_2 is set on the velocity boundary $\partial\Omega_{12}^{(2)}$ from Fig. 10a. In the time interval (2.8363 s, 3.4265 s), the mass m_α moves in domain $\Omega_1^{(\alpha)}(\alpha \in \{1, 2\})$, and the velocities of the two masses are greater than that of the belt. At time $t = 3.4265$ s, the mass m_1 reaches to the velocity boundary $\partial\Omega_{12}^{(1)}$. And the forces of per unit mass are $F_1^{(1)} < 0$ and $F_1^{(2)} > 0$ for the mass m_1 at this moment. Therefore, the conditions of the stick motion appearing for the mass m_1 on the velocity boundary in Theorem 3 are satisfied. Since the coefficients of kinetic friction and static friction are different, the flow barriers exist in this dynamical system. The discontinuity of the friction force on the velocity boundary causes the existence of the stick motion along the boundary $\partial\Omega_{12}^{(1)}$. For simplicity, the notation $F_\alpha^{(0\succ 0_\lambda)}$ is used to instead of $F_\alpha^{(0\succ 0_\lambda)}(\mathbf{x}_m^{(\alpha)}, t_m, \tau^{(\lambda)})(\lambda, \alpha \in \{1, 2\})$. When the mass m_1 begins to stick with the belt, the kinetic friction force is changed to the static friction force between the mass and the belt. So the force of the boundary barrier $F_1^{(0\succ 0_\lambda)}(\lambda \in \{1, 2\})$ is used to judge the existence and vanishing of the stick motion. As shown in Fig. 10d, the forces of the boundary flow barrier are $F_1^{(0\succ 0_1)} < 0$ (red solid curve) and $F_1^{(0\succ 0_2)} > 0$ (blue solid curve) in the time interval (3.4265 s, 6.0642 s). In the process of the stick motion, the velocity of the mass m_1 is equal to the belt's, so the trajectory of the mass m_1 is a straight line as shown in Fig. 10a. At time $t = 6.0642$ s, the forces of the boundary flow barrier are $F_1^{(0\succ 0_2)} = 0$, $F_1^{(0\succ 0_1)} < 0$ and the first-order force of the boundary flow barrier is $DF_1^{(0\succ 0_2)} < 0$ (as shown in Fig. 10d and e). So the vanishing conditions of stick motion in Theorem 4 are satisfied, therefore the stick motion disappears at time $t = 6.0642$ s. When the stick motion vanishes on the velocity boundary $\partial\Omega_{12}^{(1)}$, the relative motion occurs between the mass m_1 and the belt, so the static friction force is changed to the kinetic friction force at once. From Fig. 10d, it can be observed that the corresponding force of per unit mass jumps from zero to a negative at time $t = 6.0642$ s. After this time, the mass m_1 enters into the domain $\Omega_2^{(1)}$ because the forces of per unit mass are $F_1^{(1)} < 0$ and $F_1^{(2)} < 0$ (as shown in Fig. 10d). At time $t = 6.2358$ s, the mass m_2 reaches to the velocity boundary $\partial\Omega_{12}^{(2)}$ again. In such process of the motion, the mass m_2 has passable motions on the velocity boundary $\partial\Omega_{12}^{(2)}$ with the mapping structure $p_3^{(2)} \circ p_1^{(2)}$.

Consider another set of system parameters as $m_1 = 4$ kg, $m_2 = 0.8$ kg, $k_1 = 10$ N/m, $k_2 = 3$ N/m, $r_1 = 2$ N/m^2, $r_2 = 2.5$ N/m^2, $B_1 = -20$ N, $B_2 = 5$ N, $\varphi_1 = 2.5$ rad, $\varphi_2 = 5.5$ rad, $A_1 = 2$ N, $A_2 = 10$ N, $\Omega = 1.1$ rad/s, $\mu_k = 0.25$, $g = 9.8$ m/s^2, $V = 2$ m/s, $d = 6$ m, $R = 0.75$ and the initial conditions $t_0 = 2.55$ s, $x_{10} = -5$ m, $\dot{x}_{10} = 2$ m/s, $x_{20} = -3$ m, $\dot{x}_{20} = 2$ m/s to determine the impact motion of the mass m_2. The process of the impact motion is shown in Fig. 11. In Fig. 11d, the forces $F_1^{(1)}$, $F_1^{(2)}$, $F_2^{(1)}$, $F_2^{(2)}$ are denoted by solid lines colored with red, blue, black and purple, respectively. The yellow filled circles represent the impact points in this group of figures. In Fig. 11a, the initial points of masses m_1 and m_2 are both set on the velocity boundary $\partial\Omega_{12}^{(\alpha)}$ $(\alpha \in \{1, 2\})$. After time $t = 2.55$ s, the two masses enter into the domain $\Omega_1^{(\alpha)}$ $(\alpha \in \{1, 2\})$, that is to say the velocities of the two masses are both greater than the belt's V (as shown in Fig. 11c). The motion of the mass m_2 exists in domain $\Omega_1^{(2)}$ until it reaches to the impact boundary $\partial\Omega_{1(+\infty)}^{(2)}$ at $t = 3.9796$ s. At this time, the mass m_2 impacts with the right-hand fixed rigid obstacle, and its velocity is greater than that of the belt. After impact, the direction of motion for the mass m_2 changes immediately, and the velocity of the mass m_2 after impact (as shown in Fig. 11a and c) can be computed by Eq. (12). In the

time interval (3.9796 s, 4.0339 s), the mass m_1 is still in domain $\Omega_1^{(1)}$ and the mass m_2 exists in domain $\Omega_2^{(2)}$. At time $t = 4.0339$ s, the mass m_1 reaches to the boundary $\partial\Omega_{12}^{(1)}$, the forces of per unit mass $F_1^{(1)}$ and $F_1^{(2)}$ are both less than zero (as shown in Fig. 11d), so the mass m_1 will pass through the velocity boundary and enter to domain $\Omega_2^{(1)}$ according to Theorem 1. The velocities of two masses are both less than the belt's V in the time interval (4.0339 s, 6.4372 s). At time $t = 6.4372$ s, the velocity of the mass m_1 is equal to the belt's, the mass m_1 reaches to the velocity boundary $\partial\Omega_{12}^{(1)}$ again. The mass m_1 has the passable motion with the mapping structure $p_3^{(1)} \circ p_1^{(1)}$ in the above process of motion. The impact motion about the system is just discussed here.

Using the group of system parameters as $m_1 = 4$ kg, $m_2 = 1$ kg, $k_1 = 4$ N/m, $k_2 = 1$ N/m, $r_1 = 0.05$ N/m^2, $r_2 = 0.5$ N/m^2, $B_1 = -15$ N, $B_2 = 15$ N, $\varphi_1 = 0$ rad, $\varphi_2 = 0$ rad, $A_1 = 0$ N, $A_2 = 0$ N, $\Omega = 1.5$ rad/s, $\mu_k = 0.65$, $g = 9.8$ m/s^2, $V = -26.5$ m/s, $d = 10$ m to describe a grazing motion for the mass m_2. Under the initial conditions $t_0 = 1s, x_{10} = 4.7155m, \dot{x}_{10} = -3$ m/s, $x_{20} = -4.5$ m, $\dot{x}_{20} = 5$ m/s, the corresponding pictures of the grazing motion are given in Fig. 12a–e. The force of per unit mass $F_\alpha^{(\lambda)}(\alpha, \lambda \in \{1, 2\})$ and the first-order force of per unit mass $DF_2^{(1)}$ are depicted in Fig. 12d and e, respectively. In the group of figures, the grazing points are pictured by purple filled dots. As shown in Fig. 12a, the initial points of the two masses are both set in domain $\Omega_1^{(\alpha)}$ $(\alpha \in \{1, 2\})$. After the initial time $t_0 = 1$ s, we can see that the velocity of the mass m_1 decreases at first and then increases, but the velocity of the mass m_2 increases at first and then decreases from Fig. 12c until time $t = 3.5643$ s. The mass m_2 reaches to the velocity boundary $\partial\Omega_{12}^{(2)}$ at time $t = 3.5643$ s, i.e., the velocity of the mass m_2 is equal to the belt's V, and the force of per unit mass is $F_2^{(1)} = 0$ and the first-order force of per unit mass is $DF_2^{(1)} > 0$. So the conditions of the grazing motion on the boundary $\partial\Omega_{12}^{(2)}$ in domain $\Omega_1^{(2)}$ are satisfied from Theorem 5 (i). After the time $t = 3.5643$ s, the mass m_2 returns to the domain $\Omega_1^{(2)}$ and the velocity of the mass m_2 is greater than that of the belt.

The process of passable periodic motion for the mass $m_\alpha(\alpha \in \{1, 2\})$ is pictured in Fig. 13a–f. This group of figures are obtained from the following system parameters and initial conditions: $m_1 = 4$ kg, $m_2 = 1kg$, $k_1 = 4$ N/m, $k_2 = 1$ N/m, $r_1 = 0.05$ N/m^2, $r_2 = 0.5$ N/m^2, $B_1 = 15$ N, $B_2 = -15$ N, $\varphi_1 = 0$ rad, $\varphi_2 = 0$ rad, $A_1 = 0$ N, $A_2 = 0$ N, $\Omega = 1.6$ rad/s, $\mu_k = 0.15$, $g = 9.8$ m/s^2, $V = 2$ m/s, $d = 10$ m, $t_0 = 2.5083$ s, $x_{10} = 3.1002$ m, $\dot{x}_{10} = -1.5826$ m/s, $x_{20} = -7.1436$ m, $\dot{x}_{20} = 2$ m/s. The velocity and displacement histories of the force of per unit mass $F_\alpha^{(\lambda)}$ $(\alpha, \lambda \in \{1, 2\})$ are depicted in Fig. 13e and f, respectively. For the mass m_1, the initial point is placed in the domain $\Omega_2^{(1)}$, and the initial point for the mass m_2 is set on the velocity boundary $\partial\Omega_{12}^{(2)}$ (as shown in Fig. 13a). At the initial time $t_0 = 2.5083$ s, it is clearly seen that the mass m_2 satisfies the passable conditions $F_2^{(\lambda)} > 0(\lambda = 1, 2)$ on the velocity boundary in Theorem 1 from Fig. 13d, so the mass m_2 enters to the domain $\Omega_1^{(2)}$ after the initial time. In the time interval (2.5083 s, 4.2669 s), the velocity decreases at first and then increases for the mass m_1 but it is just the opposite for the mass m_2 (as shown in Fig. 13c). At time $t = 4.2669$ s, the mass m_2 reaches to the velocity boundary $\partial\Omega_{12}^{(2)}$ again and then the mass m_2 will pass through the velocity boundary and enter to the domain $\Omega_2^{(2)}$ according to Theorem 1 because the forces of per unit mass satisfy $F_2^{(\lambda)} < 0(\lambda = 1, 2)$ (as shown in Fig. 13d). At time $t = 4.438$ s, the mass m_1 reaches to the velocity boundary and the forces of per unit mass are $F_1^{(\lambda)} > 0(\lambda = 1, 2)$ (as shown in Fig. 13d). So the mass m_1 will enter to the domain $\Omega_1^{(1)}$ at the next time. In the time interval $(4.438s, 5.8505$ s), the velocity of the mass m_1 is greater than that of the belt, and it is equal to the velocity of the belt at time $t = 5.8505$ s. That is to say, the mass m_1 touches to the velocity boundary at this time. At time $t = 6.4353$ s, the two masses m_1 and m_2 return to the initial points. Then the next periodic motion begins, the corresponding trajectories of the two masses are completely coincide with the ones in the previous period (as shown in Fig. 13a or b and c). At time $t = 10.3623$ s, the second periodic motion finishes. The periodic motion will continue and remain the same as before. From Fig. 13e and f, the periodicity of motion can be also observed.

By using the system parameters $m_1 = 4$ kg, $m_2 = 1$ kg, $k_1 = 3$ N/m, $k_2 = 1$ N/m, $r_1 = 0.05$ N/m^2, $r_2 = 0.5$ N/m^2, $B_1 = 20$ N, $B_2 = -15$ N, $\varphi_1 = 0$ rad, $\varphi_2 = 0$ rad, $A_1 = 0$ N, $A_2 = 0$ N, $\Omega = 1.65$ rad/s, $\mu_k = 0.15$, $g = 9.8$ m/s^2, $V = 2$ m/s, $d = 6$ m, $R = 0.75$ and the initial conditions $t_0 = 2.1783$ s, $x_{10} = 0.945$ m, $\dot{x}_{10} = 0.025$ m/s, $x_{20} = -17$ m, $\dot{x}_{20} = 2$ m/s, the impact periodic motion for the mass m_2 and

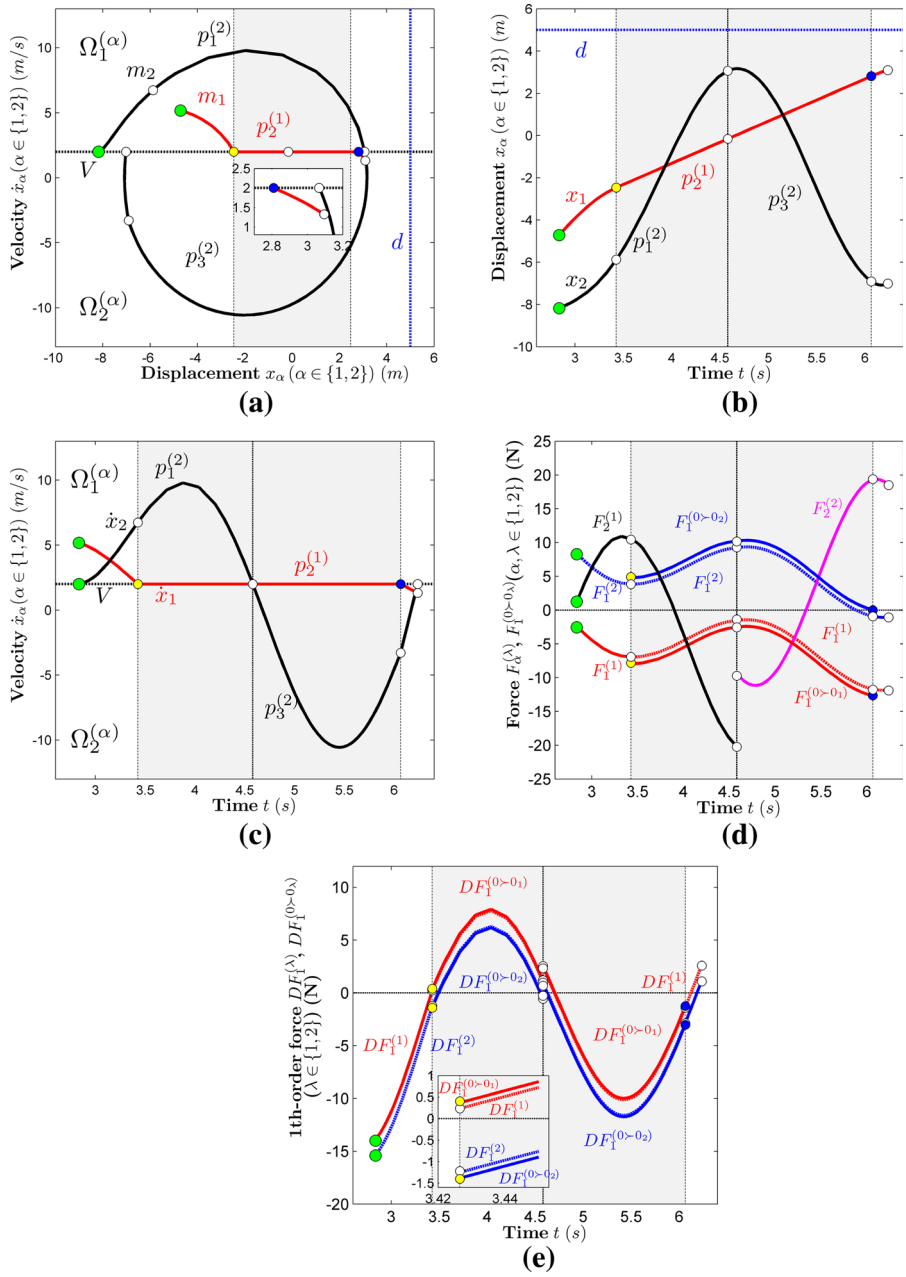

Fig. 10 Numerical simulation of the stick motion for the mass m_1: **a** phase trajectory, **b** displacement–time history, **c** velocity–time history, **d** force of per unit mass–time history, **e** first-order force of per unit mass–time history. (Color figure online)

the passable periodic motion for the mass m_1 are illustrated by Fig. 14a–f. To observe the variation tendency of per unit mass force more widely, the velocity history of the force of per unit mass and the displacement history of the force of per unit mass are given in Fig. 14e and f. In this group of figures, the yellow filled circles represent the impact points. It can be seen that the initial point for the mass m_2 is set on the velocity boundary $\partial\Omega_{12}^{(2)}$. At the time $t_0 = 2.1783$ s, the velocity of the mass m_1 is less than the belt's V, and the velocity of the mass m_2 is equal to the velocity of the belt (as shown in Fig. 14a and c) and the forces of per unit mass are $F_2^{(\lambda)} > 0(\lambda = 1, 2)$ (as shown in Fig. 14d) for the mass m_2, so the mass m_2 enters to the domain $\Omega_1^{(2)}$ after time $t = 2.1783$ s (referring to Theorem 1). At time $t = 3.8229$ s, the displacement of the mass m_2 is equal to the distance d, that is to say the mass m_2 touches with the fixed rigid obstacle on the right hand

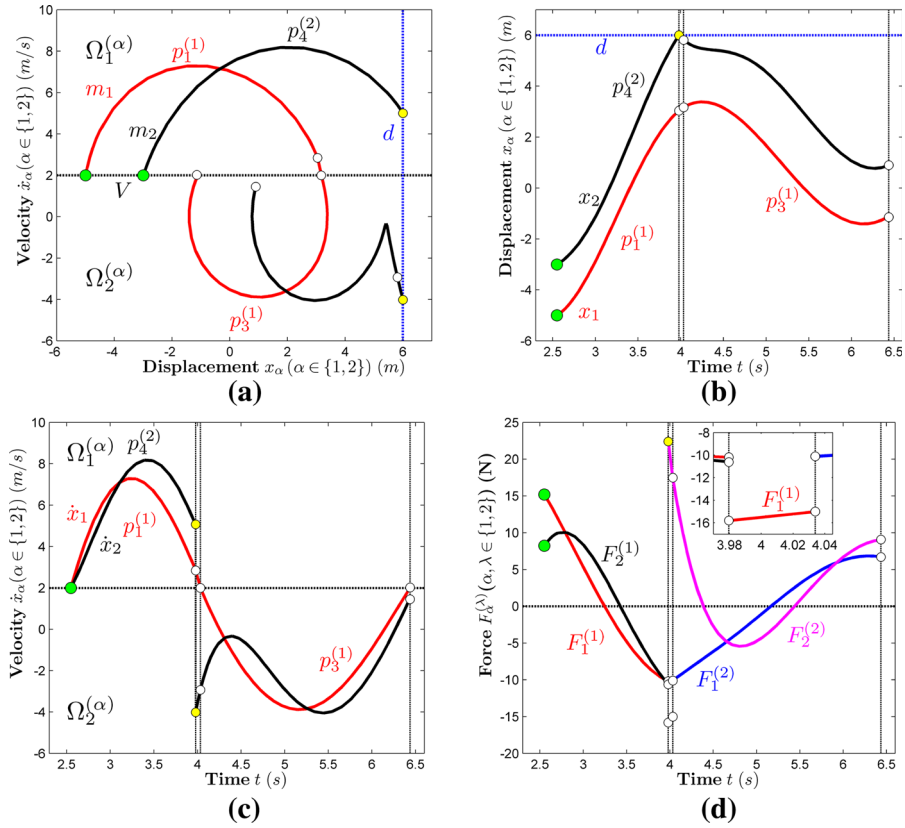

Fig. 11 Numerical simulation of the impact motion for the mass m_2: **a** phase trajectory, **b** displacement–time history, **c** velocity–time history, **d** force of per unit mass–time history. (Color figure online)

(as shown in Fig. 14b), and the velocity of the mass m_2 is greater than the belt's (as shown in Fig. 14c), so the impact motion occurs. The mass m_2 impacts with the fixed rigid obstacle at time $t = 3.8229$ s, and leaves the obstacle immediately. The velocity of the mass m_2 after impact can be computed by Eq. (12). After time $t = 3.8229$ s, the velocity's direction of the mass m_2 is changed to negative. From Fig. 14a and c, the trajectory of the mass $m_\alpha(\alpha \in \{1, 2\})$ exists in the domain $\Omega_2^{(\alpha)}(\alpha \in \{1, 2\})$ in the time interval (3.8229 s, 4.3028 s). The mass m_1 reaches to the velocity boundary $\partial\Omega_{12}^{(1)}$ at time $t = 4.3028$ s. At this time, the forces of per unit mass $F_1^{(1)}$ and $F_1^{(2)}$ are both greater than zero (as shown in Fig. 14d). So the mass m_1 comes into the domain $\Omega_1^{(1)}$ after time $t = 4.3028$ s by Theorem 1. The mass m_1 arrives at the velocity boundary again at time $t = 5.5453$ s and passes through the velocity boundary after this time. In the time interval (5.5453 s, 5.9863 s), the two masses move in the domain $\Omega_2^{(\alpha)}(\alpha \in \{1, 2\})$. At time $t = 5.9863$ s, the mass m_2 reaches to the velocity boundary and the two masses return to their respective starting points. The first periodic motion finishes at this time. The second periodic motion begins at the same time, and the trajectories of the two masses stay the same with the ones in the first periodic motion (as shown in Fig. 14b–f). At time $t = 9.7943$ s, the third periodic motion starts and keeps the same trajectories as before. In addition, the periodicity of motion for the masses m_1(with passable motion) and m_2 (with impact motion) can be also seen from Fig. 14e and f.

Consider the stick periodic motion of the mass m_2 with the mapping structure $p_2^{(2)} \circ p_3^{(2)} \circ p_2^{(2)} \circ p_1^{(2)}$ and a passable periodic motion of the mass m_1 with the initial conditions $t_0 = 16.7595$ s, $x_{10} = 0.7652$ m, $\dot{x}_{10} = -0.3045$ m/s, $x_{20} = 0.7285$ m, $\dot{x}_{20} = 2$ m/s. The frequency is $\Omega = 0.2$ rad/s, the static friction coefficient is $\mu_s = 0.18$, the kinetic friction coefficient is $\mu_k = 0.13$ and the distance between the mass m_2 and the fixed rigid obstacle on the right hand is $d = 22$ m. The rest system parameters are the same as the example in Fig. 13. The corresponding pictures of the stick periodic motion are expressed in Fig. 15a–g, where Figs. 15d–15g are the force and first-order force of per unit mass–time histories, the velocity and displacement histories

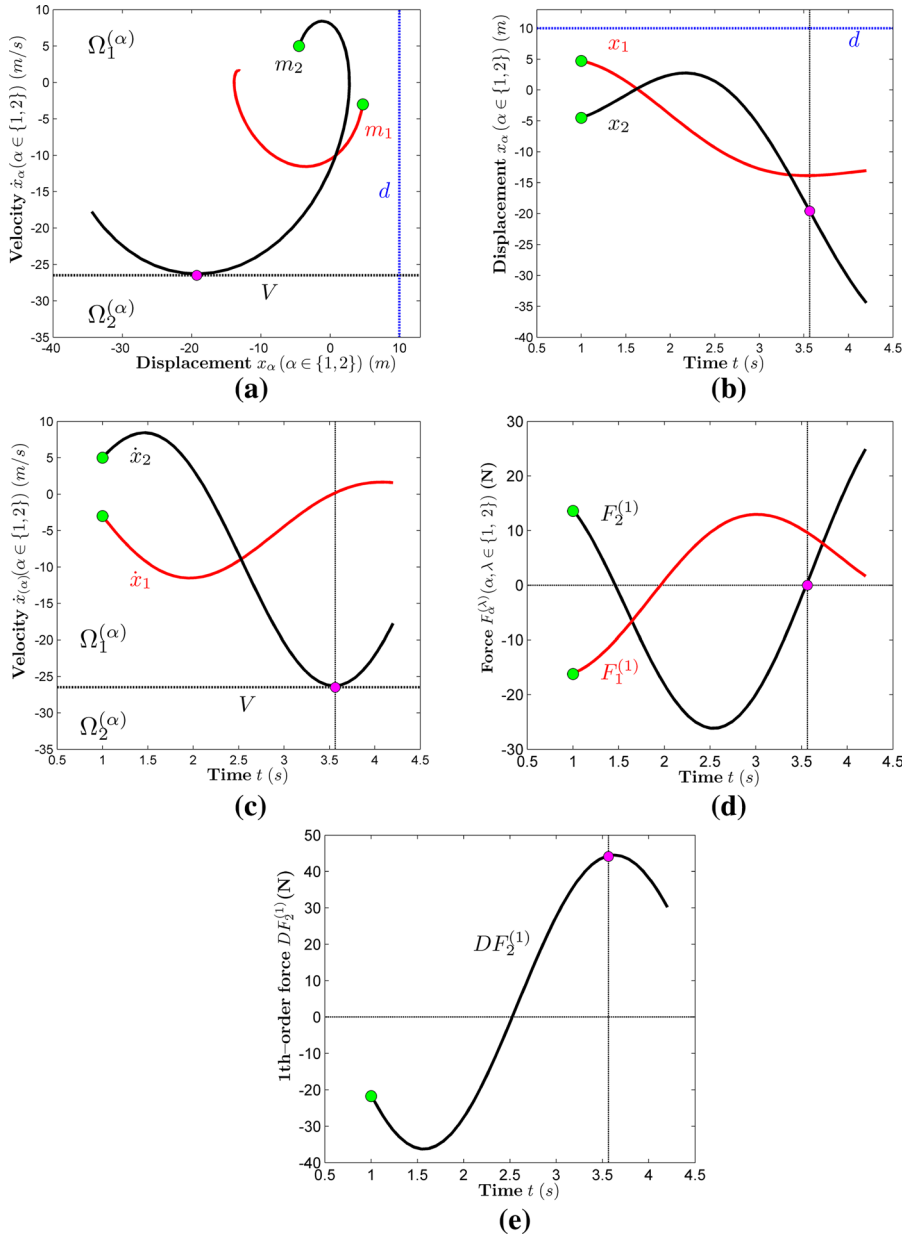

Fig. 12 Numerical simulation of the grazing motion for the mass m_2: **a** phase trajectory, **b** displacement–time history, **c** velocity–time history, **d** force of per unit mass–time history, **e** first-order force of per unit mass–time history. (Color figure online)

of force of per unit mass for the mass m_2, respectively. In the group of figures, the yellow filled circle and the blue filled circle represent the starting and vanishing points of stick motion, respectively. And the stick domains for the mass m_2 are filled by the gray color. In Fig. 15d–g, the forces and first-order forces of per unit mass in domains $\Omega_1^{(2)}$ and $\Omega_2^{(2)}$ for the mass m_2 are represented by black and purple lines, respectively. In the whole process of motion, the mass m_1 always stays in the domain $\Omega_2^{(1)}$. At the initial time $t_0 = 16.7595$ s, the starting point of the mass m_2 is fixed on the velocity boundary $\partial\Omega_{12}^{(2)}$. And the forces of per unit mass $F_2^{(1)}$ and $F_2^{(2)}$ are both greater than zero from Fig. 15d. So the conditions of passable motion in Theorem 1 are satisfied. The mass m_2 enters into the domain $\Omega_1^{(2)}$ after time $t_0 = 16.7595$ s. It exists in the domain $\Omega_1^{(2)}$ in the time interval (16.7595 s, 21.5693 s) and reaches to the velocity boundary again at time $t = 21.5693$ s. The forces of per unit mass are $F_2^{(1)} < 0$ and $F_2^{(2)} > 0$ (as shown in Fig. 15d) at this time, so the stick motion

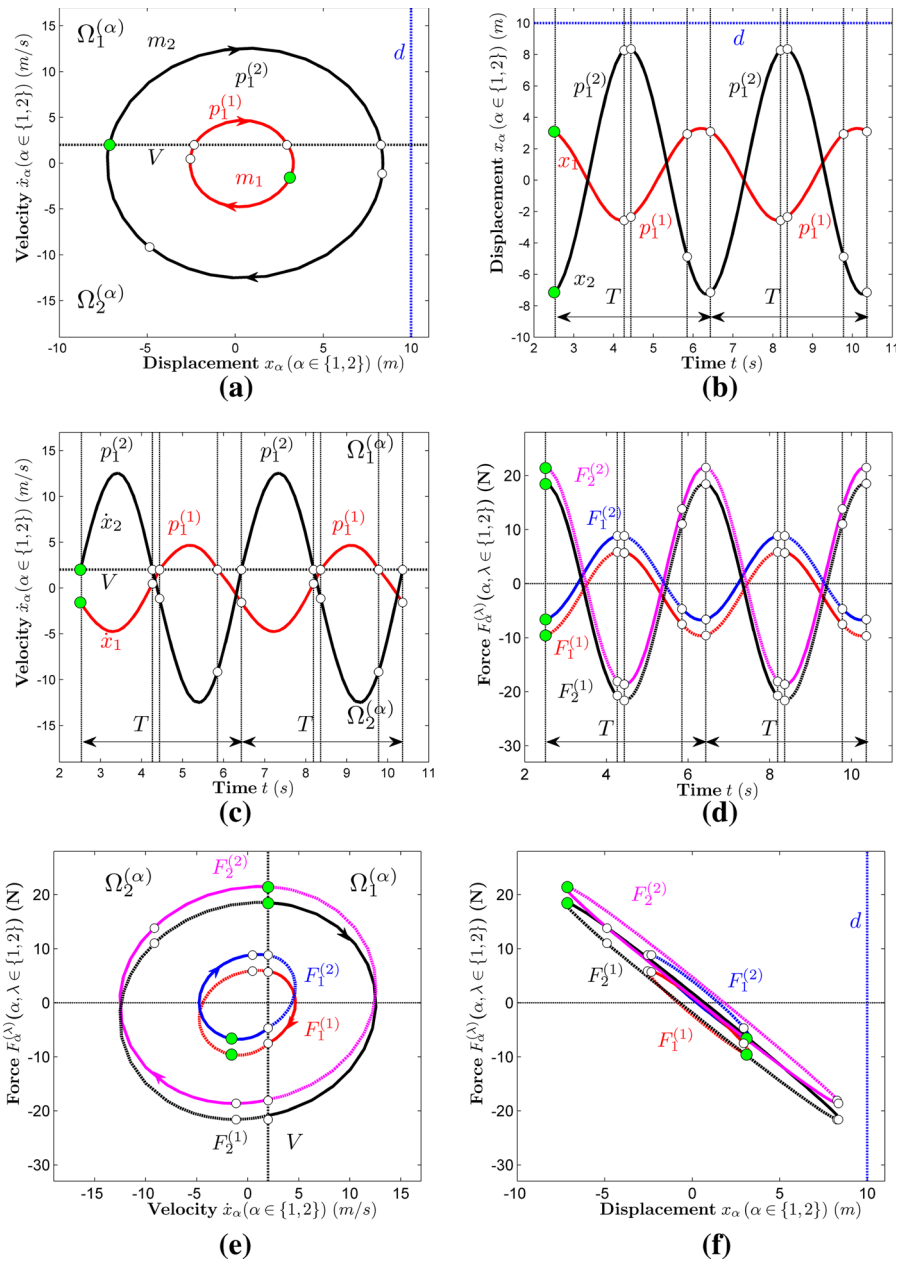

Fig. 13 Numerical simulation of the passable periodic motion for the mass $m_\alpha(\alpha \in \{1, 2\})$: **a** phase trajectory, **b** displacement–time history, **c** velocity–time history, **d** force of per unit mass–time history, **e** force of per unit mass–velocity history, **f** force of per unit mass–displacement history. (Color figure online)

of the mass m_2 appears according to Theorem 3, i.e., the relative motion between the mass m_2 and the belt does not exist. So the friction force between the mass and the belt is changed to static friction force at the stick stage, and the flow barrier is formed. In the time interval (21.5693 s, 23.1805 s), the forces of boundary flow barrier $F_2^{(0\succ 0_1)} < 0$ and $F_2^{(0\succ 0_2)} > 0$ (as shown in Fig. 15d), so the stick motion exists according to Theorem 2. As shown in Fig. 15d and e, it is obviously observed that the forces of boundary flow barrier are $F_2^{(0\succ 0_1)} < 0$, $F_2^{(0\succ 0_2)} = 0$ and the first-order force of boundary flow barrier is $DF_2^{(0\succ 0_2)} < 0$ at time $t = 23.1805$ s. It qualifies the vanishing conditions of stick motion in Theorem 4. So the mass m_2 enters to the domain $\Omega_2^{(2)}$ after time $t = 23.1805$ s. In the time interval (23.1805 s, 43.9398 s), the velocity of the mass m_2 is less than the belt's V and it equals to the belt's V at time $t = 43.9398$ s. That is to say the mass m_2 reaches

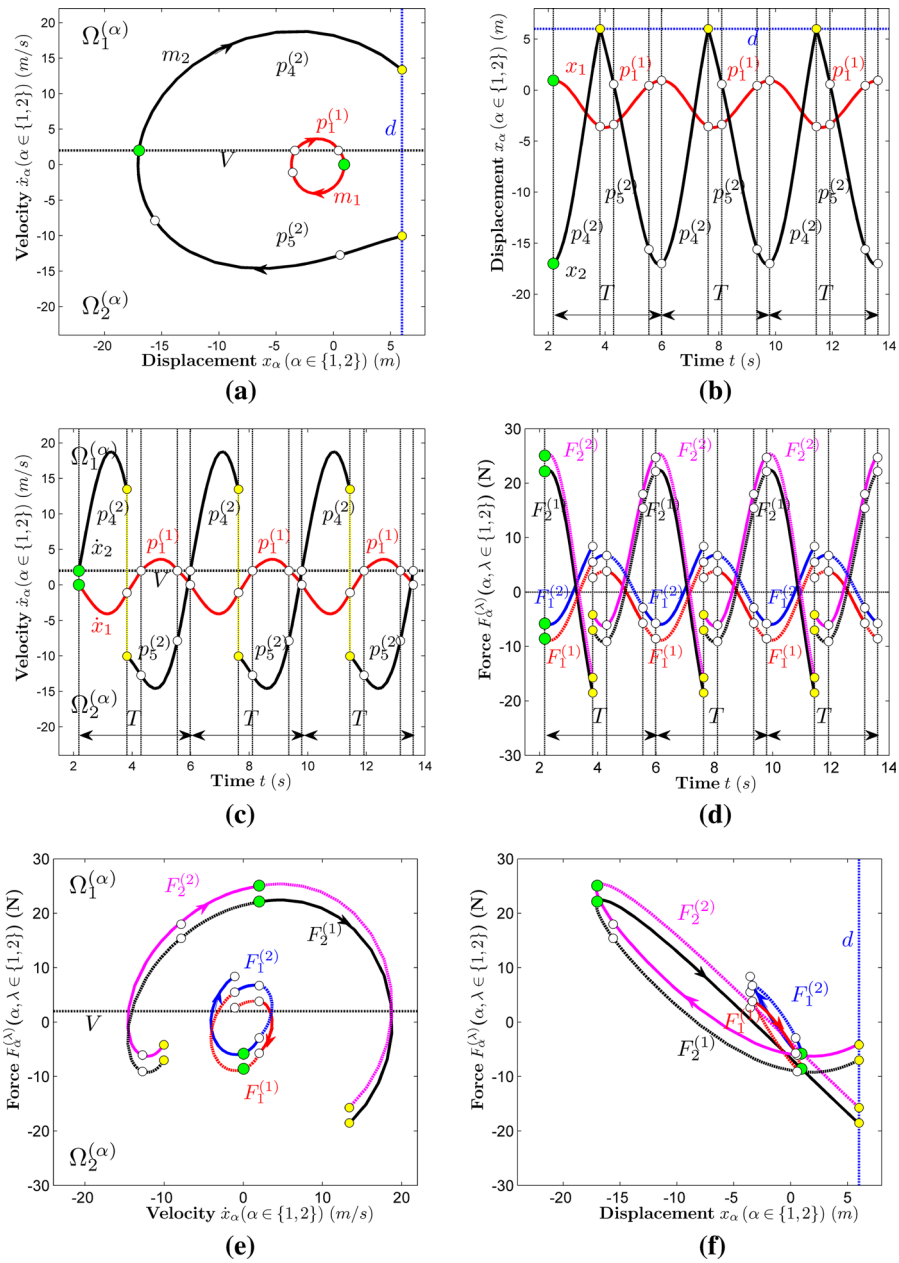

Fig. 14 Numerical simulation of the passable periodic motion for the mass m_1 and the impact periodic motion for the mass m_2: **a** phase trajectory, **b** displacement–time history, **c** velocity–time history, **d** force of per unit mass–time history, **e** force of per unit mass–velocity history, **f** force of per unit mass–displacement history. (Color figure online)

to the velocity boundary at this time. The stick motion appears because the forces of per unit mass $F_2^{(1)} < 0$ and $F_2^{(2)} > 0$ satisfy the conditions in Theorem 3. The mass m_2 sticks with the belt again in the time interval (43.9398 s, 48.1754 s). In this term, the friction force between the mass m_2 and the belt is static friction force, and the mass m_2 moves together with the belt. At time $t = 48.1754$ s, the displacement and the velocity of the mass m_2 are the same it was as in the initial point. So the trajectory at this time comes back to its starting points for the mass m_2. At the same time, the forces of boundary flow barrier are $F_2^{(0\succ 0_2)} > 0$ and $F_2^{(0\succ 0_1)} = 0$ and the first-order force of boundary flow barrier is $DF_2^{(0\succ 0_1)} > 0$ from Fig. 15d and e. So the stick motion of the mass m_2 vanishes, and the first stick periodic motion finishes. And the position of the mass m_1 in phase plane at this time is the same as the position at the initial time, so the first passable periodic

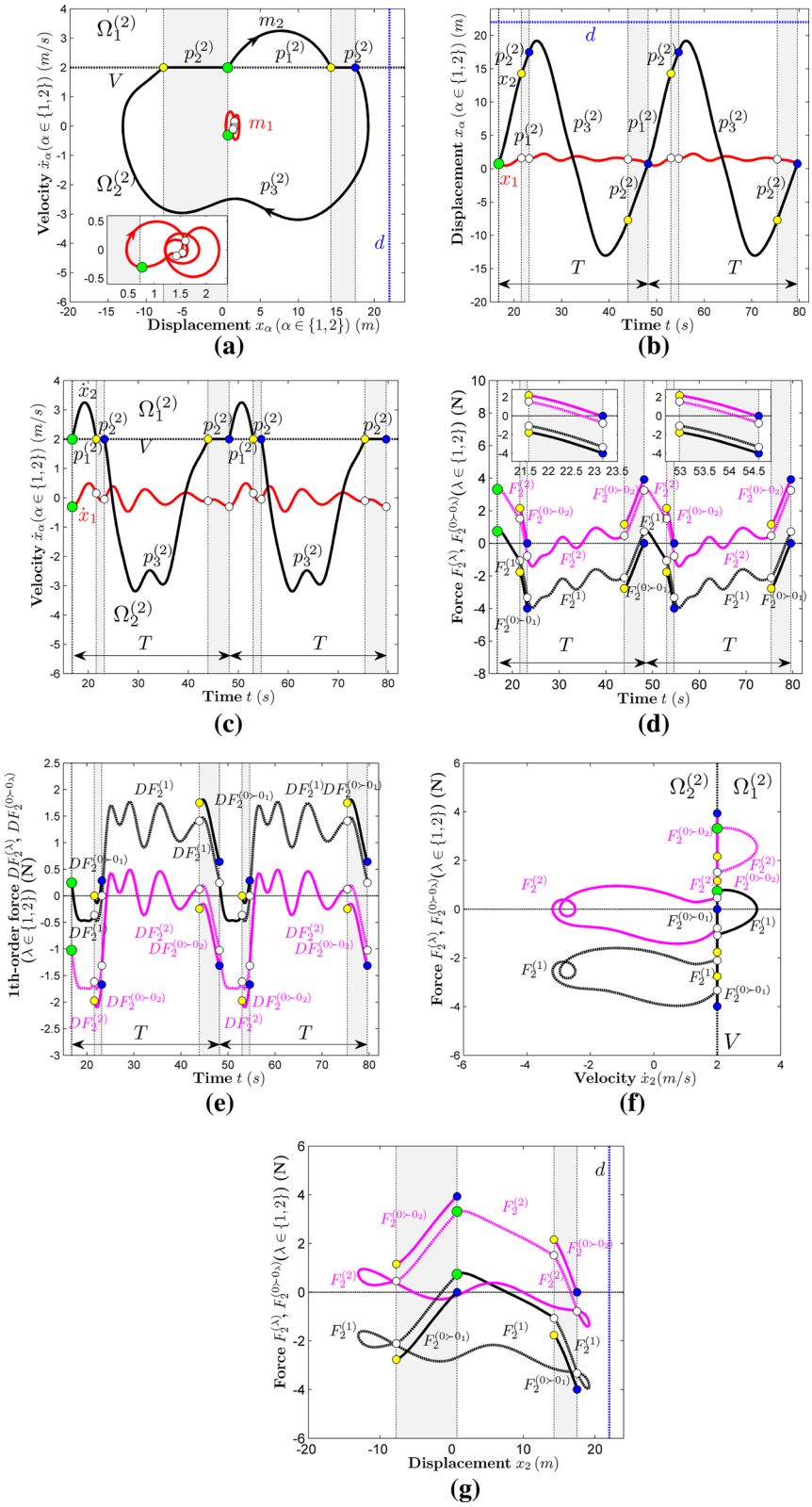

Fig. 15 Numerical simulation of the passable periodic motion for the mass m_1 and the stick periodic motion for the mass m_2: **a** phase trajectory, **b** displacement–time history, **c** velocity–time history, **d** force of per unit mass–time history, **e** first-order force of per unit mass–time history, **f** force of per unit mass–velocity history, **g** force of per unit mass–displacement history. (Color figure online)

motion for the mass m_1 finishes at the same time. In the time interval (48.1754 s, 79.5913 s), the second periodic motion for the masses m_1 and m_2 occurs, as shown in Fig. 15 b and c or a. In addition, the periodicity of the mass m_2 can be also observed from Fig. 15d and e or f and g.

7 Conclusions

In this paper, the analytical predictions of the 2-DOF friction-induced oscillator with one-sided impact on a conveyor belt were given through the theory of flow switchability for discontinuous dynamical systems. Due to the friction and impact discontinuities, different domains and boundaries were defined. The flow barrier on the separate boundary was introduced. The analytical conditions of the passable, stick, grazing, impact and stuck motions were presented in the form of theorem to show the complexity of switching motion in such friction–impact system. For a better understanding of the motion in this system, the switching sets and mapping structures were adopted to describe the different periodic motions with stick, impact and stuck in the friction–impact system. The numerical simulations were given to illustrate the different motions in this system. The obtained results reveal the mechanism of friction or collision between objects in discontinuous dynamical systems, and provide the theoretical basis for science and technology engineering to use or control the friction and collision and reference for the choice of system parameters.

Acknowledgements This research was supported by the National Natural Science Foundation of China (No. 11571208) and the Natural Science Foundation of Shandong Province (No.ZR2019MA048).

Compliance with ethical standards

Conflict of interest The authors declare that they have no conflict of interest.

Appendix A

Firstly, the switching sets will be defined and then the basic mappings will be obtained from them.

Based on the discontinuous boundaries in Eq. (15), the switching sets of the masses m_1 and m_2 are defined as

$$\begin{aligned}
\Sigma_{12}^{(1)} &= \Sigma_{21}^{(1)} \\
&= \{(x_k^{(1)}, \dot{x}_k^{(1)}, t_k) \mid \dot{x}_k^{(1)} = V, k \in \mathbb{N}\}, \\
{}^{+}\Sigma_{12}^{(1)} &= \{(x_k^{(1)}, \dot{x}_k^{(1)}, t_k) \mid \dot{x}_k^{(1)} = V^{+}, k \in \mathbb{N}\}, \\
{}^{-}\Sigma_{12}^{(1)} &= \{(x_k^{(1)}, \dot{x}_k^{(1)}, t_k) \mid \dot{x}_k^{(1)} = V^{-}, k \in \mathbb{N}\};
\end{aligned} \tag{A.1}$$

and

$$\begin{aligned}
\Sigma_{12}^{(2)} &= \Sigma_{21}^{(2)} \\
&= \{(x_k^{(2)}, \dot{x}_k^{(2)}, t_k) \mid \\
&\quad x_k^{(2)} \in (-\infty, d), \dot{x}_k^{(2)} = V, k \in \mathbb{N}\}, \\
{}^{+}\Sigma_{12}^{(2)} &= \{(x_k^{(2)}, \dot{x}_k^{(2)}, t_k) \mid \\
&\quad x_k^{(2)} \in (-\infty, d), \dot{x}_k^{(2)} = V^{+}, k \in \mathbb{N}\}, \\
{}^{-}\Sigma_{12}^{(2)} &= \{(x_k^{(2)}, \dot{x}_k^{(2)}, t_k) \mid \\
&\quad x_k^{(2)} \in (-\infty, d), \dot{x}_k^{(2)} = V^{-}, k \in \mathbb{N}\},
\end{aligned} \tag{A.2}$$

$$\begin{aligned}
\Sigma_{1(+\infty)}^{(2)} &= \{(x_k^{(2)}, \dot{x}_k^{(2)}, t_k) \mid \\
&\quad x_k^{(2)} = d, \dot{x}_k^{(2)} \in (V, +\infty), k \in \mathbb{N}\}, \\
\Sigma_{2(+\infty)}^{(2)} &= \{(x_k^{(2)}, \dot{x}_k^{(2)}, t_k) \mid \\
&\quad x_k^{(2)} = d, \dot{x}_k^{(2)} \in (-\infty, V) \\
&\quad \text{and } \dot{x}_k^{(2)} \neq 0, k \in \mathbb{N}\},
\end{aligned} \tag{A.3}$$

$$\begin{aligned}
\Sigma_{23}^{(2)} &= \{(x_k^{(2)}, \dot{x}_k^{(2)}, t_k) \mid x_k^{(2)} = d, \dot{x}_k^{(2)} = 0^{+}, \\
&\quad F_2^{(3)} > 0, k \in \mathbb{N}\}, \\
\Sigma_{32}^{(2)} &= \{(x_k^{(2)}, \dot{x}_k^{(2)}, t_k) \mid x_k^{(2)} = d, \dot{x}_k^{(2)} = 0^{-}, \\
&\quad F_2^{(3)} = 0, k \in \mathbb{N}\},
\end{aligned} \tag{A.4}$$

where $x_k^{(\alpha)} = x^{(\alpha)}(t_k)$ and $\dot{x}_k^{(\alpha)} = \dot{x}^{(\alpha)}(t_k)$, $x_k^{(\alpha)}$ and $\dot{x}_k^{(\alpha)}$ represent the switching displacement and the switching velocity for the mass $m_\alpha (\alpha \in \{1, 2\})$ at the switching time t_m. The switching set $\Sigma_{12}^{(\alpha)} (\alpha \in \{1, 2\})$ is defined on the velocity boundary $\partial\Omega_{12}^{(\alpha)} (\alpha \in \{1, 2\})$. And the switching sets $\Sigma_{i(+\infty)}^{(2)} (i = 1, 2)$ are defined on the impact boundaries $\partial\Omega_{i(+\infty)}^{(2)} (i = 1, 2)$ for the mass m_2. The switching sets $\Sigma_{23}^{(2)}$ and $\Sigma_{32}^{(2)}$ are defined

on the stuck boundary $\partial\Omega_{23}$ for the mass m_2. In fact, $\Sigma_{23}^{(2)}$ and $\Sigma_{32}^{(2)}$ are the same switching set, they represent appearing and vanishing of the stuck motion by restricting different conditions.

Furthermore, the 4-dimensional switching sets of the two masses can be defined by the form of direct product in the following:

$$
\begin{aligned}
\Sigma_{12}^{(a)} &= \Sigma_{12}^{(1)} \otimes \Sigma_{12}^{(2)} \\
&= \{(x_k^{(1)}, \dot{x}_k^{(1)}, x_k^{(2)}, \dot{x}_k^{(2)}, t_k) \mid \\
&\quad x_k^{(2)} \in (-\infty, d), \dot{x}_k^{(1)} = \dot{x}_k^{(2)} = V, \\
&\quad k \in \mathbb{N}\}, \\
\Sigma_{12}^{(b)} &=^{+} \Sigma_{12}^{(1)} \otimes^{+} \Sigma_{12}^{(2)} \\
&= \{(x_k^{(1)}, \dot{x}_k^{(1)}, x_k^{(2)}, \dot{x}_k^{(2)}, t_k) \mid \\
&\quad x_k^{(2)} \in (-\infty, d), \dot{x}_k^{(1)} = V^{+}, \\
&\quad \dot{x}_k^{(2)} = V^{+}, k \in \mathbb{N}\}, \\
\Sigma_{12}^{(c)} &=^{-} \Sigma_{12}^{(1)} \otimes^{-} \Sigma_{12}^{(2)} \\
&= \{(x_k^{(1)}, \dot{x}_k^{(1)}, x_k^{(2)}, \dot{x}_k^{(2)}, t_k) \mid \\
&\quad x_k^{(2)} \in (-\infty, d), \dot{x}_k^{(1)} = V^{-}, \\
&\quad \dot{x}_k^{(2)} = V^{-}, k \in \mathbb{N}\}; \qquad \text{(A.5)} \\
\Sigma_{12}^{(d)} &=^{+} \Sigma_{12}^{(1)} \otimes \Sigma_{12}^{(2)} \\
&= \{(x_k^{(1)}, \dot{x}_k^{(1)}, x_k^{(2)}, \dot{x}_k^{(2)}, t_k) \mid \\
&\quad x_k^{(2)} \in (-\infty, d), \dot{x}_k^{(1)} = V^{+}, \\
&\quad \dot{x}_k^{(2)} = V, k \in \mathbb{N}\}, \\
\Sigma_{12}^{(e)} &=^{+} \Sigma_{12}^{(1)} \otimes^{-} \Sigma_{12}^{(2)}, \\
&= \{(x_k^{(1)}, \dot{x}_k^{(1)}, x_k^{(2)}, \dot{x}_k^{(2)}, t_k) \mid \\
&\quad x_k^{(2)} \in (-\infty, d), \dot{x}_k^{(1)} = V^{+}, \\
&\quad \dot{x}_k^{(2)} = V^{-}, k \in \mathbb{N}\} \\
\Sigma_{12}^{(f)} &= \Sigma_{12}^{(1)} \otimes^{+} \Sigma_{12}^{(2)} \\
&= \{(x_k^{(1)}, \dot{x}_k^{(1)}, x_k^{(2)}, \dot{x}_k^{(2)}, t_k) \mid \\
&\quad x_k^{(2)} \in (-\infty, d), \dot{x}_k^{(1)} = V, \\
&\quad \dot{x}_k^{(2)} = V^{+}, k \in \mathbb{N}\}; \qquad \text{(A.6)} \\
\Sigma_{12}^{(g)} &= \Sigma_{12}^{(1)} \otimes^{-} \Sigma_{12}^{(2)} \\
&= \{(x_k^{(1)}, \dot{x}_k^{(1)}, x_k^{(2)}, \dot{x}_k^{(2)}, t_k) \mid \\
&\quad x_k^{(2)} \in (-\infty, d), \dot{x}_k^{(1)} = V, \\
&\quad \dot{x}_k^{(2)} = V^{-}, k \in \mathbb{N}\}, \\
\Sigma_{12}^{(h)} &=^{-} \Sigma_{12}^{(1)} \otimes^{+} \Sigma_{12}^{(2)} \\
&= \{(x_k^{(1)}, \dot{x}_k^{(1)}, x_k^{(2)}, \dot{x}_k^{(2)}, t_k) \mid \\
&\quad x_k^{(2)} \in (-\infty, d), \dot{x}_k^{(1)} = V^{-}, \\
&\quad \dot{x}_k^{(2)} = V^{+}, k \in \mathbb{N}\}, \\
\Sigma_{12}^{(i)} &=^{-} \Sigma_{12}^{(1)} \otimes \Sigma_{12}^{(2)} \\
&= \{(x_k^{(1)}, \dot{x}_k^{(1)}, x_k^{(2)}, \dot{x}_k^{(2)}, t_k) \mid \\
&\quad x_k^{(2)} \in (-\infty, d), \dot{x}_k^{(1)} = V^{-}, \\
&\quad \dot{x}_k^{(2)} = V, k \in \mathbb{N}\}; \qquad \text{(A.7)} \\
\Sigma_{1(+\infty)}^{(a)} &=^{+} \Sigma_{12}^{(1)} \otimes \Sigma_{1(+\infty)}^{(2)} \\
&= \{(x_k^{(1)}, \dot{x}_k^{(1)}, x_k^{(2)}, \dot{x}_k^{(2)}, t_k) \mid \\
&\quad x_k^{(2)} = d, \dot{x}_k^{(1)} = V^{+}, \dot{x}_k^{(2)} > V, \\
&\quad k \in \mathbb{N}\}, \\
\Sigma_{1(+\infty)}^{(b)} &= \Sigma_{12}^{(1)} \otimes \Sigma_{1(+\infty)}^{(2)} \\
&= \{(x_k^{(1)}, \dot{x}_k^{(1)}, x_k^{(2)}, \dot{x}_k^{(2)}, t_k) \mid \\
&\quad x_k^{(2)} = d, \dot{x}_k^{(1)} = V, \dot{x}_k^{(2)} > V, \\
&\quad k \in \mathbb{N}\}, \\
\Sigma_{1(+\infty)}^{(c)} &=^{-} \Sigma_{12}^{(1)} \otimes \Sigma_{1(+\infty)}^{(2)} \\
&= \{(x_k^{(1)}, \dot{x}_k^{(1)}, x_k^{(2)}, \dot{x}_k^{(2)}, t_k) \mid \\
&\quad x_k^{(2)} = d, \dot{x}_k^{(1)} = V^{-}, \dot{x}_k^{(2)} > V, \\
&\quad k \in \mathbb{N}\}; \qquad \text{(A.8)} \\
\Sigma_{2(+\infty)}^{(a)} &=^{+} \Sigma_{12}^{(1)} \otimes \Sigma_{2(+\infty)}^{(2)} \\
&= \{(x_k^{(1)}, \dot{x}_k^{(1)}, x_k^{(2)}, \dot{x}_k^{(2)}, t_k) \mid \\
&\quad x_k^{(2)} = d, \dot{x}_k^{(1)} = V^{+}, \dot{x}_k^{(2)} < V \\
&\quad \text{and } \dot{x}_k^{(2)} \neq 0, k \in \mathbb{N}\}, \\
\Sigma_{2(+\infty)}^{(b)} &= \Sigma_{12}^{(1)} \otimes \Sigma_{2(+\infty)}^{(2)} \\
&= \{(x_k^{(1)}, \dot{x}_k^{(1)}, x_k^{(2)}, \dot{x}_k^{(2)}, t_k) \mid \\
&\quad x_k^{(2)} = d, \dot{x}_k^{(1)} = V, \dot{x}_k^{(2)} < V \\
&\quad \text{and } \dot{x}_k^{(2)} \neq 0, k \in \mathbb{N}\}, \\
\Sigma_{2(+\infty)}^{(c)} &=^{-} \Sigma_{12}^{(1)} \otimes \Sigma_{2(+\infty)}^{(2)} \\
&= \{(x_k^{(1)}, \dot{x}_k^{(1)}, x_k^{(2)}, \dot{x}_k^{(2)}, t_k) \mid \\
&\quad x_k^{(2)} = d, \dot{x}_k^{(1)} = V^{-}, \dot{x}_k^{(2)} < V \\
&\quad \text{and } \dot{x}_k^{(2)} \neq 0, k \in \mathbb{N}\}; \qquad \text{(A.9)} \\
\Sigma_{23}^{(a)} &=^{+} \Sigma_{12}^{(1)} \otimes \Sigma_{23}^{(2)} \\
&= \{(x_k^{(1)}, \dot{x}_k^{(1)}, x_k^{(2)}, \dot{x}_k^{(2)}, t_k) \mid \\
&\quad x_k^{(2)} = d, \dot{x}_k^{(1)} = V^{+}, \dot{x}_k^{(2)} = 0^{+}, \\
&\quad F_2^{(3)} > 0, k \in \mathbb{N}\}, \\
\Sigma_{23}^{(b)} &= \Sigma_{12}^{(1)} \otimes \Sigma_{23}^{(2)}
\end{aligned}
$$

$$
\begin{aligned}
&= \{(x_k^{(1)}, \dot{x}_k^{(1)}, x_k^{(2)}, \dot{x}_k^{(2)}, t_k) \mid \\
&\quad x_k^{(2)} = d, \dot{x}_k^{(1)} = V, \dot{x}_k^{(2)} = 0^+, \\
&\quad F_2^{(3)} > 0, k \in \mathbb{N}\}, \\
\Sigma_{23}^{(c)} &=^- \Sigma_{12}^{(1)} \otimes \Sigma_{23}^{(2)} \\
&= \{(x_k^{(1)}, \dot{x}_k^{(1)}, x_k^{(2)}, \dot{x}_k^{(2)}, t_k) \mid \\
&\quad x_k^{(2)} = d, \dot{x}_k^{(1)} = V^-, \dot{x}_k^{(2)} = 0^+, \\
&\quad F_2^{(3)} > 0, k \in \mathbb{N}\}; \qquad \text{(A.10)} \\
\Sigma_{32}^{(a)} &=^+ \Sigma_{12}^{(1)} \otimes \Sigma_{32}^{(2)} \\
&= \{(x_k^{(1)}, \dot{x}_k^{(1)}, x_k^{(2)}, \dot{x}_k^{(2)}, t_k) \mid \\
&\quad x_k^{(2)} = d, \dot{x}_k^{(1)} = V^+, \dot{x}_k^{(2)} = 0^-, \\
&\quad F_2^{(3)} = 0, k \in \mathbb{N}\}, \\
\Sigma_{32}^{(b)} &= \Sigma_{12}^{(1)} \otimes \Sigma_{32}^{(2)} \\
&= \{(x_k^{(1)}, \dot{x}_k^{(1)}, x_k^{(2)}, \dot{x}_k^{(2)}, t_k) \mid \\
&\quad x_k^{(2)} = d, \dot{x}_k^{(1)} = V, \dot{x}_k^{(2)} = 0^-, \\
&\quad F_2^{(3)} = 0, k \in \mathbb{N}\}, \\
\Sigma_{32}^{(c)} &=^- \Sigma_{12}^{(1)} \otimes \Sigma_{32}^{(2)} \\
&= \{(x_k^{(1)}, \dot{x}_k^{(1)}, x_k^{(2)}, \dot{x}_k^{(2)}, t_k) \mid \\
&\quad x_k^{(2)} = d, \dot{x}_k^{(1)} = V^-, \dot{x}_k^{(2)} = 0^-, \\
&\quad F_2^{(3)} = 0, k \in \mathbb{N}\}. \qquad \text{(A.11)}
\end{aligned}
$$

For the 2-DOF friction-induced oscillator with one-side impact on a conveyer belt described in Sect. 2, the basic mappings for the mass m_1 are

$$
\begin{aligned}
&p_1^{(1)} :^+ \Sigma_{12}^{(1)} \to^+ \Sigma_{12}^{(1)}, \\
&p_2^{(1)} : \Sigma_{12}^{(1)} \to \Sigma_{12}^{(1)}, \qquad \text{(A.12)} \\
&p_3^{(1)} :^- \Sigma_{12}^{(1)} \to^- \Sigma_{12}^{(1)}.
\end{aligned}
$$

And the basic mappings for the mass m_2 are

$$
\begin{aligned}
&p_1^{(2)} :^+ \Sigma_{12}^{(2)} \to^+ \Sigma_{12}^{(2)}, \\
&p_2^{(2)} : \Sigma_{12}^{(2)} \to \Sigma_{12}^{(2)}, \\
&p_3^{(2)} :^- \Sigma_{12}^{(2)} \to^- \Sigma_{12}^{(2)}; \qquad \text{(A.13)} \\
&p_4^{(2)} :^+ \Sigma_{12}^{(2)} \to \Sigma_{1(+\infty)}^{(2)}, \\
&p_5^{(2)} : \Sigma_{2(+\infty)}^{(2)} \to^- \Sigma_{12}^{(2)}, \\
&p_6^{(2)} :^- \Sigma_{12}^{(2)} \to \Sigma_{23}^{(2)}; \qquad \text{(A.14)} \\
&p_7^{(2)} : \Sigma_{23}^{(2)} \to \Sigma_{32}^{(2)}, \\
&p_8^{(2)} : \Sigma_{32}^{(2)} \to \Sigma_{23}^{(2)}, \\
&p_9^{(2)} : \Sigma_{32}^{(2)} \to^- \Sigma_{12}^{(2)}; \qquad \text{(A.15)} \\
&p_{10}^{(2)} :^- \Sigma_{12}^{(2)} \to \Sigma_{2(+\infty)}^{(2)}. \qquad \text{(A.16)}
\end{aligned}
$$

The corresponding mapping structures for the mass m_1 and mass m_2 are sketched in Fig. 16a and b, respectively. The above basic mappings can be divided into two kinds of global mapping and local mapping. The global mapping means that the motion switches from one switching set to another one; and the local mapping means that the motion switches from one switching set to itself. By the above definitions, the global mappings are defined as

$$
\begin{aligned}
&p_4^{(2)} : (x_k^{(2)}, V^+, t_k) \to (d, \dot{x}_{k+1}^{(2)}, t_{k+1}), \\
&p_5^{(2)} : (d, \dot{x}_k^{(2)}, t_k) \to (x_{k+1}^{(2)}, V^-, t_{k+1}), \\
&p_6^{(2)} : (x_k^{(2)}, V^-, t_k) \to (d, 0, t_{k+1}), \qquad \text{(A.17)} \\
&p_9^{(2)} : (d, 0, t_k) \to (x_{k+1}^{(2)}, V^-, t_{k+1}), \\
&p_{10}^{(2)} : (x_k^{(2)}, V^-, t_k) \to (d, \dot{x}_k^{(2)}, t_{k+1});
\end{aligned}
$$

and the local mappings are defined as

$$
\begin{aligned}
&p_1^{(1)} : (x_k^{(1)}, V^+, t_k) \to (x_{k+1}^{(1)}, V^+, t_{k+1}), \\
&p_1^{(2)} : (x_k^{(2)}, V^+, t_k) \to (x_{k+1}^{(2)}, V^+, t_{k+1}); \qquad \text{(A.18)} \\
&p_2^{(1)} : (x_k^{(1)}, V, t_k) \to (x_{k+1}^{(1)}, V, t_{k+1}), \\
&p_2^{(2)} : (x_k^{(2)}, V, t_k) \to (x_{k+1}^{(2)}, V, t_{k+1}); \qquad \text{(A.19)} \\
&p_3^{(1)} : (x_k^{(1)}, V^-, t_k) \to (x_{k+1}^{(1)}, V^-, t_{k+1}), \\
&p_3^{(2)} : (x_k^{(2)}, V^-, t_k) \to (x_{k+1}^{(2)}, V^-, t_{k+1}); \qquad \text{(A.20)} \\
&p_7^{(2)} : (d, 0, t_k) \to (d, 0, t_{k+1}), \\
&p_8^{(2)} : (d, 0, t_k) \to (d, 0, t_{k+1}). \qquad \text{(A.21)}
\end{aligned}
$$

Based on the above discussion, the 4-dimensional resultant mappings of the friction-induced oscillator with one-sided impact can be given as follows.

$$
\begin{aligned}
&P_{1a} = (p_2^{(1)}, p_2^{(2)}) : \Sigma_{12}^{(a)} \to \Sigma_{12}^{(a)}, \\
&P_{1b} = (p_1^{(1)}, p_1^{(2)}) : \Sigma_{12}^{(b)} \to \Sigma_{12}^{(b)}, \\
&P_{1c} = (p_3^{(1)}, p_3^{(2)}) : \Sigma_{12}^{(c)} \to \Sigma_{12}^{(c)}; \qquad \text{(A.22)} \\
&P_{1d} = (p_1^{(1)}, p_2^{(2)}) : \Sigma_{12}^{(d)} \to \Sigma_{12}^{(d)}, \\
&P_{1e} = (p_1^{(1)}, p_3^{(2)}) : \Sigma_{12}^{(e)} \to \Sigma_{12}^{(e)}; \qquad \text{(A.23)} \\
&P_{1f} = (p_2^{(1)}, p_1^{(2)}) : \Sigma_{12}^{(f)} \to \Sigma_{12}^{(f)}, \\
&P_{1g} = (p_2^{(1)}, p_3^{(2)}) : \Sigma_{12}^{(g)} \to \Sigma_{12}^{(g)}; \qquad \text{(A.24)} \\
&P_{1h} = (p_3^{(1)}, p_1^{(2)}) : \Sigma_{12}^{(h)} \to \Sigma_{12}^{(h)}, \\
&P_{1i} = (p_3^{(1)}, p_2^{(2)}) : \Sigma_{12}^{(i)} \to \Sigma_{12}^{(i)}; \qquad \text{(A.25)}
\end{aligned}
$$

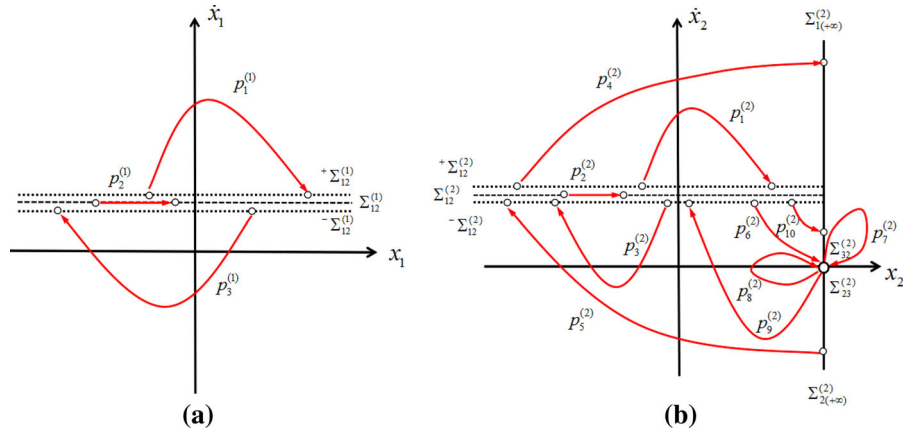

Fig. 16 The mapping structures for the two masses $m_\alpha(\alpha = 1, 2)$: **a** mass m_1 and **b** mass m_2

$$
\begin{aligned}
P_{2a} &= (p_1^{(1)}, p_4^{(2)}) : \Sigma_{12}^{(b)} \to \Sigma_{1(+\infty)}^{(a)},\\
P_{2b} &= (p_2^{(1)}, p_4^{(2)}) : \Sigma_{12}^{(f)} \to \Sigma_{1(+\infty)}^{(b)},\\
P_{2c} &= (p_3^{(1)}, p_4^{(2)}) : \Sigma_{12}^{(h)} \to \Sigma_{1(+\infty)}^{(c)}; \qquad \text{(A.26)}\\
P_{3a} &= (p_1^{(1)}, p_5^{(2)}) : \Sigma_{2(+\infty)}^{(a)} \to \Sigma_{12}^{(e)},\\
P_{3b} &= (p_2^{(1)}, p_5^{(2)}) : \Sigma_{2(+\infty)}^{(b)} \to \Sigma_{12}^{(g)},\\
P_{3c} &= (p_3^{(1)}, p_5^{(2)}) : \Sigma_{2(+\infty)}^{(c)} \to \Sigma_{12}^{(c)}; \qquad \text{(A.27)}\\
P_{4a} &= (p_1^{(1)}, p_6^{(2)}) : \Sigma_{12}^{(e)} \to \Sigma_{23}^{(a)},\\
P_{4b} &= (p_2^{(1)}, p_6^{(2)}) : \Sigma_{12}^{(g)} \to \Sigma_{23}^{(b)},\\
P_{4c} &= (p_3^{(1)}, p_6^{(2)}) : \Sigma_{12}^{(i)} \to \Sigma_{23}^{(c)}; \qquad \text{(A.28)}\\
P_{5a} &= (p_1^{(1)}, p_7^{(2)}) : \Sigma_{23}^{(a)} \to \Sigma_{32}^{(a)},\\
P_{5b} &= (p_2^{(1)}, p_7^{(2)}) : \Sigma_{23}^{(b)} \to \Sigma_{32}^{(b)},\\
P_{5c} &= (p_3^{(1)}, p_7^{(2)}) : \Sigma_{23}^{(c)} \to \Sigma_{32}^{(c)}; \qquad \text{(A.29)}\\
P_{6a} &= (p_1^{(1)}, p_8^{(2)}) : \Sigma_{32}^{(a)} \to \Sigma_{23}^{(a)},\\
P_{6b} &= (p_2^{(1)}, p_8^{(2)}) : \Sigma_{32}^{(b)} \to \Sigma_{23}^{(b)},\\
P_{6c} &= (p_3^{(1)}, p_8^{(2)}) : \Sigma_{32}^{(c)} \to \Sigma_{23}^{(c)}; \qquad \text{(A.30)}\\
P_{7a} &= (p_1^{(1)}, p_9^{(2)}) : \Sigma_{32}^{(a)} \to \Sigma_{12}^{(e)},\\
P_{7b} &= (p_2^{(1)}, p_9^{(2)}) : \Sigma_{32}^{(b)} \to \Sigma_{12}^{(g)},\\
P_{7c} &= (p_3^{(1)}, p_9^{(2)}) : \Sigma_{32}^{(c)} \to \Sigma_{12}^{(c)}; \qquad \text{(A.31)}\\
P_{8a} &= (p_1^{(1)}, p_{10}^{(2)}) : \Sigma_{32}^{(a)} \to \Sigma_{2(+\infty)}^{(a)},\\
P_{8b} &= (p_2^{(1)}, p_{10}^{(2)}) : \Sigma_{32}^{(b)} \to \Sigma_{2(+\infty)}^{(b)},\\
P_{8c} &= (p_3^{(1)}, p_{10}^{(2)}) : \Sigma_{32}^{(c)} \to \Sigma_{2(+\infty)}^{(c)}. \qquad \text{(A.32)}
\end{aligned}
$$

For convenience, we introduce an index set $\mathcal{N} = \{1\sigma|\sigma = a, b, \ldots, i\} \cup \{\sigma_1\sigma_2|\sigma_1 = 2, 3, \ldots, 8; \sigma_2 = a, b, c\}$.

Based on the above definitions of the basic mappings, the governing equations for the 4-dimensional resultant mapping P_δ $(\delta \in \mathcal{N})$ of the two masses $m_\alpha(\alpha = 1, 2)$ can be expressed by

$$\mathbf{f}^{(\delta)}(\mathbf{m}_k, \mathbf{m}_{k+1}) = 0 \quad \text{for } P_\delta \ (\delta \in \mathcal{N}) \qquad \text{(A.33)}$$

with

$$
\begin{aligned}
\mathbf{m}_k &= (x_k^{(1)}, \dot{x}_k^{(1)}, x_k^{(2)}, \dot{x}_k^{(2)}, t_k)^{\mathrm{T}},\\
\mathbf{m}_{k+1} &= (x_{k+1}^{(1)}, \dot{x}_{k+1}^{(1)}, x_{k+1}^{(2)}, \dot{x}_{k+1}^{(2)}, t_{k+1})^{\mathrm{T}}, \qquad \text{(A.34)}\\
\mathbf{f}^{(\delta)} &= (f_1^{(\delta)}, f_2^{(\delta)}, f_3^{(\delta)}, f_4^{(\delta)})^{\mathrm{T}},
\end{aligned}
$$

where

$$
\begin{aligned}
&f_1^{(\delta)}(x_k^{(1)}, \dot{x}_k^{(1)}, x_k^{(2)}, \dot{x}_k^{(2)}, t_k, x_{k+1}^{(1)}, \dot{x}_{k+1}^{(1)},\\
&\quad x_{k+1}^{(2)}, \dot{x}_{k+1}^{(2)}, t_{k+1}) = 0,\\
&f_2^{(\delta)}(x_k^{(1)}, \dot{x}_k^{(1)}, x_k^{(2)}, \dot{x}_k^{(2)}, t_k, x_{k+1}^{(1)}, \dot{x}_{k+1}^{(1)},\\
&\quad x_{k+1}^{(2)}, \dot{x}_{k+1}^{(2)}, t_{k+1}) = 0,\\
&f_3^{(\delta)}(x_k^{(1)}, \dot{x}_k^{(1)}, x_k^{(2)}, \dot{x}_k^{(2)}, t_k, x_{k+1}^{(1)}, \dot{x}_{k+1}^{(1)},\\
&\quad x_{k+1}^{(2)}, \dot{x}_{k+1}^{(2)}, t_{k+1}) = 0,\\
&f_4^{(\delta)}(x_k^{(1)}, \dot{x}_k^{(1)}, x_k^{(2)}, \dot{x}_k^{(2)}, t_k, x_{k+1}^{(1)}, \dot{x}_{k+1}^{(1)},\\
&\quad x_{k+1}^{(2)}, \dot{x}_{k+1}^{(2)}, t_{k+1}) = 0.
\end{aligned} \qquad \text{(A.35)}
$$

References

1. Levitan, E.: Forced oscillation of a spring-mass system having combined Coulomb and viscous damping. J. Acoust. Soc. Am. **32**, 1265–1269 (1960)

2. Filippov, A.F.: Differential equations with discontinuous right-hand side. Am. Math. Soc. Transl. **2**(42), 99–231 (1964)
3. Filippov, A.F.: Differential Equations with Discontinuous Righthand Sides. Kluwer Academic Publishers, Dordrecht (1988)
4. Holmes, P.: The dynamics of repeated impacts with a sinusoidally vibrating table. J. Sound Vibr. **84**(2), 173–189 (1982)
5. Shaw, S.: On the dynamic response of a system with dry-friction. J. Sound Vibr. **108**(2), 305–325 (1986)
6. Natsiavas, S.: Stability of piecewise linear oscillator with viscous and dry friction damping. J. Sound Vibr. **217**, 507–522 (1998)
7. Andreaus, U., Casini, P.: Dynamics of friction oscillators excited by a moving base and driving force. J. Sound Vibr. **245**, 685–699 (2000)
8. Andreaus, U., Casini, P.: Friction oscillator excited by moving base and colliding with a rigid or deformable obstacle. Int. J. Non-linear Mech. **37**, 117–133 (2002)
9. Casini, P., Vestroni, F.: Bifurcation in hybrid mechanical systems with discontinuity boundaries. Int. J. Bifurc. Chaos **15**(6), 2003–2013 (2005)
10. Casini, P., Giannini, O., Vestroni, F.: Experimental evidence of non-standard bifurcations in non-smooth oscillator dynamics. Nonlinear Dyn. **46**, 259–272 (2006)
11. Shaw, S., Holmes, P.: A periodically forced impact oscillator with large dissipation. J. Appl. Mech. **50**(4), 849–857 (1983)
12. Shaw, S.: The dynamics of a harmonically excited system having rigid amplitude constraints part 1: subharmonic motions and local bifurcations. J. Appl. Mech. **52**, 453–458 (1985)
13. Shaw, S.: The dynamics of a harmonically excited system having rigid amplitude constraints part 2: Subharmonic motions and local bifurcations. J. Appl. Mech. **52**, 459–464 (1985)
14. Whiston, G.: The vibro-impact response of a harmonically excited and preloaded one-dimensional linear oscillator. J. Sound Vibr. **115**(2), 303–319 (1987)
15. Whiston, G.: Global dynamics of a vibro-impacting linear oscillator. J. Sound Vibr. **118**(3), 395–429 (1987)
16. Nordmark, A.: Non-periodic motion caused by grazing incidence in an impact oscillator. J. Sound Vibr. **145**(2), 279–297 (1991)
17. Awrejcewicz, J., Delfs, J.: Dynamics of a self-excited stick-slip oscillator with two degrees of freedom, part I. Investig. Equilib. Eur. J. Mech. **9**(4), 269–282 (1990)
18. Awrejcewicz, J., Delfs, J.: Dynamics of a self-excited stick-slip oscillator with two degrees of freedom, II. Slip-stick, slip-slip, stick-slip transitions, periodic and chaotic orbits. Eur. J. Mech. **9**(5), 397–418 (1990)
19. Foale, S., Bishop, S.: Dynamical complexities of forced impacting systems. Philos. Trans. R. Lond. A. **338**(1651), 547–556 (1992)
20. Hinrichs, N., Oestreich, M., Popp, K.: Dynamics of oscillators with impact and friction. Chaos Solitons Fractals **8**(4), 535–558 (1997)
21. Hinrichs, N., Oestreich, M., Popp, K.: On the modeling of friction oscillators. J. Sound Vibr. **216**(3), 435–459 (1997)
22. Pascal, M.: Dynamics and stability of a two degree of freedom oscillator with an elastic stop. J. Appl. Math. Mech. **1**(1), 94–102 (2006)
23. Pascal, M.: Dynamics of coupled oscillators excited by dry friction. ASME J. Comput. Nonlinear Dyn. **3**(3), 20–26 (2008)
24. Pascal, M.: New events in stick-slip oscillators behavior. J. Appl. Math. Mech. **75**(3), 402–409 (2011)
25. Pascal, M.: A new model of dry friction oscillator colliding with a rigid obstacle. Nonlinear Dyn. **91**, 2541–2550 (2018)
26. Balachandran, B., Nayfeh, A.: Nonlinear motions of beam-mass structure. Nonlinear Dyn. **1**(1), 39–61 (1990)
27. Balachandran, B., Zhao, M., Li, Y.: Dynamics of elastic structures subjected to impact excitations. In: Moon, F.C. (ed.) Appl. Nonlinear Chaotic Dyn. Mech. Kluwer, Dordrecht (1997)
28. Balachandran, B.: Dynamics of an elastic structure excited by harmonic and aharmonic impactor motions. J. Vib. Control **9**, 265–279 (2003)
29. Balachandran, B.: Nonlinear dynamics of milling process. Philos. Trans. R. Soc. Lond. A **359**, 793–819 (2001)
30. Lenci, S., Clementi, F.: Axial-transversal coupling in the nonlinear dynamics of a beam with an inclined roller. Int. J. Mech. Sci. **144**, 490–501 (2018)
31. Demeio, L., Lenci, S.: Dynamic analysis of a ball bouncing on a flexible beam. J. Sound Vibr. **441**, 152–164 (2019)
32. Li, X., Song, S.: Impulsive control for existence, uniqueness and global stability of periodic solutions of recurrent neural networks with discrete and continuously distributed delays. IEEE Trans. Neural Netw. Learn. **24**(6), 868–877 (2013)
33. Li, X., Bohner, M., Wang, C.: Impulsive differential equations: periodic solutions and applications. Automatica **52**, 173–178 (2015)
34. Li, H., Wang, Y., Xie, L.: Output tracking control of Boolean control networks via state feedback: constant reference signal case. Automatica **59**, 54–59 (2015)
35. Li, X., Wu, J.: Stability of nonlinear differential systems with state-dependent delayed impulses. Automatica **64**, 63–69 (2016)
36. Li, H., Xie, L., Wang, Y.: On robust control invariance of Boolean control networks. Automatica **68**, 392–396 (2016)
37. Li, X., Zhang, X., Song, S.: Effect of delayed impulses on input-to-state stability of nonlinear systems. Automatica **76**, 378–382 (2017)
38. Li, X., Song, S.: Stabilization of delay systems: delay-dependent impulsive control. IEEE Trans. Autom. Control. **62**(1), 406–411 (2017)
39. Zhang, X., Li, X.: Input-to-state stability of non-linear systems with distributed-delayed impulses. IET Control Theory Appl. **11**(1), 81–89 (2017)
40. Li, X., Cao, J.: An impulsive delay inequality involving unbounded time-varying delay and applications. IEEE Trans. Autom. Control. **62**(7), 3618–3625 (2017)
41. Li, H., Xie, L., Wang, Y.: Output regulation of Boolean control networks. IEEE Trans. Autom. Control. **62**(6), 2993–2998 (2017)
42. Li, H., Wang, Y.: Further results on feedback stabilization control design of Boolean control networks. Automatica **83**, 303–308 (2017)

43. Liu, Y., Zheng, Y., Li, H., Alsaadi, F., Ahmad, B.: Control design for output tracking of delayed Boolean control networks. J. Comput. Appl. Math. **327**, 188–195 (2018)
44. Galvanetto, U.: Some discontinuous bifurcations in a two-block stick-slip systems. J. Sound Vibr. **248**(4), 653–669 (2001)
45. Leine, R., Nijmeijer, H.: Dynamics and Bifurcations of Non-Smooth Mechanical Systems. Number 18 in Lecture Notes in Applied and Computational Mechanics. Springer-Verlag, Berlin (2004)
46. Bernardo, M., Budd, C.J., Champneys, A.R., Kowalczyk, P.: Piecewise-Smooth Dynamical Systems: Theory and Applications. Springer, New York (2008)
47. Lancioni, G., Lenci, S., Galvanetto, U.: Dynamics of windscreen wiper blades: squeal noise, reversal noise and chattering. Int. J. Non-linear Mech. **80**, 132–143 (2016)
48. Luo, A.: A theory for nonsmooth dynamical systems on connectable domains. Commun. Nonlinear Sci. Numer. Simul. **10**, 1–55 (2005)
49. Luo, A.: Imaginary, sink and source flows in the vicinity of the separatrix of nonsmooth dynamic system. J. Sound Vibr. **285**, 443–456 (2005)
50. Luo, A., Gegg, B.: Stick and non-stick periodic motions in periodically forced oscillators with dry friction. J. Sound Vibr. **291**(1–2), 132–168 (2006)
51. Luo, A.: A theory for flow swtichability in discontinuous dynamical systems. Nonlinear Anal. Hybrid Syst. **2**, 1030–1061 (2008)
52. Luo, A., Thapa, S.: On nonlinear dynamics of simplified brake dynamical systems. In: International Mechanical Engineering Congress and Exposition 1849–1859 (2007)
53. Luo, A., Mao, T.: On motion switchability in a two degree of freedom, friction-induced oscillator traveling on constant speed belts. International Mechanical Engineering Congress and Exposition 965–980 (2009)
54. Luo, A.: Discontinuous Dynamical Systems on Time-Varying Domains. Higher Education Press, Beijing (2009)
55. Luo, A.: Discontinuous Dynamical Systems. Higher Education Press, Beijing (2010)
56. Luo, A., Huang, J.: Discontinuous dynamics of a non-linear, self-excited, friction-induced, periodically forced oscillator. Nonlinear Anal. Real World Appl. **13**, 241–257 (2012)
57. Zheng, S., Fu, X.: Periodic motion of the van der Pol equation with impulsive effect. Int. J. Bifurcation Chaos **25**(9), 1550119 (2015)
58. Zhang, Y., Fu, X.: On periodic motions of an inclined impact pair. Commun. Nonlinear Sci. Numer. Simul. **20**, 1033–1042 (2015)
59. Fu, X., Zhang, Y.: Stick motions and grazing flows in an inclined impact oscillator. Chaos Solitons Fractals **76**, 218–230 (2015)
60. Chen, G., Fan, J.: Analysis of dynamical behaviors of a double belt friction-oscillator model. Wseas Trans. Math. **15**, 357–373 (2016)
61. Fan, J., Li, S., Chen, G.: On dynamical behavior of a friction-induced oscillator with 2-DOF on a speed-varying traveling belt, Math. Prob. Eng. 2017, 1208563 (2017). https://doi.org/10.1155/2017/1208563
62. Fan, J., Xue, S., Li, S.: Analysis of dynamical behaviors of a friction-induced oscillator with switching control law. Chaos Solitons Fractals **103**, 513–531 (2017)
63. Xue, S., Fan, J.: Discontinuous dynamical behaviors in a vibro-impact system with multiple constraints. Int. J. Non-Linear Mech. **98**, 75–101 (2018)
64. Fan, J., Xue, S., Chen, G.: On discontinuous dynamics of a periodically forced double-belt friction oscillator. Chaos Solitons Fractals **109**, 280–302 (2018)
65. Fan, J., Liu, P., Liu, T., Xue, S., Yang, Z.: Analysis of discontinuous dynamical behaviors of a friction-induced oscillator with an elliptic control law, Math. Prob. Eng. 2018, 5301747 (2018). https://doi.org/10.1155/2018/5301747
66. Fan, J., Liu, T., Liu, P.: Analysis of discontinuous dynamical behavior of a class of friction oscillators with impact. Int. J. Non-linear Mech. **106**, 38–54 (2018)
67. Fan, J., Yang, Z.: Analysis of dynamical behaviors of a 2-DOF vibro-impact system with dry friction. Chaos Solitons Fractals **116**, 176–201 (2018)
68. Liu, T., Fan, J., Xue, S.: Synchronization of a Duffing oscillator with a Van der Pol equation under sinusoidal constraints. Int. J. Math. Comput. (IJMC) **29**(3), 1–25 (2018)
69. Chen, S., Fan, J., Liu, T.: On discontinuous dynamics of a 2-DOF friction-influenced oscillator with multiple elastic constraints. Int. J. Non-linear Mech. **110**, 131–150 (2019)
70. Li, C., Fan, J., Yang, Z., Xue, S.: On discontinuous dynamical behaviors of a 2-DOF impact oscillator with friction and a periodically forced excitation. Mech. Mach. Theory **135**, 81–108 (2019)